Charles University, Prague
Faculty of Mathematics and Physics

MASTER THESIS

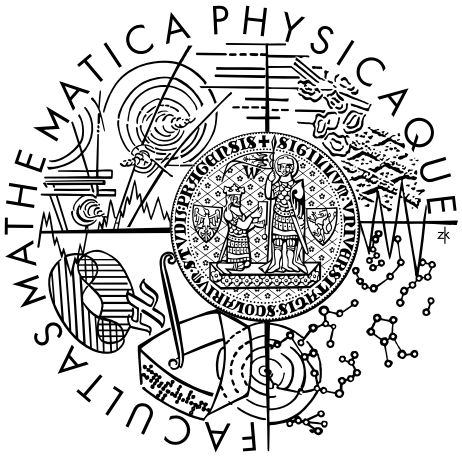

Libor Inovecký

Postglacial Relaxation of the Earth's Models in Cylindrically Symmetric Geometry

Institute of Theoretical Physics

Supervisor: Doc. RNDr. Ctirad Matyska, DrSc.

Study branch: Mathematical and Computer Modeling

I would like to express my vast thanks to Doc. RNDr. Ctirad Matyska, DrSc. for his tremendous support, guidance, attention and help with this work. Other thanks go to Doc. RNDr. Josef Málek, CSc., Mgr. Milan Pokorný, Ph.D. and RNDr. Ladislav Hanyk, Ph.D. for numerous fruitful discussions and additional literature sources. A special acknowledgement goes to Mgr. Jaroslav Hron, Ph.D., who not only provided his Navier–Stokes code, but even spent hours and days helping me to adapt the code to my needs. Last but not least, I am very grateful to my parents for their support, patience and encouragement during my studies. This work was partly supported by the Charles Univ. Grant no. 238/2001/B-GEO/MFF.

Prohlašuji, že jsem svou diplomovou práci napsal samostatně a výhradně s použitím citovaných pramenů. Souhlasím se zapůjčováním práce.

V Praze dne 12. 12. 2003 Libor Inovecký

Contents

Název práce: Postglaciální relaxace modelů Země s válcově symetrickou geometrií

Autor: Libor Inovecký

Katedra (ústav): Ústav teoretické fyziky

Vedoucí diplomové práce: Doc. RNDr. Ctirad Matyska, DrSc., Katedra geofyziky

e-mail vedoucího: cm@karel.troja.mff.cuni.cz

Abstrakt: Cylindricky symetrický model Země s elastickou a viskoelastickou reologií byl použit ke studiu vlivu laterálních heterogenit viskozity na postglaciální zdvih. Je uveden postup odvození rovnic popisujících malé deformace Země a tyto rovnice jsou přeformulovány ve slabém smyslu. Dále je dokázána existence a jednoznačnost slabých řesení. Slabá formulace je poté přepsána do cylindrických souřadnic a zdiskretizována v prostoru (metodou konečných prvků) a v čase. Jsou provedeny počítačové simulace pro různé geofyzikální modely. Uvažují se dva tvary ledovce, dvě jednoduché a jedna realistická časová závislost zátěže a především několik pozic astenosféry. Pro některé z modelů jsou uvedeny grafy deformace, napětí a disipace. Kompletní výsledky ve formě filmů lze nalézt na přiloženém CD.

Klíčová slova: postglaciální zdvih, viskoelasticita, laterální heterogenita, slabá formulace, metoda konečných prvků

Title: Postglacial relaxation of the Earth's models in cylindrically symmetric geometry

Author: Libor Inovecký

Department: Institute of Theoretical Physics

Supervisor: Doc. RNDr. Ctirad Matyska, DrSc., Department of Geophysics

Supervisor's e-mail address: cm@karel.troja.mff.cuni.cz

Abstract: A cylindrically symmetric flat-earth finite element model of the elastic and viscoelastic Earth is used to study the impact of lateral heterogeneities of viscosity on the postglacial rebound. It is shown how to derive the equations describing the Earth's infinitesimal deformations and how to formulate them in the weak sense (for the flat-earth approximation). Existence and uniqueness is proved for the weak formulations. The equations are reformulated for the case of cylindrical symmetry and discretized in space and time. Computer simulations for various geophysical models are performed. We consider two different shapes of the glacier, two simple and one realistic loading history and most importantly, several positions of the asthenosphere. Graphs of displacement, stress and dissipation are given for some models. Complete results in the form of movies can be found on the enclosed CD.

Keywords: postglacial rebound, viscoelasticity, lateral heterogeneity, weak formulation, finite element method

1 Introduction

This work deals with the postglacial rebound (also known as glacial isostatic adjustment), i.e. the Earth's deformations due to the loading and unloading of realistic glaciers. For many years, the most popular method for calculations of the postglacial rebound was the normal-mode approach. In this approach, the partial differential equations governing the post-glacial rebound are transformed into the Laplace domain and subjected to the spherical harmonic decomposition. Later, the so-called initial value approach was developed [8]. In this approach the problem is solved using the method of lines in the time-domain and using the spherical harmonic decomposition in space. Such studies usually assume radially symmetric distributions of Earth's material properties. However, seismological evidence has revealed significant lateral variations in the viscosity [18].

Recently, the finite element method has been found very useful to study postglacial rebound in the case of lateral heterogeneities (e.g. [12]). In most cases, the Earth is treated as flat to reduce the computational complexity [22]. Furthermore, the Cowling approximation [19] is usually adopted, which means that the perturbation of the Earth's gravitational potential is neglected. In the present work we will use the finite element method (with both these approximations) to study the impact of lateral heterogeneities of the viscosity.

Throughout this work, it will be assumed that all the material properties of the Earth with the exception of the viscosity vary only with depth. The viscosity will be allowed to vary laterally as well. We will consider only the forward problem, where the viscosity distribution is known beforehand. In reality, this distribution is not well determined, so the task is often to solve the inverse problem, i.e. to estimate the viscosity distribution in the mantle so as to match the measured surface deformation.

The outline of this work is as follows. We will show how the equations describing the Earth's deformations can be derived, in order to give at least the basic idea, what approximations these equations involve and where the unusual terms appearing in the equilibrium equation come from. Next, we adopt the flat-earth approximation and discuss the conditions when such an approximation is reasonable. The main intent of the present work is to rigorously derive the weak formulation of the equations describing the Earth's deformations, to prove the existence and uniqueness of the solutions, to propose a discretization of the problem in space and time and finally, to implement the discretization by means of a computer program. Then, the program is used to perform simulations of the Fennoscandian glacier for different glacier shapes, loading histories and most importantly, for several viscosity distributions. Among other models, we will study the instability of PREM [16], different cases of the position of the asthenosphere, the energy dissipation in the mantle. The last case has so far deserved very little attention in the literature (apart from [9]—in preparation).

2 Equations Describing the Earth's Deformations

In this section it will be shown, how to derive the equations that describe the deformation of the elastic or viscoelastic inhomogeneous Earth. The necessity to derive special equations for such a case arises from two important facts—the Earth is a pre-stressed and self-gravitating body. It means that the stress is non-zero even when no external force is applied. Once it is applied, the already existing stress, displacement and gravitational fields are slightly altered. However, we are interested only in the fields' changes generated by the additionally applied external force and this fact will lead to the concept of incremental quantities (incremental stress, incremental displacement and incremental gravitational potential). Moreover the Earth itself is influenced by its gravitational field. Whenever the Earth is deformed, its gravitational field is affected, thereby altering the forces acting on the Earth. This gives rise to coupling between the gravitational potential and the deformation.

The general problem of infinitesimal deformations superimposed on a finite initial strain was studied by Biot [1] and other investigators. A very detailed derivation with emphasis on the case of the Earth was carried out e.g. in [2], [13]. To complete the model of the Earth, we will introduce equations describing the two rheologies that will be dealt with throughout this work.

2.1 Equations of Motion of a Pre-stressed Body

Let us assume that there exists an original configuration, where no stresses are present and no forces act on the body occupying the domain Ω_0. This stress-free configuration is called the natural configuration and it will be denoted B_0. Some static forces begin to act on the body, thus forcing it to establish a new equilibrium. The newly-adopted (strained) configuration will be denoted B, the newly-occupied domain Ω and the space coordinate $\boldsymbol{x}$. The equilibrium condition (in the Eulerian reference frame) is expressed as

$$\nabla \cdot \boldsymbol{\tau}_0 + \rho_0 \boldsymbol{f}_0 = 0 \qquad \text{in } \Omega, \tag{2.1}$$

where $\boldsymbol{\tau}_0$ is the Cauchy tensor of initial static stress, ρ_0 the material density in configuration B and $\boldsymbol{f}_0$ the initial body force per unit mass, which will be discussed later.

The body in configuration B is subject to additional forces varying in both space and time, superimposed on the original static forces. The body will be deformed from configuration B to configuration B', a material point will move from its position $\boldsymbol{x}$ to a new position $\boldsymbol{x}'$. The additional forces are assumed to be small compared to the initial forces, therefore we shall restrict ourselves to the (linear) small strain theory. In such case, the curvilinear coordinate systems in B and B' can be considered as identical. It is more advantageous to take the coordinate system of B as a reference

frame rather than that of the natural configuration B_0. In the case of the Earth, the natural (stress-free) configuration does not even exist. The positions of all points will thus be expressed in the coordinate system of the configuration B, which corresponds to the Lagrangian approach (when dealing with the deformation from B to B').

Under the above assumptions, the stress and displacement are approximated as

$$\boldsymbol{T}(\boldsymbol{x},t) = \boldsymbol{\tau}_0(\boldsymbol{x}) + \varepsilon\overline{\boldsymbol{T}}(\boldsymbol{x},t) \tag{2.2}$$

$$\boldsymbol{x}'(\boldsymbol{x},t) = \boldsymbol{x} + \varepsilon\boldsymbol{u}(\boldsymbol{x},t), \tag{2.3}$$

where $\boldsymbol{T}$ stands for the Piola-Kirchhoff stress tensor, $\varepsilon\overline{\boldsymbol{T}}$ for its increment and $\varepsilon\boldsymbol{u}$ for the displacement field. Let us denote the deformation gradient and the deformation Jacobian

$$\boldsymbol{F} = \frac{\partial \boldsymbol{x}'}{\partial \boldsymbol{x}}, \qquad j = \det(\boldsymbol{F}), \tag{2.4}$$

which, in the present case, yields

$$\boldsymbol{F} = \boldsymbol{I} + \varepsilon(\nabla\boldsymbol{u})^T, \qquad j \doteq 1 + \varepsilon\nabla\cdot\boldsymbol{u}, \qquad j^{-1} \doteq 1 - \varepsilon\nabla\cdot\boldsymbol{u}. \tag{2.5}$$

Using these relations and the relation between the Piola-Kirchhoff and the Cauchy stress tensor $\boldsymbol{\tau}$ [13]

$$\boldsymbol{\tau} = j^{-1}\boldsymbol{F}\boldsymbol{T}, \tag{2.6}$$

we can rewrite (2.2) as

$$\boldsymbol{\tau} = \boldsymbol{\tau}_0 + \varepsilon\overline{\boldsymbol{\tau}}, \tag{2.7}$$

where

$$\overline{\boldsymbol{\tau}} = \overline{\boldsymbol{T}} + (\nabla\boldsymbol{u})^T\cdot\boldsymbol{\tau}_0 - (\nabla\cdot\boldsymbol{u})\boldsymbol{\tau}_0. \tag{2.8}$$

According to [13], the equations of motion of the body are

$$\nabla\cdot\boldsymbol{T}(\boldsymbol{x},t) + \rho_0\boldsymbol{f}(\boldsymbol{x}',t) = \varepsilon\rho_0\frac{\partial^2\boldsymbol{u}(\boldsymbol{x},t)}{\partial t^2}, \tag{2.9}$$

where the body force $\boldsymbol{f}(\boldsymbol{x}')$ can be expanded using the Taylor series

$$\boldsymbol{f}(\boldsymbol{x}',t) = \boldsymbol{f}(\boldsymbol{x},t) + \varepsilon\boldsymbol{u}(\boldsymbol{x},t)\cdot\nabla\boldsymbol{f}(\boldsymbol{x},t) + o(\varepsilon^2). \tag{2.10}$$

The force $\boldsymbol{f}(\boldsymbol{x})$ is considered to be only a linear perturbation of the initial force $\boldsymbol{f}_0(\boldsymbol{x})$

$$\boldsymbol{f}(\boldsymbol{x},t) = \boldsymbol{f}_0(\boldsymbol{x}) + \varepsilon\boldsymbol{f}_1(\boldsymbol{x},t). \tag{2.11}$$

By combining the previous two expansions and neglecting the terms quadratic in ε, we have

$$\boldsymbol{f}(\boldsymbol{x}',t) = \boldsymbol{f}_0(\boldsymbol{x}) + \varepsilon\boldsymbol{u}(\boldsymbol{x},t)\cdot\nabla\boldsymbol{f}_0(\boldsymbol{x}) + \varepsilon\boldsymbol{f}_1(\boldsymbol{x},t). \tag{2.12}$$

After substituting this result into the equation of motion (2.9) and considering the equilibrium equation (2.1), we obtain

$$\nabla \cdot \overline{\boldsymbol{T}} + \rho_0(\boldsymbol{u} \cdot \nabla \boldsymbol{f}_0 + \boldsymbol{f}_1) = \rho_0 \frac{\partial^2 \boldsymbol{u}}{\partial t^2}. \tag{2.13}$$

Finally, this equation can be expressed in terms of the increment of the Cauchy stress tensor, using the relation (2.8) and the initial equilibrium condition (2.1) as

$$\nabla \cdot \overline{\boldsymbol{\tau}} - \nabla \cdot [(\nabla \boldsymbol{u})^T \cdot \boldsymbol{\tau}_0] + \nabla(\nabla \cdot \boldsymbol{u}) \cdot \boldsymbol{\tau}_0 + \rho_0[\boldsymbol{u} \cdot \nabla \boldsymbol{f}_0 - (\nabla \cdot \boldsymbol{u})\boldsymbol{f}_0 + \boldsymbol{f}_1] = \rho_0 \frac{\partial^2 \boldsymbol{u}}{\partial t^2}. \tag{2.14}$$

The acting body forces $\boldsymbol{f}_0$, $\boldsymbol{f}_1$ and the initial static stress $\boldsymbol{\tau}_0$ are of a completely general nature as yet.

2.2 Body Forces Acting on the Earth

Let us now determine the initial body force per unit mass $\boldsymbol{f}_0$. In the case of the Earth, it is due to the Earth's own gravitational field and the centrifugal force and can be expressed in terms of the geopotential

$$\Phi_0 = \varphi_0 + \psi \tag{2.15}$$

as

$$\boldsymbol{f}_0 = -\nabla \Phi_0. \tag{2.16}$$

Considering the fact that in the equilibrium configuration B the Earth rotates uniformly with angular frequency $\boldsymbol{\omega}$ about the origin located in its center of gravity, the potential of the centrifugal force is

$$\psi = -\frac{1}{2}\left[|\boldsymbol{\omega}|^2 |\boldsymbol{x}|^2 - (\boldsymbol{\omega} \cdot \boldsymbol{x})^2\right]. \tag{2.17}$$

The gravitational potential is given by Poisson's equation

$$\Delta \varphi_0 = 4\pi G \rho_0 \tag{2.18}$$

and is required to vanish in the infinity. G is the universal gravitational constant.

The geopotential $\Phi(\boldsymbol{x}, t)$ at point x after the deformation can be expressed as

$$\Phi(\boldsymbol{x}, t) = \Phi_0(\boldsymbol{x}) + \varepsilon \Phi_1(\boldsymbol{x}, t), \tag{2.19}$$

where $\Phi_1(\boldsymbol{x}, t)$ is the increment of the geopotential and can be expressed as the sum of the increment of the gravitational potential and the increment of the potential

of the centrifugal force. However, the latter one is of the order of ε^2 and therefore drops out due to the linearization. Hence, we can write

$$\Phi_1(\boldsymbol{x}, t) = \varphi_1(\boldsymbol{x}, t). \tag{2.20}$$

The gravitational potential after the deformation is approximated by

$$\varphi(\boldsymbol{x}, t) = \varphi_0(\boldsymbol{x}) + \varepsilon\varphi_1(\boldsymbol{x}, t) \tag{2.21}$$

and must fulfill Poisson's equation

$$\Delta\varphi = 4\pi G\rho. \tag{2.22}$$

In order to obtain a similar equation for the incremental gravitational potential φ_1, we must approximate the density ρ after the deformation at point $\boldsymbol{x}$. From the law of the mass conservation, we have

$$\rho(\boldsymbol{x}', t) = \rho_0(\boldsymbol{x}, t)/j \doteq \rho_0[1 - \varepsilon\nabla \cdot \boldsymbol{u}(\boldsymbol{x}, t)], \tag{2.23}$$

where $\rho(\boldsymbol{x}', t)$ is the density after the deformation in the configuration B'. To calculate the density after the deformation in the configuration B, we must use the Taylor expansion in the neighbourhood of point $\boldsymbol{x}$

$$\rho(\boldsymbol{x}', t) = \rho(\boldsymbol{x}, t) + \varepsilon\nabla\rho(\boldsymbol{x}, t) \cdot \boldsymbol{u}(\boldsymbol{x}, t) + o(\varepsilon^2) \doteq \rho(\boldsymbol{x}, t) + \varepsilon\nabla\rho_0(\boldsymbol{x}) \cdot \boldsymbol{u}(\boldsymbol{x}, t). \tag{2.24}$$

Finally, the density after the deformation at point $\boldsymbol{x}$ is expressed as

$$\rho(\boldsymbol{x}, t) = \rho_0(\boldsymbol{x}) + \varepsilon\rho_1(\boldsymbol{x}, t), \tag{2.25}$$

where

$$\rho_1(\boldsymbol{x}, t) = -\rho_0(\boldsymbol{x})\nabla \cdot \boldsymbol{u}(\boldsymbol{x}, t) - \nabla\rho_0(\boldsymbol{x}) \cdot \boldsymbol{u}(\boldsymbol{x}, t) = -\nabla \cdot (\rho_0\boldsymbol{u}). \tag{2.26}$$

By substituting this result into Poisson's equation after the deformation (2.22) and taking into account Poisson's equation at the equilibrium (2.18), we obtain the equation for the incremental gravitational potential

$$\Delta\varphi_1 + 4\pi G\ \nabla \cdot (\rho_0\boldsymbol{u}) = 0. \tag{2.27}$$

Also the incremental gravitational potential φ_1 must vanish in the infinity.

It is important to note that Poisson's equation is always written in the Eulerian reference frame. The deformations are considered to be small, so we could linearly approximate Poisson's equation in the Lagrangian reference frame. Since the boundary becomes curved when undergoing the deformation from B to B', there arises a term for the apparent surface mass density due to the normal displacement of the

boundary (for details, see [13]). This term will appear in the boundary conditions for the incremental gravitational potential.

The body force per unit mass after the deformation was expected to be a linear perturbation of the initial field

$$\boldsymbol{f}(\boldsymbol{x},t) = \boldsymbol{f}_0(\boldsymbol{x}) + \varepsilon \boldsymbol{f}_1(\boldsymbol{x},t), \tag{2.28}$$

where the increment of the body force per unit mass is now given by

$$\boldsymbol{f}_1(\boldsymbol{x},t) = -\nabla\varphi_1(\boldsymbol{x},t). \tag{2.29}$$

The equation of motion (2.9) can be modified using the introduced potentials to the form

$$\begin{aligned} &\nabla\cdot\overline{\boldsymbol{\tau}} - \nabla\cdot[(\nabla\boldsymbol{u})^T\cdot\boldsymbol{\tau}_0] + \nabla(\nabla\cdot\boldsymbol{u})\cdot\boldsymbol{\tau}_0 \\ &= \rho_0\left[\frac{\partial^2\boldsymbol{u}}{\partial t^2} + 2\boldsymbol{\omega}\times\frac{\partial\boldsymbol{u}}{\partial t} + \nabla\varphi_1 + \boldsymbol{u}\cdot\nabla(\nabla\Phi_0) - (\nabla\cdot\boldsymbol{u})\nabla\Phi_0\right]. \end{aligned} \tag{2.30}$$

2.3 Initial Static Stress

From this section on, the terms arising from the Earth's rotation will be neglected. The initial static stress $\boldsymbol{\tau}_0$ is assumed to be hydrostatic

$$\boldsymbol{\tau}_0(\boldsymbol{x}) = -p_0(\boldsymbol{x})\boldsymbol{I}, \tag{2.31}$$

where $p_0(\boldsymbol{x})$ is the hydrostatic pressure in the initial equilibrium configuration, described by equations (2.1) and (2.16), which, in this case, yields

$$\nabla p_0 = -\rho_0\nabla\varphi_0. \tag{2.32}$$

Let us now assume that the initial density ρ_0 is dependent on the radial distance r from the center of gravity of the Earth only. By Poisson's equation (2.18), we see that the initial gravitational potential is also dependent on r only. Finally, from the two above-appearing equations, we see that p_0 and $\boldsymbol{\tau}_0$ also depend on r only.

The gravitational acceleration in the initial configuration is

$$\boldsymbol{g}_0 = -\nabla\varphi_0 = -\frac{\mathrm{d}\varphi_0}{\mathrm{d}r}\boldsymbol{e}_r = -g_0(r)\boldsymbol{e}_r, \qquad g_0(r) > 0. \tag{2.33}$$

By substituting the assumption on the initial static stress (2.31) into the relation (2.30), we have

$$\nabla\cdot\overline{\boldsymbol{\tau}} = \rho_0\left[\frac{\partial^2\boldsymbol{u}}{\partial t^2} + \nabla\varphi_1 + \nabla(\boldsymbol{u}\cdot\nabla\varphi_0) - (\nabla\cdot\boldsymbol{u})\nabla\varphi_{1_0}\right]. \tag{2.34}$$

Finally, we substitute for $\nabla\varphi_0$, and obtain the result

$$\nabla\cdot\overline{\boldsymbol{\tau}}-\rho_0\nabla\varphi_1+\rho_0(\nabla\cdot\boldsymbol{u})g_0\boldsymbol{e}_r-\rho_0\nabla(g_0\boldsymbol{u}\cdot\boldsymbol{e}_r)=\rho_0\frac{\partial^2\boldsymbol{u}}{\partial t^2}. \tag{2.35}$$

Since $\rho_0=\rho_0(r)$, the previous equation can be rewritten in the form, in which it is usually stated in the literature dealing with the postglacial rebound. Furthermore, the changes are usually assumed to be gradual, so we can consider the static equilibrium rather than the motion equation:

$$\nabla\cdot\overline{\boldsymbol{\tau}}-\rho_0\nabla\varphi_1+\nabla\cdot(\rho_0\boldsymbol{u})g_0\boldsymbol{e}_r-\nabla(\rho_0 g_0\boldsymbol{u}\cdot\boldsymbol{e}_r)=0. \tag{2.36}$$

This equation and Poisson's equation (2.27) are the two equations that model small static (or quasi-static) deformations of the inhomogeneous non-rotating Earth.

To simplify the notation, the incremental stress field $\overline{\boldsymbol{\tau}}$ will be denoted simply $\boldsymbol{\tau}$ hereafter.

2.4 Boundary Conditions

Without going into further details, we will provide the above-derived equations with appropriate boundary conditions.

Since the Earth comprises of several spherical layers of highly differing physical properties, there exist certain internal surfaces of discontinuity in the density, Lamé coefficients etc. Let Σ be such a surface of discontinuity separating the domains Ω^+ and Ω^-. On the surface Σ, we will apply the jump conditions

$$[\boldsymbol{u}]^+_-=0, \qquad [\boldsymbol{\tau}\cdot\boldsymbol{n}]^+_-=0 \tag{2.37}$$

$$[\varphi_1]^+_-=0, \qquad [(\nabla\varphi_1+4\pi G\rho_0\boldsymbol{u})\cdot\boldsymbol{n}]^+_-=0 \tag{2.38}$$

for a solid-solid boundary and

$$[\boldsymbol{u}\cdot\boldsymbol{n}]^+_-=0, \qquad [\boldsymbol{\tau}\cdot\boldsymbol{n}]^+_-=0 \tag{2.39}$$

$$[\varphi_1]^+_-=0, \qquad [(\nabla\varphi_1+4\pi G\rho_0\boldsymbol{u})\cdot\boldsymbol{n}]^+_-=0 \tag{2.40}$$

for a solid-liquid boundary. Furthermore, in the case of solid-liquid boundary, it is required that the tangential forces vanish on the boundary:

$$\boldsymbol{\tau}\cdot\boldsymbol{n}-(\boldsymbol{n}\cdot\boldsymbol{\tau}\cdot\boldsymbol{n})\boldsymbol{n}=0 \qquad \text{on } \Sigma. \tag{2.41}$$

The symbol $[\xi]^+_-$ indicates the jump of the quantity ξ across Σ, vector $\boldsymbol{n}$ is a unit normal to the surface Σ, pointing toward the domain Ω^+.

The external surface of the Earth will be subject to an external load f, signifying the pressure at a given surface point. This evidently imposes a boundary condition

on the incremental stress field. However, it also influences the jump condition for the incremental potential, since the load corresponds to a certain surface distribution of mass. The conditions on the external surface are

$$\boldsymbol{\tau}(\boldsymbol{x}) \cdot \boldsymbol{n} = f(\boldsymbol{x}, t)\ \boldsymbol{n}, \qquad [\varphi_1]^+_- = 0 \tag{2.42}$$

$$[\nabla \varphi_1]^+_- \cdot \boldsymbol{n} = 4\pi G(\rho_0 \boldsymbol{u} \cdot \boldsymbol{n} - f/g_R), \tag{2.43}$$

where $\boldsymbol{n}$ is the outward unit normal to the surface of the Earth. The constant $g_R > 0$ is the value of the initial gravitational acceleration $g_0(r)$ at the Earth's surface.

2.5 Rheological Models

The above derived equation of static equilibrium and Poisson's equation are independent of the rheological model used, provided that we stay in the framework of small deformations. To complete the description of the Earth, we will now supply these equations with two alternative rheological models. One of them is the elastic rheology given by Hooke's law

$$\boldsymbol{\tau} - \lambda(\nabla \cdot \boldsymbol{u})\boldsymbol{I} - 2\mu\, \boldsymbol{\varepsilon}(\boldsymbol{u}) = 0, \tag{2.44}$$

the other one is the time-dependent Maxwell viscoelastic rheology given by the formula

$$\frac{\partial}{\partial t}\boldsymbol{\tau} - \frac{\partial}{\partial t}\left[\lambda(\nabla \cdot \boldsymbol{u})\boldsymbol{I} + 2\mu\, \boldsymbol{\varepsilon}(\boldsymbol{u})\right] + \frac{\mu}{\eta}\left[\boldsymbol{\tau} - K(\nabla \cdot \boldsymbol{u})\boldsymbol{I}\right] = 0, \tag{2.45}$$

empirically derived from the RSL (relative sea level) data.

The small strain tensor $\boldsymbol{\varepsilon}(\boldsymbol{u})$ is defined as

$$\boldsymbol{\varepsilon}(\boldsymbol{u}) = \frac{1}{2}\left(\nabla \boldsymbol{u} + (\nabla \boldsymbol{u})^T\right). \tag{2.46}$$

The symbols μ and λ represent the elastic Lamé coefficients and K, the bulk modulus, can be expressed as their linear combination

$$K = \lambda + \frac{2}{3}\mu. \tag{2.47}$$

The symbol η denotes the dynamic viscosity.

In case of the Maxwell viscoelasticity, there is a non-zero dissipation density, which can be evaluated as [9]

$$\Phi = \frac{\boldsymbol{\tau}_S : \boldsymbol{\tau}_S}{2\eta}, \qquad \text{where} \quad \boldsymbol{\tau}_S = \boldsymbol{\tau} - K(\nabla \cdot \boldsymbol{u})\boldsymbol{I}. \tag{2.48}$$

For modeling the Earth's liquid core, a different rheological model is necessary. However, as already explained before, we will concentrate on local problems, so the core can be completely excluded.

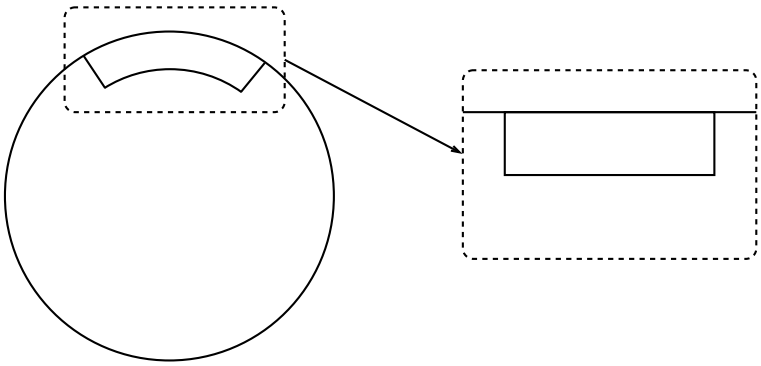

Fig. 1: Passing to the local problem

3 Local Problem Formulation

In the previous section, the equations describing the deformation of the Earth as a whole were derived. In the present work we deal with the elastic and viscoelastic response of the Earth to the presence of a glacier on its surface. Depending on the glacier's size, this may be considered to be a local problem, i.e. a problem, where the driving forces and deformations are present only in a limited region of the Earth. Hence, we can abandon the spherical nature and geometry of the problem, and limit ourselves to the local orthogonal geometry, which will be later replaced by cylindrical geometry (for a cylindrically symmetric case). This is the so-called flat-earth approximation. The validity of such an approximation was studied in [22], where it was shown that it is credible in the case of a glacier, whose size is smaller than or comparable to that of the Fennoscandian glacier.

Hereafter, the vertical coordinate (pointing in the direction away from the Earth's center) will always be denoted z in place of r, in order to avoid confusion with the radial coordinate in the local cylindrical coordinate system.

We must realize that such a simplification involves two possible sources of discrepancies. The first comes from the fact that the real geometry is curved, whereas the local one is not. The second is due to the necessity to impose boundary conditions at the edges of the local geometry. These boundary conditions do not come from the model of the Earth, they come from the assumption that the Earth is not affected by the glacier outside the local domain at all.

To make the problems' formulations clear, we will summarize the equations, the boundary conditions, the jump conditions of the incremental gravitational potential on the free boundary and the initial conditions describing the elastic and the viscoelastic problem. The internal jump conditions (2.37), corresponding to the discontinuities in the Earth's properties, need not be considered. In the weak formulation, discontinuous coefficients are generally assumed.

3.1 Elastic Problem

We aim to solve the equation system

$$\nabla \cdot \boldsymbol{\tau} - \rho_0 \nabla \varphi_1 + \nabla \cdot (\rho_0 \boldsymbol{u}) g_0 \boldsymbol{e}_z - \nabla(\rho_0 g_0 \boldsymbol{e}_z \cdot \boldsymbol{u}) = 0 \qquad \text{in } \Omega \tag{3.1a}$$

$$\nabla \cdot (\nabla \varphi_1 + 4\pi G \rho_0 \boldsymbol{u}) = 0 \qquad \text{in } \Omega \tag{3.1b}$$

$$\Delta \varphi_1 = 0 \qquad \text{in } \Omega^C \tag{3.1c}$$

$$\boldsymbol{\tau} - \lambda (\nabla \cdot \boldsymbol{u}) \boldsymbol{I} - 2\mu\, \boldsymbol{\varepsilon}(\boldsymbol{u}) = 0 \qquad \text{in } \Omega, \tag{3.1d}$$

for the unknown incremental displacement (vector field) $\boldsymbol{u} = \boldsymbol{u}(\boldsymbol{x})$, the incremental gravitational potential (scalar field) $\varphi_1 = \varphi_1(\boldsymbol{x})$ and the incremental stress (symmetric tensor field) $\boldsymbol{\tau} = \boldsymbol{\tau}(\boldsymbol{x})$. $\Omega \subset R^3$ is a bounded domain with a lipschitzian boundary and $\Omega^C = \mathcal{R}^3 \setminus \Omega$ its complement. $\boldsymbol{\varepsilon}(\boldsymbol{u})$ denotes the small strain tensor.

The vector $\boldsymbol{e}_z$ is a unit vector pointing in the direction of the z-coordinate. The parameters ρ_0, g_0 are assumed to depend only on z. λ and μ are the elastic Lamé coefficients. G is the universal gravitational constant.

The equations are supplied with the boundary (or limit) conditions

$$\boldsymbol{u}(\boldsymbol{x}) = 0 \qquad \text{on } \Gamma_1 \tag{3.2a}$$

$$\boldsymbol{\tau}(\boldsymbol{x}) \cdot \boldsymbol{n} = f(\boldsymbol{x})\, \boldsymbol{n} \qquad \text{on } \Gamma_2 \tag{3.2b}$$

$$\varphi_1(\boldsymbol{x}) \approx \frac{1}{|\boldsymbol{x}|} \qquad \text{for } |\boldsymbol{x}| \to \infty \tag{3.2c}$$

and the jump conditions

$$[\varphi_1]^+_- = 0 \qquad \text{on } \partial\Omega \tag{3.3a}$$

$$[\nabla \varphi_1]^+_- \cdot \boldsymbol{n} = 0 \qquad \text{on } \Gamma_1 \tag{3.3b}$$

$$[\nabla \varphi_1]^+_- \cdot \boldsymbol{n} = 4\pi G(\rho_0 \boldsymbol{u} \cdot \boldsymbol{n} - f/g_R) \qquad \text{on } \Gamma_2, \tag{3.3c}$$

where $\boldsymbol{n}$ is the vector of the outward unit normal to $\partial\Omega$ and the sets Γ_1 and Γ_2 are non-empty and open with respect to $\partial\Omega$. $g_R > 0$ is the value of the initial gravitational acceleration at the Earth's surface.

Figure 2 shows a typical domain Ω under consideration. As the figure suggests, for the case of postglacial rebound, the upper face of the cylinder will be considered as the part Γ_2 of the boundary (i.e. the part, where the stress condition is given) and the remainder of the surface as the part Γ_1 (i.e. the part, where the displacement condition is given).

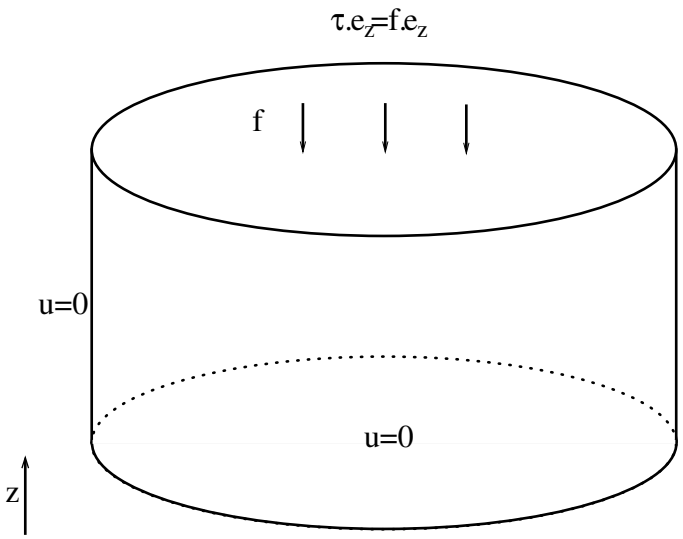

Fig. 2: A cylindrical 3D region

3.2 Viscoelastic Problem

In this problem, Hooke's law is replaced with the Maxwell rheology and the problem becomes time-dependent, thus yielding the following equation system:

$$\nabla \cdot \boldsymbol{\tau} - \rho_0 \nabla \varphi_1 + \nabla \cdot (\rho_0 \boldsymbol{u}) g_0 \boldsymbol{e}_z - \nabla(\rho_0 g_0 \boldsymbol{e}_z \cdot \boldsymbol{u}) = 0 \qquad \text{in } \Omega \times I \qquad (3.4a)$$

$$\nabla \cdot (\nabla \varphi_1 + 4\pi G \rho_0 \boldsymbol{u}) = 0 \qquad \text{in } \Omega \times I \qquad (3.4b)$$

$$\Delta \varphi_1 = 0 \qquad \text{in } \Omega^C \times I \qquad (3.4c)$$

$$\frac{\partial}{\partial t}\boldsymbol{\tau} - \frac{\partial}{\partial t}\left[\lambda(\nabla \cdot \boldsymbol{u})\boldsymbol{I} + 2\mu\,\boldsymbol{\varepsilon}(\boldsymbol{u})\right] + \frac{\mu}{\eta}\left[\boldsymbol{\tau} - K(\nabla \cdot \boldsymbol{u})\boldsymbol{I}\right] = 0 \qquad \text{in } \Omega \times I, \qquad (3.4d)$$

where the unknowns $\boldsymbol{u} = \boldsymbol{u}(\boldsymbol{x}, t)$, $\varphi_1 = \varphi_1(\boldsymbol{x}, t)$, $\boldsymbol{\tau} = \boldsymbol{\tau}(\boldsymbol{x}, t)$ are now time-dependent. $I = [0, T]$, $T > 0$, is the time interval under consideration. The bulk modulus K is defined through the elastic Lamé coefficients λ and μ as $K = \lambda + 2/3\mu$. η is the dynamic viscosity. All the coefficients ρ_0, g_0, λ, μ, K and η are considered to be independent of time. The time and space dependence will be omitted hereafter, whenever there is no risk of confusion.

The problem is provided with the initial conditions

$$\boldsymbol{u}(\boldsymbol{x}, 0) = \boldsymbol{u}_0(\boldsymbol{x}) \qquad \text{in } \Omega \qquad (3.5a)$$

$$\boldsymbol{\tau}(\boldsymbol{x}, 0) = \boldsymbol{\tau}_0(\boldsymbol{x}) \qquad \text{in } \Omega, \qquad (3.5b)$$

the boundary (or limit) conditions

$$\boldsymbol{u}(\boldsymbol{x},t) = 0 \qquad \text{on } \Gamma_1 \ \times I \tag{3.6a}$$
$$\boldsymbol{\tau}(\boldsymbol{x},t)\cdot\boldsymbol{n} = f(\boldsymbol{x},t)\,\boldsymbol{n} \qquad \text{on } \Gamma_2 \times I \tag{3.6b}$$
$$\varphi_1(\boldsymbol{x},t) \approx \frac{1}{|\boldsymbol{x}|} \qquad \text{for } |\boldsymbol{x}| \to \infty,\ \forall t \in I \tag{3.6c}$$

and the skip conditions

$$[\varphi_1]^+_- = 0 \qquad \text{on } \partial\Omega \times I \tag{3.7a}$$
$$[\nabla\varphi_1]^+_-\cdot\boldsymbol{n} = 0 \qquad \text{on } \Gamma_1 \times I \tag{3.7b}$$
$$[\nabla\varphi_1]^+_-\cdot\boldsymbol{n} = 4\pi G(\rho_0\boldsymbol{u}\cdot\boldsymbol{n} - f/g_R) \qquad \text{on } \Gamma_2 \times I. \tag{3.7c}$$

4 Weak Formulation of the Problems

We will derive the weak formulations of the elastic and the viscoelastic problem. Existence and uniqueness will be proved for these weak formulations. The weak formulations will later be used for the discrete approximation of the problems.

Martinec [14] has derived the variational formulation (i.e. formulation in terms of energy functionals) of an incompressible viscoelastic problem discretized in time using the standard θ-scheme. To our knowledge, the weak formulation of the fully time-dependent problem has not yet been presented in the literature. The conditions for the existence and uniqueness of the solution of the elastic and the viscoelastic problem as well as the proof itself also seem to be an original result.

4.1 Elastic Problem

Let us now derive the weak formulation of the elastic problem.

Equation (3.1a) is multiplied by an arbitrary vector test function

$$\boldsymbol{U} \in \tilde{V} \equiv \left\{\boldsymbol{v} \in [\mathcal{C}^\infty(\Omega)]^3; \boldsymbol{v}\big|_{\Gamma_1} = 0\right\} \tag{4.1}$$

and integrated over the domain Ω:

$$\begin{aligned}\int_\Omega (\nabla\cdot\boldsymbol{\tau})\cdot\boldsymbol{U}\ \mathrm{d}x + \int_\Omega [\nabla\cdot(\rho_0\boldsymbol{u})g_0\boldsymbol{e}_z - \nabla(\rho_0 g_0\boldsymbol{e}_z\cdot\boldsymbol{u})]\cdot\boldsymbol{U}\ \mathrm{d}x \\ - \int_\Omega \rho_0\nabla\varphi_1\cdot\boldsymbol{U}\ \mathrm{d}x = 0.\end{aligned} \tag{4.2}$$

Then, integrating by parts the term with $(\nabla \cdot \boldsymbol{\tau})$, using the symmetry of $\boldsymbol{\tau}$ and the definition of the small strain tensor (2.46), we have

$$\begin{aligned}\int_\Omega (\nabla \cdot \boldsymbol{\tau}) \cdot \boldsymbol{U} \, \mathrm{d}x &= \int_\Omega \sum_{i,j=1}^{3} \frac{\partial \tau_{ij}}{\partial x_i} U_j \, \mathrm{d}x = -\int_\Omega \sum_{i,j=1}^{3} \tau_{ij} \frac{\partial U_j}{\partial x_i} \, \mathrm{d}x + \int_{\partial\Omega} \boldsymbol{n} \cdot \boldsymbol{\tau} \cdot \boldsymbol{U} \, \mathrm{d}S \\ &= -\int_\Omega \boldsymbol{\tau} : \nabla \boldsymbol{U} \, \mathrm{d}x + \int_{\partial\Omega} \boldsymbol{n} \cdot \boldsymbol{\tau} \cdot \boldsymbol{U} \, \mathrm{d}S = -\int_\Omega \boldsymbol{\tau} : \boldsymbol{\varepsilon}(\boldsymbol{U}) \, \mathrm{d}x + \int_{\partial\Omega} \boldsymbol{n} \cdot \boldsymbol{\tau} \cdot \boldsymbol{U} \, \mathrm{d}S,\end{aligned} \tag{4.3}$$

so the previous equation becomes

$$\begin{aligned}-\int_\Omega \boldsymbol{\tau} : \boldsymbol{\varepsilon}(\boldsymbol{U}) \, \mathrm{d}x + \int_\Omega [\nabla \cdot (\rho_0 \boldsymbol{u}) g_0 \boldsymbol{e}_z - \nabla(\rho_0 g_0 \boldsymbol{e}_z \cdot \boldsymbol{u})] \cdot \boldsymbol{U} \, \mathrm{d}x \\ - \int_\Omega \rho_0 \nabla \varphi_1 \cdot \boldsymbol{U} \, \mathrm{d}x + \int_{\partial\Omega} \boldsymbol{n} \cdot \boldsymbol{\tau} \cdot \boldsymbol{U} \, \mathrm{d}S = 0.\end{aligned} \tag{4.4}$$

Next, we take into consideration the imposed boundary conditions for $\boldsymbol{U}$ and $\boldsymbol{\tau}$ in the surface integral, thus obtaining

$$\begin{aligned}-\int_\Omega \boldsymbol{\tau} : \boldsymbol{\varepsilon}(\boldsymbol{U}) \, \mathrm{d}x + \int_\Omega [\nabla \cdot (\rho_0 \boldsymbol{u}) g_0 \boldsymbol{e}_z - \nabla(\rho_0 g_0 \boldsymbol{e}_z \cdot \boldsymbol{u})] \cdot \boldsymbol{U} \, \mathrm{d}x \\ - \int_\Omega \rho_0 \nabla \varphi_1 \cdot \boldsymbol{U} \, \mathrm{d}x + \int_{\Gamma_2} f \, \boldsymbol{n} \cdot \boldsymbol{U} \, \mathrm{d}S = 0.\end{aligned} \tag{4.5}$$

Considering the fact that $\rho_0 = \rho_0(z)$, we have the equality

$$\nabla \cdot (\rho_0 \boldsymbol{u}) g_0 \boldsymbol{e}_z - \nabla(\rho_0 g_0 \boldsymbol{e}_z \cdot \boldsymbol{u}) = \rho_0 \left[(\nabla \cdot \boldsymbol{u}) g_0 \boldsymbol{e}_z - \nabla(g_0 \boldsymbol{e}_z \cdot \boldsymbol{u}) \right]. \tag{4.6}$$

Finally, we substitute for $\boldsymbol{\tau}$ from Equation (3.1d), to get

$$\begin{aligned}&\int_\Omega 2\mu \, \boldsymbol{\varepsilon}(\boldsymbol{u}) : \boldsymbol{\varepsilon}(\boldsymbol{U}) \, \mathrm{d}x + \int_\Omega \lambda (\nabla \cdot \boldsymbol{u})(\nabla \cdot \boldsymbol{U}) \, \mathrm{d}x + \int_\Omega \rho_0 \nabla \varphi_1 \cdot \boldsymbol{U} \, \mathrm{d}x \\ &+ \int_\Omega \rho_0 \left[\nabla(g_0 \boldsymbol{e}_z \cdot \boldsymbol{u}) - (\nabla \cdot \boldsymbol{u}) g_0 \boldsymbol{e}_z \right] \cdot \boldsymbol{U} \, \mathrm{d}x = \int_{\Gamma_2} f \, \boldsymbol{n} \cdot \boldsymbol{U} \, \mathrm{d}S \qquad \forall \boldsymbol{U} \in \tilde{V}.\end{aligned} \tag{4.7}$$

To derive the weak form of Equation (3.1d), we simply multiply it (using the double-dot product) by a symmetric tensor test function

$$\boldsymbol{\mathcal{T}} \in \tilde{P} \equiv \left\{ \boldsymbol{A} \in [\mathcal{C}^\infty(\Omega)]^{3\times 3}; \boldsymbol{A} = \boldsymbol{A}^T \right\} \tag{4.8}$$

and integrate the result over Ω:

$$\int_\Omega \boldsymbol{\tau} : \boldsymbol{\mathcal{T}} \, \mathrm{d}x = \int_\Omega 2\mu \, \boldsymbol{\varepsilon}(\boldsymbol{u}) : \boldsymbol{\mathcal{T}} \, \mathrm{d}x + \int_\Omega \lambda (\nabla \cdot \boldsymbol{u}) \operatorname{Tr} \boldsymbol{\mathcal{T}} \, \mathrm{d}x \qquad \forall \boldsymbol{\mathcal{T}} \in \tilde{P}. \tag{4.9}$$

The weak formulation of Poisson's equation (3.1b) is the most delicate. We take an arbitrary test function $\Phi \in \tilde{F} \equiv \mathcal{C}_0^\infty(\mathcal{R}^3)$. We multiply both Equations (3.1b) and (3.1c) by Φ and integrate the first one over Ω and the second one over $\Omega^C = \mathcal{R}^3 \setminus \Omega$. As a result, we obtain

$$\int_\Omega (\Delta\varphi_1)\Phi \,\mathrm{d}x + \int_{\Omega^C} (\Delta\varphi_1)\Phi \,\mathrm{d}x + 4\pi G \int_\Omega \nabla\cdot(\rho_0 \boldsymbol{u})\Phi \,\mathrm{d}x = 0. \tag{4.10}$$

Keeping in mind that Φ has a bounded support, we apply integration by parts to all the integrals:

$$\begin{aligned}\int_\Omega \nabla\varphi_1\cdot\nabla\Phi \,\mathrm{d}x + \int_{\Omega^C} \nabla\varphi_1\cdot\nabla\Phi \,\mathrm{d}x + 4\pi G\int_\Omega \rho_0\boldsymbol{u}\cdot\nabla\Phi \,\mathrm{d}x \\ + \int_{\partial\Omega} [\nabla\varphi_1]^+_-\cdot\boldsymbol{n}\,\Phi \,\mathrm{d}S - 4\pi G\int_{\partial\Omega}\rho_0\boldsymbol{u}\cdot\boldsymbol{n}\,\Phi\,\mathrm{d}S = 0.\end{aligned}$$

Adding the first two integrals together and using the prescribed boundary and jump conditions (namely (3.2a), (3.3b), (3.3c)), we get

$$\begin{aligned}\int_{\mathcal{R}^3} \nabla\varphi_1\cdot\nabla\Phi \,\mathrm{d}x + 4\pi G\int_\Omega \rho_0\boldsymbol{u}\cdot\nabla\Phi\,\mathrm{d}x \\ + 4\pi G\int_{\Gamma_2}(\rho_0\boldsymbol{u}\cdot\boldsymbol{n} - f/g_R)\Phi\,\mathrm{d}S - 4\pi G\int_{\Gamma_2}\rho_0\boldsymbol{u}\cdot\boldsymbol{n}\,\Phi\,\mathrm{d}S = 0.\end{aligned} \tag{4.11}$$

Two terms in the boundary integrals cancel out, so the weak formulation of the potential equation is

$$\frac{1}{4\pi G}\int_{\mathcal{R}^3}\nabla\varphi_1\cdot\nabla\Phi\,\mathrm{d}x + \int_\Omega \rho_0\boldsymbol{u}\cdot\nabla\Phi\,\mathrm{d}x = \int_{\Gamma_2}\frac{f}{g_R}\Phi\,\mathrm{d}S \qquad \forall\Phi\in\tilde{F}. \tag{4.12}$$

We will now close the above-presented test function spaces in the right norm in order to ensure the existence of all the integrals appearing in the derived equations and the fulfillment of the Dirichlet boundary condition for the displacement. The solutions will be sought in the same spaces and this choice will be later justified by the proof of existence and uniqueness. The solution and test function spaces are

$$\boldsymbol{u}, \boldsymbol{U} \in V \equiv \left\{\boldsymbol{v}\in\left[W^{1,2}(\Omega)\right]^3; \boldsymbol{v}\big|_{\Gamma_1} = 0\right\} \tag{4.13a}$$

$$\boldsymbol{\tau}, \boldsymbol{\mathcal{T}} \in P \equiv \left\{\boldsymbol{A}\in\left[L^2(\Omega)\right]^{3\times 3}; \boldsymbol{A} = \boldsymbol{A}^T\right\} \tag{4.13b}$$

$$\varphi_1, \Phi \in F \equiv D_0^{1,2}(\mathcal{R}^3), \tag{4.13c}$$

where the space $D_0^{1,2}$ is a homogeneous Sobolev space. The definitions and some properties of the homogeneous Sobolev spaces $D^{m,q}$ and $D_0^{m,q}$ can be found in Appendix A and we will refer to them as they will be used throughout the text. We observe that for $\boldsymbol{u}\in V$ we have $\boldsymbol{\varepsilon}(\boldsymbol{u})\in P$.

We must also specify the conditions for the coefficients:

$$\mu, \lambda, \rho_0 \in L^\infty(\Omega), \quad g_0 \in W^{1,\infty}(\Omega), \quad f \in L^2(\Gamma_2). \tag{4.14}$$

All the spaces V, P and F are Hilbert spaces, equipped with the scalar products

$$(\boldsymbol{U}, \boldsymbol{V})_V \equiv \sum_{i=1}^{3} \int_\Omega U_i V_i \, \mathrm{d}x + \sum_{i,j=1}^{3} \int_\Omega \frac{\partial U_i}{\partial x_j} \frac{\partial V_i}{\partial x_j} \, \mathrm{d}x \tag{4.15a}$$

$$(\boldsymbol{\mathcal{T}}, \boldsymbol{\mathcal{S}})_P \equiv \sum_{i,j=1}^{3} \int_\Omega T_{ij} S_{ij} \, \mathrm{d}x \tag{4.15b}$$

$$(\Phi, \Psi)_F \equiv \int_{\mathcal{R}^3} \nabla\Phi \cdot \nabla\Psi \, \mathrm{d}x \tag{4.15c}$$

and the corresponding norms $\|\cdot\|_V = \|\cdot\|_{1,2,\Omega}$, $\|\cdot\|_P = \|\cdot\|_{2,\Omega}$ and $\|\cdot\|_F = |\cdot|_{1,2,\mathcal{R}^3}$.

From the definition of homogeneous Sobolev space we only know that the gradient of φ_1 lies in the space $L^2(\mathcal{R}^3)$. According to Lemmas A.4 and A.5, φ_1 lies in some better spaces, namely

$$\varphi_1 \in L^6(\mathcal{R}^3), \qquad \|\varphi_1\|_{6,\mathcal{R}^3} \le \frac{2}{\sqrt{3}} \|\varphi_1\|_F \tag{4.16}$$

and

$$\forall \boldsymbol{x}_0 \in \mathcal{R}^3 : \quad \frac{\varphi_1}{|\boldsymbol{x} - \boldsymbol{x}_0|} \in L^2(\mathcal{R}^3), \qquad \left\| \frac{\varphi_1}{|\boldsymbol{x} - \boldsymbol{x}_0|} \right\|_{2,\mathcal{R}^3} \le 2 \|\varphi_1\|_F . \tag{4.17}$$

The weak solutions can be found as functions from the above-defined spaces, fulfilling Equations (4.7), (4.9) and (4.12) for all test functions $\boldsymbol{U} \in V$, $\Phi \in F$, $\boldsymbol{\tau} \in P$. To put these equations into a more compact form, we introduce the bilinear forms

$$a : V \times V \to \mathcal{R}, \quad a(\boldsymbol{U}, \boldsymbol{V}) \equiv \int_\Omega 2\mu \, \boldsymbol{\varepsilon}(\boldsymbol{U}) : \boldsymbol{\varepsilon}(\boldsymbol{V}) \, \mathrm{d}x + \int_\Omega \lambda (\nabla \cdot \boldsymbol{U})(\nabla \cdot \boldsymbol{V}) \, \mathrm{d}x \tag{4.18a}$$

$$b : V \times V \to \mathcal{R}, \quad b(\boldsymbol{U}, \boldsymbol{V}) \equiv \int_\Omega \rho_0 \left[\nabla(g_0 \boldsymbol{e}_z \cdot \boldsymbol{U}) - (\nabla \cdot \boldsymbol{U}) g_0 \boldsymbol{e}_z \right] \cdot \boldsymbol{V} \, \mathrm{d}x \tag{4.18b}$$

$$c : V \times F \to \mathcal{R}, \quad c(\boldsymbol{U}, \Phi) \equiv \int_\Omega \rho_0 \, \boldsymbol{U} \cdot \nabla\Phi \, \mathrm{d}x \tag{4.18c}$$

$$d : V \times P \to \mathcal{R}, \quad d(\boldsymbol{U}, \boldsymbol{\mathcal{T}}) \equiv \int_\Omega 2\mu \, \boldsymbol{\varepsilon}(\boldsymbol{U}) : \boldsymbol{\mathcal{T}} \, \mathrm{d}x + \int_\Omega \lambda (\nabla \cdot \boldsymbol{U})(\mathrm{Tr}\, \boldsymbol{\mathcal{T}}) \, \mathrm{d}x \tag{4.18d}$$

and the linear forms

$$F_1(\boldsymbol{U}) \equiv \int_{\Gamma_2} f\,\boldsymbol{n}\cdot\boldsymbol{U}\ \mathrm{d}S \tag{4.19a}$$

$$F_2(\Phi) \equiv \int_{\Gamma_2} \frac{f}{g_R}\Phi\ \mathrm{d}S. \tag{4.19b}$$

The existence of the boundary integral in the definition of F_2 is justified by Lemma A.3 and the trace theorem.

Now, the weak formulation of the elastic problem can be rewritten in the compact form

$$a(\boldsymbol{u},\boldsymbol{U}) + b(\boldsymbol{u},\boldsymbol{U}) + c(\boldsymbol{U},\varphi_1) = F_1(\boldsymbol{U}) \qquad \forall \boldsymbol{U}\in V \tag{4.20a}$$

$$\frac{1}{4\pi G}(\varphi_1,\Phi)_F + c(\boldsymbol{u},\Phi) = F_2(\Phi) \qquad \forall \Phi\in F \tag{4.20b}$$

$$(\boldsymbol{\tau},\boldsymbol{\mathcal{T}})_P - d(\boldsymbol{u},\boldsymbol{\mathcal{T}}) = 0 \qquad \forall \boldsymbol{\mathcal{T}}\in P. \tag{4.20c}$$

4.2 Existence and Uniqueness of the Solution of the Elastic Problem

Equation (4.20c) for $\boldsymbol{\tau}$ can be regarded as explicit and $\boldsymbol{\tau}$ does not appear anywhere else in the equation system. It is therefore evident that once we have a unique solution $\boldsymbol{u}$, there also exists a unique solution $\boldsymbol{\tau}$. Furthermore, it is bounded by

$$\|\boldsymbol{\tau}\|_P \le (2\|\mu\|_\infty + 3\|\lambda\|_\infty)\,\|\boldsymbol{u}\|_V\,. \tag{4.21}$$

Thus, in the following proof we will only deal with $\boldsymbol{u}$ and φ_1. The proof will be carried out using the Lax-Milgram theorem.

Step 1: Properties of the defined bilinear and linear forms
First, it is necessary to prove some basic properties of the above-defined bilinear and linear forms, namely the boundedness and ellipticity.

Using the Hölder inequality and the inequalities

$$\|\nabla\cdot\boldsymbol{U}\|_2^2 \le 3\|\nabla\boldsymbol{U}\|_2^2, \quad \|\boldsymbol{\varepsilon}(\boldsymbol{U})\|_2 \le \|\nabla\boldsymbol{U}\|_2 \qquad \forall \boldsymbol{U}\in V, \tag{4.22}$$

we show that the bilinear forms $a(\cdot,\cdot)$, $b(\cdot,\cdot)$, $c(\cdot,\cdot)$ are bounded on the spaces, where they are defined:

$$|a(\boldsymbol{U},\boldsymbol{V})| \le (2\|\mu\|_\infty + 3\|\lambda\|_\infty)\,\|\boldsymbol{U}\|_V\,\|\boldsymbol{V}\|_V =: \|a\|\,\|\boldsymbol{U}\|_V\,\|\boldsymbol{V}\|_V \tag{4.23a}$$

$$|b(\boldsymbol{U},\boldsymbol{V})| \le (1+\sqrt{3})\,\|\rho_0\|_\infty\,\|g_0\|_{1,\infty}\,\|\boldsymbol{U}\|_V\,\|\boldsymbol{V}\|_V =: \|b\|\,\|\boldsymbol{U}\|_V\,\|\boldsymbol{V}\|_V \tag{4.23b}$$

$$|c(\boldsymbol{U},\Phi)| \le \|\rho_0\|_\infty\,\|\boldsymbol{U}\|_V\,\|\Phi\|_F =: \|c\|\,\|\boldsymbol{U}\|_V\,\|\Phi\|_F\,. \tag{4.23c}$$

Using the trace theorem, we find out that the linear form $F_1(\cdot)$ is bounded as well:

$$|F_1(\boldsymbol{U})| \leq \|f\|_{2,\Gamma_2} \|\boldsymbol{U}\|_V \,. \tag{4.24}$$

To prove the boundedness of the linear form $F_2(\cdot)$, we must show that $\|\Phi\|_{2,\Gamma_2}$ is controlled by $\|\Phi\|_F$. First, we employ Lemma A.4, which in our case reads

$$\Phi \in F \Rightarrow \Phi \in L^6(\mathcal{R}^3) \quad \text{and} \quad \|\Phi\|_{6,\mathcal{R}^3} \leq \frac{2}{\sqrt{3}} \|\Phi\|_F \,. \tag{4.25}$$

We also need the inequality

$$\|\Phi\|_{2,\Theta} \leq |\Theta|^{\lambda} \|\Phi\|_{6,\Theta} \tag{4.26}$$

for an arbitrary bounded domain Θ, with $|\Theta|$ being its measure and λ a real constant. Combining the previous inequalities with the trace theorem, we get

$$\begin{aligned} \|\Phi\|_{2,\Gamma_2} \leq C(\|\Phi\|_{2,\Theta_2} + |\Phi|_{1,2,\Theta_2}) &\leq C\left(|\Theta_2|^{\lambda} \|\Phi\|_{6,\Theta_2} + |\Phi|_{1,2,\Theta_2}\right) \\ &\leq C\left(\frac{2}{\sqrt{3}} |\Theta_2|^{\lambda} + 1\right) \|\Phi\|_F \,, \end{aligned} \tag{4.27}$$

where the domain Θ_2 is any bounded locally lipschitzian domain such that it has Γ_2 as a boundary part. Employing this result in the definition of $F_2(\cdot)$, we conclude that it is, indeed, bounded:

$$|F_2(\Phi)| \leq C_2 \|f\|_{2,\Gamma_2} \|\Phi\|_F \,, \tag{4.28}$$

with C_2 being a positive real constant depending on the domain Θ_2.

The bilinear form $a(\cdot,\cdot)$ is V-elliptic under certain supplementary conditions. In order to prove it, we will make use of the following theorem (for proof and further details, see [15]):

Theorem 4.1 (Korn's inequality)
Let $\boldsymbol{U} \in V \equiv \left\{\boldsymbol{v} \in [W^{1,2}(\Omega)]^3 \,;\, \boldsymbol{v}\big|_{\Gamma_1} = 0\right\}$, *where* Γ_1 *is a non-empty set open with respect to* $\partial\Omega$. *Then there exists a constant* C_K *(depending on* Ω *and* Γ_1*) such that*

$$\int_\Omega \boldsymbol{\varepsilon}(\boldsymbol{U}) : \boldsymbol{\varepsilon}(\boldsymbol{U}) \, \mathrm{d}x \geq C_K \|\boldsymbol{U}\|_V^2 \,. \tag{4.29}$$

Under the assumption that the Lamé coefficients obey the inequalities

$$0 \leq \lambda(\boldsymbol{x}), \quad 0 < \mu_0 \leq \mu(\boldsymbol{x}) \qquad \text{a.e. in } \Omega, \tag{4.30}$$

the bilinear form $a(\cdot,\cdot)$ fulfills

$$a\left(\boldsymbol{U},\boldsymbol{U}\right)=\int_{\Omega}2\mu\,\boldsymbol{\varepsilon}(\boldsymbol{U}):\boldsymbol{\varepsilon}(\boldsymbol{U})\,\mathrm{d}x+\int_{\Omega}\lambda|\nabla\cdot\boldsymbol{U}|^{2}\,\mathrm{d}x\geq 2\mu_{0}\int_{\Omega}\boldsymbol{\varepsilon}(\boldsymbol{U}):\boldsymbol{\varepsilon}(\boldsymbol{U})\,\mathrm{d}x \quad (4.31)$$

or

$$a\left(\boldsymbol{U},\boldsymbol{U}\right)\geq 2\mu_{0}C_{K}\left\|\boldsymbol{U}\right\|_{V}^{2}\qquad\forall\boldsymbol{U}\in V. \quad (4.32)$$

The V-ellipticity of the bilinear form $a(\cdot,\cdot)$ is proved. The condition on λ is sufficient, not necessary.

From the ellipticity of the bilinear form $a(\cdot,\cdot)$ and the boundedness of the bilinear form $b(\cdot,\cdot)$, we see that the bilinear form $(a+b)(\cdot,\cdot)$ is also elliptic, under the condition

$$0<C_{ab}:=2\mu_{0}C_{K}-(1+\sqrt{3})\left\|\rho_{0}\right\|_{\infty}\left\|g_{0}\right\|_{1,\infty}. \quad (4.33)$$

In the rest of the proof, we will assume this condition to be met.

Step 2: Reformulation for the Lax-Milgram theorem
By summing Equations (4.20a) and (4.20b) we get an equivalent equation

$$\begin{aligned}a\left(\boldsymbol{u},\boldsymbol{U}\right)+b\left(\boldsymbol{u},\boldsymbol{U}\right)+\frac{1}{4\pi G}\left(\varphi_{1},\Phi\right)_{F}+c\left(\boldsymbol{u},\Phi\right)+c\left(\boldsymbol{U},\varphi_{1}\right)\\=F_{1}(\boldsymbol{U})+F_{2}(\Phi)\qquad\forall\boldsymbol{U}\in V,\ \forall\Phi\in F.\end{aligned} \quad (4.34)$$

Let us now introduce a space combining both the displacement and the potential

$$X=V\times F, \quad (4.35)$$

with the norm

$$\left\|(\boldsymbol{U},\Phi)\right\|_{X}=(\left\|\boldsymbol{U}\right\|_{V}^{2}+\left\|\Phi\right\|_{F}^{2})^{1/2},\qquad(\boldsymbol{U},\Phi)\in X. \quad (4.36)$$

The space X with the defined norm is evidently a Banach space.

Next, we can define a bilinear form representing the left hand side of the above equation:

$$\begin{aligned}&g:X\times X\to\mathcal{R},\ (\boldsymbol{U},\Phi)\in X,\ (\boldsymbol{V},\Psi)\in X,\\ &g\left((\boldsymbol{U},\Phi),(\boldsymbol{V},\Psi)\right)\equiv\\ &\quad a\left(\boldsymbol{U},\boldsymbol{V}\right)+b\left(\boldsymbol{U},\boldsymbol{V}\right)+\frac{1}{4\pi G}\left(\Phi,\Psi\right)_{F}+c\left(\boldsymbol{U},\Psi\right)+c\left(\boldsymbol{V},\Phi\right)\end{aligned} \quad (4.37)$$

and a linear form representing the right hand side:

$$K\big((\boldsymbol{U},\Phi)\big)\equiv F_{1}(\boldsymbol{U})+F_{2}(\Phi),\qquad(\boldsymbol{U},\Phi)\in X. \quad (4.38)$$

Now, Equation (4.34) or the equation system (4.20a), (4.20b) can be rewritten simply as

$$g\left((\boldsymbol{u},\varphi_1),Y\right)=K\big(Y\big)\qquad\forall Y\in X, \tag{4.39}$$

which is already applicable in the Lax-Milgram theorem. However, we must first prove some properties of the bilinear form $g(\cdot,\cdot)$ and the linear form $K(\cdot)$.

The linear form $K(\cdot)$ is bounded on the space X due to the boundedness of the linear forms $F_1(\cdot)$, $F_2(\cdot)$:

$$\begin{aligned}K\big((\boldsymbol{U},\Phi)\big)&\le\|f\|_{2,\Gamma_2}\|\boldsymbol{U}\|_V+C_2\|f\|_{2,\Gamma_2}\|\Phi\|_F\\&\le(1+C_2)\|f\|_{2,\Gamma_2}(\|\boldsymbol{U}\|_V^2+\|\Phi\|_F^2)^{1/2}.\end{aligned} \tag{4.40}$$

Similarly, owing to the boundedness of the bilinear forms $a(\cdot,\cdot)$, $b(\cdot,\cdot)$, $c(\cdot,\cdot)$, the bilinear form $g(\cdot,\cdot)$ is bounded by

$$\begin{aligned}g\left((\boldsymbol{U},\Phi),(\boldsymbol{V},\Psi)\right)&\le(\|a\|+\|b\|)(\|\boldsymbol{U}\|_V\|\boldsymbol{V}\|_V)+\frac{1}{4\pi G}\|\Phi\|_F\|\Psi\|_F\\&+\|c\|\left(\|\boldsymbol{U}\|_V\|\Psi\|_F+\|\boldsymbol{V}\|_V\|\Phi\|_F\right)\le\|g\|\left(\|\boldsymbol{U}\|_V^2+\|\Phi\|_F^2\right)^{1/2}(\|\boldsymbol{V}\|_V^2+\|\Psi\|_F^2)^{1/2},\end{aligned} \tag{4.41}$$

where

$$\|g\|:=\|a\|+\|b\|+\|c\|+\frac{1}{4\pi G}. \tag{4.42}$$

Finally, let us prove the X-ellipticity of the bilinear form $g(\cdot,\cdot)$. By putting $\boldsymbol{V}:=\boldsymbol{U}$, $\Psi:=\Phi$ in its definition (4.37), we get

$$g\left((\boldsymbol{U},\Phi),(\boldsymbol{U},\Phi)\right)=a\left(\boldsymbol{U},\boldsymbol{U}\right)+b\left(\boldsymbol{U},\boldsymbol{U}\right)+\frac{1}{4\pi G}\|\Phi\|_F^2+2c\left(\boldsymbol{U},\Phi\right). \tag{4.43}$$

Now, we make use of the V-ellipticity of the bilinear form $(a+b)(\cdot,\cdot)$ and of the boundedness of $c(\cdot,\cdot)$ to find the estimate

$$g\left((\boldsymbol{U},\Phi),(\boldsymbol{U},\Phi)\right)\ge C_{ab}\|\boldsymbol{U}\|_V^2+\frac{1}{4\pi G}\|\Phi\|_F^2-2\|\rho_0\|_\infty\|\boldsymbol{U}\|_V\|\Phi\|_F. \tag{4.44}$$

If it holds that

$$\|\rho_0\|_\infty^2<\frac{C_{ab}}{4\pi G}, \tag{4.45}$$

then the two non-negative (quadratic) terms overbalance the non-positive one using the simple inequality $a^2+b^2\ge 2ab$. Hence, we have shown the desired ellipticity:

$$g\left((\boldsymbol{U},\Phi),(\boldsymbol{U},\Phi)\right)\ge m_g(\|\boldsymbol{U}\|_V^2+\|\Phi\|_F^2)^{1/2}\qquad\forall(\boldsymbol{U},\Phi)\in X, \tag{4.46}$$

where m_g is a positive real constant and can be explicitly expressed as

$$m_g = \frac{1}{2}\left[C_{ab} + \frac{1}{4\pi G} - \sqrt{(C_{ab} - \frac{1}{4\pi G})^2 + 4\,\|\rho_0\|_\infty^2}\right]. \tag{4.47}$$

At this point, we can apply the Lax-Milgram theorem and, by summarizing all the required conditions, we have the following result:

Theorem 4.2 (Existence and uniqueness for the elastic problem)
Let the spaces V, F, P be defined by (4.13). Let the following conditions be met:

- $\mu, \lambda, \rho_0 \in L^\infty(\Omega), \quad g_0 \in W^{1,\infty}(\Omega), \quad f \in L^2(\Gamma_2)$
- $0 \leq \lambda(\boldsymbol{x}), \quad 0 < \mu_0 \leq \mu(\boldsymbol{x}) \qquad a.e.\ in\ \Omega$
- $0 < C_{ab} := 2\mu_0 C_K - (1+\sqrt{3})\,\|\rho_0\|_\infty\,\|g_0\|_{1,\infty}$
- $\|\rho_0\|_\infty^2 < \dfrac{C_{ab}}{4\pi G}$.

Then Problem (4.20) admits unique solutions $\boldsymbol{u}$, φ_1, $\boldsymbol{\tau}$. Furthermore, these solutions are continuously dependent on the boundary condition f.

4.3 Viscoelastic Problem

Next, we will derive the weak formulation of the viscoelastic problem, given by the equation system (3.4) and equipped with initial conditions (3.5), boundary conditions (3.6) and jump conditions (3.7). Since all of the equations but one are the same as in the case of the elastic problem, we will describe the weak formulation more briefly. The only differing equation is that of the Maxwell rheology:

$$\frac{\partial}{\partial t}\boldsymbol{\tau} - \frac{\partial}{\partial t}\left[\lambda(\nabla\cdot\boldsymbol{u})\boldsymbol{I} + 2\mu\,\boldsymbol{\varepsilon}(\boldsymbol{u})\right] + \frac{\mu}{\eta}\left[\boldsymbol{\tau} - K(\nabla\cdot\boldsymbol{u})\boldsymbol{I}\right] = 0, \tag{4.48}$$

where we recall that $K = \lambda + \frac{2}{3}\mu$.

We introduce an auxiliary tensor field $\boldsymbol{\sigma} = \boldsymbol{\sigma}(x,t)$, defined as

$$\boldsymbol{\sigma} = \boldsymbol{\tau} - \lambda(\nabla\cdot\boldsymbol{u})\boldsymbol{I} - 2\mu\,\boldsymbol{\varepsilon}(\boldsymbol{u}). \tag{4.49}$$

The tensor $\boldsymbol{\sigma}$ corresponds to the non-elastic part of the incremental stress tensor and is evidently symmetric. After substituting this definition into Equation (4.48), we get an equivalent formulation of the Maxwell rheology:

$$\dot{\boldsymbol{\sigma}} + \frac{\mu}{\eta}\boldsymbol{\sigma} + 2\frac{\mu^2}{\eta}\left[\boldsymbol{\varepsilon}(\boldsymbol{u}) - \frac{1}{3}(\nabla\cdot\boldsymbol{u})\boldsymbol{I}\right] = 0, \tag{4.50}$$

where the notation $\dot{\boldsymbol{\sigma}} = \frac{\partial}{\partial t}\boldsymbol{\sigma}$ was adopted and will be used hereafter. To formulate this equation ni the weak sense, we multiply it (using the double-dot product) by an arbitrary test function $\boldsymbol{\mathcal{S}} \in P$ and integrate it over Ω:

$$\int_\Omega \left[\dot{\boldsymbol{\sigma}} + \frac{\mu}{\eta}\boldsymbol{\sigma} + 2\frac{\mu^2}{\eta}\boldsymbol{\varepsilon}(\boldsymbol{u})\right] : \boldsymbol{\mathcal{S}} \,\mathrm{d}x - \int_\Omega \frac{2}{3}\,\frac{\mu^2}{\eta}(\nabla\cdot\boldsymbol{u})\,\mathrm{Tr}\,\boldsymbol{\mathcal{S}} \,\mathrm{d}x = 0 \qquad \forall \boldsymbol{\mathcal{S}} \in P \quad (4.51)$$

The weak formulation of Equation (4.49) relating $\boldsymbol{\sigma}$, $\boldsymbol{\tau}$ and $\boldsymbol{u}$ is obtained in a similar manner:

$$\int_\Omega \boldsymbol{\tau} : \boldsymbol{\mathcal{T}} \,\mathrm{d}x = \int_\Omega \boldsymbol{\sigma} : \boldsymbol{\mathcal{T}} \,\mathrm{d}x + \int_\Omega 2\mu\,\boldsymbol{\varepsilon}(\boldsymbol{u}) : \boldsymbol{\mathcal{T}} \,\mathrm{d}x + \int_\Omega \lambda(\nabla\cdot\boldsymbol{u})\,\mathrm{Tr}\,\boldsymbol{\mathcal{T}} \,\mathrm{d}x \qquad \forall \boldsymbol{\mathcal{T}} \in P \quad (4.52)$$

The weak formulation of the equilibrium equation (4.5) derived in the elastic problem formulation is valid in the present case as well, but this time we need to substitute for $\boldsymbol{\tau}$ from the definition (4.49):

$$\begin{aligned} &\int_\Omega 2\mu\,\boldsymbol{\varepsilon}(\boldsymbol{u}) : \boldsymbol{\varepsilon}(\boldsymbol{U}) \,\mathrm{d}x + \int_\Omega \lambda(\nabla\cdot\boldsymbol{u})(\nabla\cdot\boldsymbol{U}) \,\mathrm{d}x \\ &\qquad + \int_\Omega \boldsymbol{\sigma} : \boldsymbol{\varepsilon}(\boldsymbol{U}) \,\mathrm{d}x + \int_\Omega \rho_0 \nabla\varphi_1 \cdot \boldsymbol{U} \,\mathrm{d}x \\ &+ \int_\Omega \rho_0 \left[\nabla(g_0\boldsymbol{e}_z\cdot\boldsymbol{u}) - (\nabla\cdot\boldsymbol{u})g_0\boldsymbol{e}_z\right]\cdot\boldsymbol{U} \,\mathrm{d}x = \int_{\Gamma_2} f\,\boldsymbol{n}\cdot\boldsymbol{U} \,\mathrm{d}S \qquad \forall \boldsymbol{U} \in V \end{aligned} \quad (4.53)$$

The weak formulation of Poisson's equation remains unchanged from the elastic case, i.e. it is again (4.12).

The solutions $\boldsymbol{u}$, φ_1, $\boldsymbol{\tau}$ and $\boldsymbol{\sigma}$ will now be considered as mappings

$$\begin{aligned} &\boldsymbol{u} : [0,T] \to V, \qquad &&\varphi_1 : [0,T] \to F, \\ &\boldsymbol{\tau} : [0,T] \to P, \qquad &&\boldsymbol{\sigma} : [0,T] \to P. \end{aligned} \quad (4.54)$$

The test function spaces are chosen in the same way as for the elastic rheology, in addition, the space for $\boldsymbol{\mathcal{S}}$ is given,

$$\boldsymbol{U} \in V, \quad \boldsymbol{\mathcal{T}}, \boldsymbol{\mathcal{S}} \in P, \quad \Phi \in F. \quad (4.55)$$

The spaces for the coefficients also remain the same:

$$\mu, \lambda, \rho_0 \in L^\infty(\Omega), \quad g_0 \in W^{1,\infty}(\Omega), \quad f(t) \in L^2(\Gamma_2). \quad (4.56)$$

In fact, the space for f will be specified in a more precise way later on. Furthermore, a restriction for η is introduced

$$0 < \eta_0 \le \eta(\boldsymbol{x}) \quad \text{a.e. in } \Omega, \quad (4.57)$$

so that we have $\mu/\eta, \mu^2/\eta \in L^\infty(\Omega)$.

We will introduce an additional bilinear form, in order to put the equations into a more readable form:

$$e : V \times P \to \mathcal{R}, \quad e\,(\boldsymbol{U}, \boldsymbol{\mathcal{S}}) \equiv \int_\Omega 2\frac{\mu^2}{\eta}\boldsymbol{\varepsilon}(\boldsymbol{U}) : \boldsymbol{\mathcal{S}}\ \mathrm{d}x - \int_\Omega \frac{2}{3}\,\frac{\mu^2}{\eta}(\nabla \cdot \boldsymbol{U})\,\mathrm{Tr}\,\boldsymbol{\mathcal{S}}\ \mathrm{d}x. \tag{4.58}$$

The weak formulation of the viscoelastic problem can be summarized by the system of equations, holding for a.e. $t \in [0, T]$:

$$a\,(\boldsymbol{u}, \boldsymbol{U}) + b\,(\boldsymbol{u}, \boldsymbol{U}) + c\,(\boldsymbol{U}, \varphi_1) + (\boldsymbol{\sigma}, \boldsymbol{\varepsilon}(\boldsymbol{U}))_P = F_1(\boldsymbol{U}) \qquad \forall \boldsymbol{U} \in V \tag{4.59a}$$

$$\frac{1}{4\pi G}\,(\varphi_1, \Phi)_F + c\,(\boldsymbol{u}, \Phi) = F_2(\Phi) \qquad \forall \Phi \in F \tag{4.59b}$$

$$(\boldsymbol{\tau}, \boldsymbol{\mathcal{T}})_P - (\boldsymbol{\sigma}, \boldsymbol{\mathcal{T}})_P - d\,(\boldsymbol{u}, \boldsymbol{\mathcal{T}}) = 0 \qquad \forall \boldsymbol{\mathcal{T}} \in P \tag{4.59c}$$

$$(\dot{\boldsymbol{\sigma}}, \boldsymbol{\mathcal{S}})_P + \left(\frac{\mu}{\eta}\boldsymbol{\sigma}, \boldsymbol{\mathcal{S}}\right)_P + e\,(\boldsymbol{u}, \boldsymbol{\mathcal{S}}) = 0 \qquad \forall \boldsymbol{\mathcal{S}} \in P \tag{4.59d}$$

and the initial condition

$$\boldsymbol{\sigma}(\boldsymbol{x}, 0) = \boldsymbol{\sigma}_0(\boldsymbol{x}) \equiv \boldsymbol{\tau}_0(\boldsymbol{x}) - \lambda\,(\nabla \cdot \boldsymbol{u}_0(\boldsymbol{x}))\,\boldsymbol{I} - 2\mu\,\boldsymbol{\varepsilon}(\boldsymbol{u}_0(\boldsymbol{x})), \tag{4.60}$$

which is readily obtained from the definition of $\boldsymbol{\sigma}$ (4.49) and the initial conditions imposed on the incremental stress and the displacement.

It is interesting to remark that if we take the viscosity $\eta \to \infty$ and initial condition $\boldsymbol{\sigma}_0 = 0$, the problem will reduce to the equations of elasticity (4.20). This means that elasticity may be treated as a special case of viscoelasticity. More importantly, this allows us to consider certain regions of Ω as elastic and certain as viscoelastic without the need to develop a special theory for such a case.

4.4 Existence and Uniqueness of the Solution of the Viscoelastic Problem

First of all, it will be shown that Problem (4.59) can be simplified by resolving the three equations independent of time. The Galerkin method will be used to prove the existence and uniqueness of the remaining evolutionary problem, mainly following the proof performed by Evans [4] (section 7.1.2).

The solution $\boldsymbol{\sigma}$ will be approximated on finite dimensional subspaces of the solution space P using the Galerkin approximations. Next, it will be proved that such a sequence of solutions is bounded in a certain Bochner space and finally, we will show that the weak limit of the sequence is the sought solution.

Step 1: Reduction of the number of unknowns

Using the results obtained for the elastic problem, we will show that all the unknowns but $\boldsymbol{\sigma}$ can be eliminated from the system. In other words, they can be all explicitly expressed in terms of $\boldsymbol{\sigma}$.

We see that the equation system (4.59a), (4.59b) for the incremental potential and the displacement is very similar to that of the elastic problem. Thus, by summing the two equations and recalling the definition of the bilinear form $g(\cdot,\cdot)$ and the linear form $K(\cdot)$, we have an equivalent equation

$$g\left((\boldsymbol{u},\varphi_1),(\boldsymbol{U},\Phi)\right) = K\big((\boldsymbol{U},\Phi)\big) - (\boldsymbol{\sigma},\boldsymbol{\varepsilon}(\boldsymbol{U}))_P \qquad \forall(\boldsymbol{U},\Phi)\in X. \tag{4.61}$$

The right hand side represents a bounded linear form on the space X, because $K(\cdot)$ is bounded and so is the second term

$$|(\boldsymbol{\sigma},\boldsymbol{\varepsilon}(\boldsymbol{U}))_P| \le \|\boldsymbol{\sigma}\|_P \|U\|_V, \qquad \forall \boldsymbol{U}\in V, \tag{4.62}$$

provided that $\boldsymbol{\sigma}\in P$.

As already pointed out earlier, the bilinear form $g(\cdot,\cdot)$ is bounded and elliptic. Therefore, by virtue of the Lax-Milgram theorem, there exist unique solutions $\boldsymbol{u}$, φ_1 of Equation (4.61). These solutions are bounded by the right hand side terms through the inequality

$$(\|\boldsymbol{u}\|_V^2+\|\varphi_1\|_F^2)^{1/2} \le \frac{1}{m_g}(\|K\|_{X^*}+\|\boldsymbol{\sigma}\|_P) = \frac{1}{m_g}\left[(1+C_2)\,\|f\|_{2,\Gamma_2}+\|\boldsymbol{\sigma}\|_P\right], \tag{4.63}$$

where m_g is the ellipticity constant of the bilinear form $g(\cdot,\cdot)$.

Hence, for a fixed boundary condition f, there exists a continuous linear mapping $\mathcal{L}_f$ such that

$$\mathcal{L}_f : P\to V, \qquad \boldsymbol{u}=\mathcal{L}_f\boldsymbol{\sigma} \tag{4.64}$$

and $\boldsymbol{u}$, $\boldsymbol{\sigma}$ satisfy Equation (4.61).

Equation (4.59c) for $\boldsymbol{\tau}$ is explicit as in the case of the elastic problem. Furthermore, an upper bound similar to (4.21) can be found:

$$\|\boldsymbol{\tau}\|_P \le (2\,\|\mu\|_\infty + 3\,\|\lambda\|_\infty)\,\|\boldsymbol{u}\|_V + \|\boldsymbol{\sigma}\|_P, \tag{4.65}$$

where $\|\boldsymbol{u}\|_V$ is itself bounded by (4.63).

Thus, it suffices to deal with Equation (4.59d) for $\boldsymbol{\sigma}$, which, after the substitution from (4.64), reads

$$(\dot{\boldsymbol{\sigma}},\boldsymbol{\mathcal{S}})_P + \left(\frac{\mu}{\eta}\boldsymbol{\sigma},\boldsymbol{\mathcal{S}}\right)_P + e\,(\mathcal{L}_f\boldsymbol{\sigma},\boldsymbol{\mathcal{S}}) = 0 \qquad \forall\boldsymbol{\mathcal{S}}\in P, \tag{4.66}$$

plus the initial condition

$$\boldsymbol{\sigma}(\boldsymbol{x},0)=\boldsymbol{\sigma}_0(\boldsymbol{x}). \tag{4.67}$$

It is important to keep in mind that the linear operator $\mathcal{L}_f$ is time-dependent through the boundary condition $f=f(t)$.

Step 2: Galerkin approximations

The space $P \subset [L^2(\Omega)^{3\times 3}]$ is separable, hence we can choose a basis in it:

$$\{\boldsymbol{\mathcal{S}}_k\}_{k=1}^{\infty} \subset P \tag{4.68}$$

and this basis may be constructed as orthonormal in P.

The Galerkin approximations are the solutions of the projection of the evolutionary problem (4.66), (4.67) onto a finite dimensional space $P_N \equiv \text{span}\{\boldsymbol{\mathcal{S}}_k\}_{k=1}^{N}$. Therefore, they can be sought in the form

$$\boldsymbol{\sigma}^N(t) = \sum_{k=1}^{N} \alpha_k^N(t)\boldsymbol{\mathcal{S}}_k, \tag{4.69}$$

with $\boldsymbol{\sigma}^N : [0,T] \to P$ and $\alpha_k^N \in \mathcal{R},\ k = 1, ..., N$. By substituting the approximate solution $\boldsymbol{\sigma}^N$ into the initial condition (4.67) and into Equation (4.66), we obtain the initial value problem

$$\left(\boldsymbol{\sigma}^N(0), \boldsymbol{\mathcal{S}}\right)_P = (\boldsymbol{\sigma}_0, \boldsymbol{\mathcal{S}})_P \qquad \forall \boldsymbol{\mathcal{S}} \in P_N \tag{4.70a}$$

$$\left(\dot{\boldsymbol{\sigma}}^N, \boldsymbol{\mathcal{S}}\right)_P + \left(\frac{\mu}{\eta}\boldsymbol{\sigma}^N, \boldsymbol{\mathcal{S}}\right)_P + e\left(\mathcal{L}_f\boldsymbol{\sigma}^N, \boldsymbol{\mathcal{S}}\right) = 0 \qquad \forall \boldsymbol{\mathcal{S}} \in P_N. \tag{4.70b}$$

Let us show that this finite-dimensional problem admits a unique solution.

By substituting from the definition (4.69), putting the basis functions $\boldsymbol{\mathcal{S}}_j$ as test functions and taking into account the orthonormality of the chosen basis, we can rewrite the preceding problem as

$$\alpha_j^N(0) = (\boldsymbol{\sigma}_0, \boldsymbol{\mathcal{S}}_j)_P \qquad j = 1, ..., N \tag{4.71a}$$

$$\dot{\alpha}_j^N + \sum_{k=1}^{N} \alpha_k^N \left(\frac{\mu}{\eta}\boldsymbol{\mathcal{S}}_k, \boldsymbol{\mathcal{S}}_j\right)_P + \sum_{k=1}^{N} \alpha_k^N e\left(\mathcal{L}_f\boldsymbol{\mathcal{S}}_k, \boldsymbol{\mathcal{S}}_j\right) = 0 \qquad j = 1, ..., N. \tag{4.71b}$$

By defining

$$G_{jk} = \left(\frac{\mu}{\eta}\boldsymbol{\mathcal{S}}_k, \boldsymbol{\mathcal{S}}_j\right)_P, \qquad E_{jk} = e\left(\mathcal{L}_f\boldsymbol{\mathcal{S}}_k, \boldsymbol{\mathcal{S}}_j\right), \tag{4.72}$$

we can rewrite the linear ODE system (4.71b) in the matrix form

$$\dot{\boldsymbol{\alpha}}^N + \mathbb{G}\,\boldsymbol{\alpha}^N + \mathbb{E}(t)\boldsymbol{\alpha}^N = 0. \tag{4.73}$$

The matrices $\mathbb{G}$ and $\mathbb{E}$ satisfy Caratheodory's conditions, thus there exists a unique absolutely continuous function $\boldsymbol{\alpha}^N(t) = (\alpha_1^N(t), \ldots, \alpha_N^N(t))$ satisfying (4.71) locally. The global existence for a.e. $0 \le t \le T$ follows from linearity or from the energy estimates derived below. Hence, there exists a unique solution $\boldsymbol{u}^N$ to Problem (4.70).

Step 3: Energy estimates

Let us put $\boldsymbol{\mathcal{S}} := \boldsymbol{\sigma}^N$ as the test function in Equation (4.70b):

$$\left(\dot{\boldsymbol{\sigma}}^N, \boldsymbol{\sigma}^N\right)_P + \left(\frac{\mu}{\eta}\boldsymbol{\sigma}^N, \boldsymbol{\sigma}^N\right)_P + e\left(\mathcal{L}_f \boldsymbol{\sigma}^N, \boldsymbol{\sigma}^N\right) = 0. \tag{4.74}$$

Using the Hölder inequality and the inequalities

$$\|\mathrm{Tr}\,\boldsymbol{\mathcal{S}}\|_2^2 \leq 3\,\|\boldsymbol{\mathcal{S}}\|_2^2 \quad \forall \boldsymbol{\mathcal{S}} \in P, \qquad \|\nabla \cdot \boldsymbol{U}\|_2^2 \leq 3\,\|\nabla \boldsymbol{U}\|_2^2 \quad \forall \boldsymbol{U} \in V, \tag{4.75}$$

we show that the bilinear form $e(\cdot,\cdot)$ is bounded

$$e\left(\boldsymbol{U}, \boldsymbol{\mathcal{S}}\right) \leq 4 \left\| \frac{\mu^2}{\eta} \right\|_\infty \|\boldsymbol{U}\|_V \, \|\boldsymbol{\mathcal{S}}\|_P\,, \tag{4.76}$$

specially

$$\begin{aligned} e\left(\mathcal{L}_f \boldsymbol{\sigma}^N, \boldsymbol{\sigma}^N\right) &\leq \frac{4}{m_g} \left\| \frac{\mu^2}{\eta} \right\|_\infty \left\|\boldsymbol{\sigma}^N\right\|_P \left[(1+C_2)\,\|f\|_{2,\Gamma_2} + \left\|\boldsymbol{\sigma}^N\right\|_P\right] \\ &\leq \frac{2}{m_g} \left\| \frac{\mu^2}{\eta} \right\|_\infty \left[3\left\|\boldsymbol{\sigma}^N\right\|_P^2 + (1+C_2)^2\,\|f\|_{2,\Gamma_2}^2\right]. \end{aligned} \tag{4.77}$$

Considering that

$$0 \leq \frac{\mu(\boldsymbol{x})}{\eta(\boldsymbol{x})} \quad \text{a.e. in } \Omega, \tag{4.78}$$

we can estimate

$$0 \leq \left(\frac{\mu}{\eta}\boldsymbol{\sigma}^N, \boldsymbol{\sigma}^N\right)_P. \tag{4.79}$$

Finally, by making use of

$$\left(\dot{\boldsymbol{\sigma}}^N, \boldsymbol{\sigma}^N\right)_P = \frac{\mathrm{d}}{\mathrm{d}t}\left\|\boldsymbol{\sigma}^N\right\|_P^2, \tag{4.80}$$

we can use the above estimates and Equation (4.74) to get the inequality

$$\frac{\mathrm{d}}{\mathrm{d}t}\left\|\boldsymbol{\sigma}^N\right\|_P^2 \leq \frac{2}{m_g} \left\| \frac{\mu^2}{\eta} \right\|_\infty \left[3\left\|\boldsymbol{\sigma}^N\right\|_P^2 + (1+C_2)^2\,\|f\|_{2,\Gamma_2}^2\right]. \tag{4.81}$$

This inequality can be readily applied in the Gronwall's lemma, stated in the following form:

Lemma 4.3 *(Gronwall) Let $y(t), \alpha(t), \beta(t)$ be non-negative functions on $[0,T]$ such that*

$$\dot{y}(t) \leq \alpha(t)\; y(t) + \beta(t) \qquad \forall t \in (0,T). \tag{4.82}$$

Then

$$y(t) \leq e^{\int_0^t \alpha(s)\;\mathrm{d}s}\left[y(0) + \int_0^t \beta(s)\;\mathrm{d}s\right] \qquad \forall t \in (0,T). \tag{4.83}$$

In our case, this yields

$$\left\|\boldsymbol{\sigma}^N(t)\right\|_P^2 \leq e^{At}\left[\left\|\boldsymbol{\sigma}_0\right\|_P^2 + B\int_0^t \left\|f(s)\right\|_{2,\Gamma_2}^2 \,\mathrm{d}s\right] \quad \forall t \in (0,T), \tag{4.84}$$

where the constants A, B are defined as

$$A = 3B, \qquad B = \frac{2}{m_g}\left\|\frac{\mu^2}{\eta}\right\|_\infty (1+C_2)^2. \tag{4.85}$$

If we put T instead of t on the right hand side of (4.84), the value of the right hand side will not decrease, hence

$$\left\|\boldsymbol{\sigma}^N(t)\right\|_P^2 \leq e^{AT}\left[\left\|\boldsymbol{\sigma}_0\right\|_P^2 + B\left\|f\right\|_{L^2(0,T;L^2(\Gamma_2))}^2\right] \qquad \forall t \in (0,T). \tag{4.86}$$

By integrating this result with respect to t and using the assumption that

$$f \in L^2(0,T;L^2(\Gamma_2)), \tag{4.87}$$

we find out that the Galerkin approximations $\boldsymbol{\sigma}^N$ lie and are uniformly bounded in the space

$$\boldsymbol{\sigma}^N \in L^2(0,T;P) \qquad \forall N \in \mathcal{N}. \tag{4.88}$$

Let us now derive, in which space the function $\dot{\boldsymbol{\sigma}}^N$ lies. We take an arbitrary function $\boldsymbol{\mathcal{S}} \in P$, $\left\|\boldsymbol{\mathcal{S}}\right\|_P \leq 1$ and decompose it into two parts $\boldsymbol{\mathcal{S}} = \boldsymbol{\mathcal{S}}^o + \boldsymbol{\mathcal{S}}^\perp$, where $\boldsymbol{\mathcal{S}}^o \in P_N$ and $\left(\boldsymbol{\mathcal{S}}^\perp, \boldsymbol{\mathcal{S}}_k\right)_P = 0$, $k = 1, ..., N$. Since the functions $\{\boldsymbol{\mathcal{S}}_k\}_{k=1}^\infty$ are orthonormal, $\left\|\boldsymbol{\mathcal{S}}^o\right\| \leq \left\|\boldsymbol{\mathcal{S}}\right\| \leq 1$. Directly from Equation (4.70b) and from a slight modification of the previously derived estimate (4.77), we get the upper bound

$$\left|\left(\dot{\boldsymbol{\sigma}}^N, \boldsymbol{\mathcal{S}}\right)_P\right| \leq \left\|\frac{\mu}{\eta}\right\|_\infty \left\|\boldsymbol{\sigma}^N\right\|_P + \frac{4}{m_g}\left\|\frac{\mu^2}{\eta}\right\|_\infty \left[(1+C_2)\left\|f\right\|_{2,\Gamma_2} + \left\|\boldsymbol{\sigma}^N\right\|_P\right]. \tag{4.89}$$

The term on the left hand side represents the dual norm $\left\|\dot{\boldsymbol{\sigma}}^N\right\|_{P^*}$. By taking the square of the previous inequality, integrating it over $[0,T]$ and employing (4.86), we finally obtain

$$\int_0^T \left\|\dot{\boldsymbol{\sigma}}^N\right\|_{P^*}^2 \,\mathrm{d}t \leq C\left(\left\|\boldsymbol{\sigma}_0\right\|_P^2 + \left\|f\right\|_{L^2(0,T;L^2(\Gamma_2))}^2\right), \tag{4.90}$$

where C is a constant independent of N.

Thus, we have deduced that

$$\dot{\boldsymbol{\sigma}}^N \in L^2(0,T;P^*) = L^2(0,T;P) \quad \forall N \in \mathcal{N} \tag{4.91}$$

and that the approximations $\dot{\boldsymbol{\sigma}}^N$ are uniformly bounded in this space.

Step 4: Passing to weak limit

To find the solution of our evolutionary problem, we pass to the limit as $N \to \infty$. Since the sequence $\{\boldsymbol{\sigma}^N\}_{N=1}^{\infty}$ is bounded in the Bochner space $W^{1,2}(0,T;P)$, we can choose a weakly convergent subsequence $\boldsymbol{\sigma}^{N_l}$ such that

$$\boldsymbol{\sigma}^{N_l} \rightharpoonup \boldsymbol{\sigma} \qquad \text{in } W^{1,2}(0,T;P), \tag{4.92}$$

with $\boldsymbol{\sigma}$ denoting the corresponding weak limit and $\dot{\boldsymbol{\sigma}}$ being its weak time derivative.

Next, we choose a fixed integer M and a test function $\boldsymbol{\mathcal{V}} \in \mathcal{C}^1([0,T];P)$ having the form

$$\boldsymbol{\mathcal{V}}(t) = \sum_{k=1}^{M} \beta_k(t)\boldsymbol{\mathcal{S}}_k, \tag{4.93}$$

where β_k are given smooth functions. We put this test function in place of $\boldsymbol{\mathcal{S}}$ in Equation (4.70b) with $N \geq M$, and integrate the result over $[0,T]$:

$$\int_0^T \left[\left(\dot{\boldsymbol{\sigma}}^N, \boldsymbol{\mathcal{V}}\right)_P + \left(\frac{\mu}{\eta}\boldsymbol{\sigma}^N, \boldsymbol{\mathcal{V}}\right)_P + e\left(\mathcal{L}_f\boldsymbol{\sigma}^N, \boldsymbol{\mathcal{V}}\right)\right] \mathrm{d}t = 0. \tag{4.94}$$

By setting $N = N_l$ and then passing to the limit as $N_l \to \infty$, we obtain

$$\int_0^T \left[\left(\dot{\boldsymbol{\sigma}}, \boldsymbol{\mathcal{V}}\right)_P + \left(\frac{\mu}{\eta}\boldsymbol{\sigma}, \boldsymbol{\mathcal{V}}\right)_P + e\left(\mathcal{L}_f\boldsymbol{\sigma}, \boldsymbol{\mathcal{V}}\right)\right] \mathrm{d}t = 0. \tag{4.95}$$

By density argument, this equality holds for all $\boldsymbol{\mathcal{V}} \in \mathcal{L}^2(0,T;P)$. In particular, this yields

$$\left(\dot{\boldsymbol{\sigma}}, \boldsymbol{\mathcal{S}}\right)_P + \left(\frac{\mu}{\eta}\boldsymbol{\sigma}, \boldsymbol{\mathcal{S}}\right)_P + e\left(\mathcal{L}_f\boldsymbol{\sigma}, \boldsymbol{\mathcal{S}}\right) = 0 \qquad \text{for a.e. } t \in [0,T], \forall \boldsymbol{\mathcal{S}} \in P. \tag{4.96}$$

As a result, we have found the weak solution $\boldsymbol{\sigma} \in W^{1,2}(0,T;P)$ of Equation (4.66). According to [4], this implies that $\boldsymbol{\sigma} \in \mathcal{C}([0,T];P)$ and

$$\max_{0\leq t\leq T} \|\boldsymbol{\sigma}(t)\|_P \leq C\left(\|\boldsymbol{\sigma}_0\|_P^2 + \|f\|^2_{L^2(0,T;L^2(\Gamma_2))}\right), \tag{4.97}$$

which directly yields the uniqueness of the solution.

It remains to show that the initial condition (4.67) is fulfilled. We will now choose a test function $\boldsymbol{\mathcal{V}} \in \mathcal{C}^1([0,T];P)$ with $\boldsymbol{\mathcal{V}}(T) = 0$. Using integration by parts in (4.94), we get

$$\int_0^T \left[-\left(\boldsymbol{\sigma}^N, \dot{\boldsymbol{\mathcal{V}}}\right)_P + \left(\frac{\mu}{\eta}\boldsymbol{\sigma}^N, \boldsymbol{\mathcal{V}}\right)_P + e\left(\mathcal{L}_f\boldsymbol{\sigma}^N, \boldsymbol{\mathcal{V}}\right)\right] \mathrm{d}t + \left(\boldsymbol{\sigma}^N(0), \boldsymbol{\mathcal{V}}(0)\right)_P = 0. \tag{4.98}$$

Employing the discrete version of the initial condition (4.71a) and passing to the limit similarly as before, we find out that

$$\int_0^T \left[-\left(\boldsymbol{\sigma}, \dot{\boldsymbol{\mathcal{V}}}\right)_P + \left(\frac{\mu}{\eta}\boldsymbol{\sigma}, \boldsymbol{\mathcal{V}}\right)_P + e\left(\mathcal{L}_f\boldsymbol{\sigma}, \boldsymbol{\mathcal{V}}\right) \right] \mathrm{d}t + \left(\boldsymbol{\sigma}_0, \boldsymbol{\mathcal{V}}(0)\right)_P = 0. \tag{4.99}$$

On the other hand, integrating by parts (4.95), we have

$$\int_0^T \left[-\left(\boldsymbol{\sigma}, \dot{\boldsymbol{\mathcal{V}}}\right)_P + \left(\frac{\mu}{\eta}\boldsymbol{\sigma}, \boldsymbol{\mathcal{V}}\right)_P + e\left(\mathcal{L}_f\boldsymbol{\sigma}, \boldsymbol{\mathcal{V}}\right) \right] \mathrm{d}t + \left(\boldsymbol{\sigma}(0), \boldsymbol{\mathcal{V}}(0)\right)_P = 0. \tag{4.100}$$

Finally, subtracting the two preceding equations, we conclude that the initial condition is satisfied.

Step 5: Spaces for the other unknowns

In the end, let us occupy ourselves with the question, in what spaces the solutions $\boldsymbol{u}$, $\boldsymbol{\tau}$ and φ_1 lie. By virtue of the bounds (4.63), (4.65), we can easily show that under the assumption (4.87), the solutions obey

$$\boldsymbol{u} \in L^2(0,T;V), \quad \varphi_1 \in L^2(0,T;F), \quad \boldsymbol{\tau} \in L^2(0,T;P). \tag{4.101}$$

However, we have no estimate for the derivative, so to show that they are, in fact, continuous in time, we must use a different approach. We write the time-independent Equations (4.59a), (4.59b), (4.59c) for two times t_1 and t_2 and subtract the two systems, equation by equation, thus obtaining

$$a\left(\boldsymbol{u}(t_1) - \boldsymbol{u}(t_2), \boldsymbol{U}\right) + b\left(\boldsymbol{u}(t_1) - \boldsymbol{u}(t_2), \boldsymbol{U}\right) + c\left(\boldsymbol{U}, \varphi_1(t_1) - \varphi_1(t_2)\right) + \left(\boldsymbol{\sigma}(t_1) - \boldsymbol{\sigma}(t_2), \boldsymbol{\varepsilon}(\boldsymbol{U})\right)_P = 0 \tag{4.102a}$$

$$\frac{1}{4\pi G}\left(\varphi_1(t_1) - \varphi_1(t_2), \Phi\right)_F + c\left(\boldsymbol{u}(t_1) - \boldsymbol{u}(t_2), \Phi\right) = 0 \tag{4.102b}$$

$$\left(\boldsymbol{\tau}(t_1) - \boldsymbol{\tau}(t_2), \boldsymbol{\mathcal{T}}\right)_P - \left(\boldsymbol{\sigma}(t_1) - \boldsymbol{\sigma}(t_2), \boldsymbol{\mathcal{T}}\right)_P - d\left(\boldsymbol{u}(t_1) - \boldsymbol{u}(t_2), \boldsymbol{\mathcal{T}}\right) = 0 \tag{4.102c}$$

holding for all $\boldsymbol{U} \in V$, $\Phi \in F$, $\boldsymbol{\mathcal{T}} \in P$. By using the previously derived bounds for the solutions, but keeping in mind that now we have a case corresponding to $f(t) = 0$, we get the bounds

$$\left\|\boldsymbol{u}(t_1) - \boldsymbol{u}(t_2)\right\|_V \leq K_1 \left\|\boldsymbol{\sigma}(t_1) - \boldsymbol{\sigma}(t_2)\right\|_P \tag{4.103a}$$

$$\left\|\varphi_1(t_1) - \varphi_1(t_2)\right\|_F \leq K_2 \left\|\boldsymbol{\sigma}(t_1) - \boldsymbol{\sigma}(t_2)\right\|_P \tag{4.103b}$$

$$\left\|\boldsymbol{\tau}(t_1) - \boldsymbol{\tau}(t_2)\right\|_P \leq K_3 \left\|\boldsymbol{\sigma}(t_1) - \boldsymbol{\sigma}(t_2)\right\|_P \ , \tag{4.103c}$$

with constants K_1, K_2, K_3 independent of time. Considering that $\boldsymbol{\sigma} \in \mathcal{C}([0,T];P)$, we immediately have

$$\boldsymbol{u} \in \mathcal{C}([0,T];V), \quad \varphi_1 \in \mathcal{C}([0,T];F), \quad \boldsymbol{\tau} \in \mathcal{C}([0,T];P). \tag{4.104}$$

Bounds in these spaces similar to (4.97) can be easily derived.

We have constructively proved the following theorem:

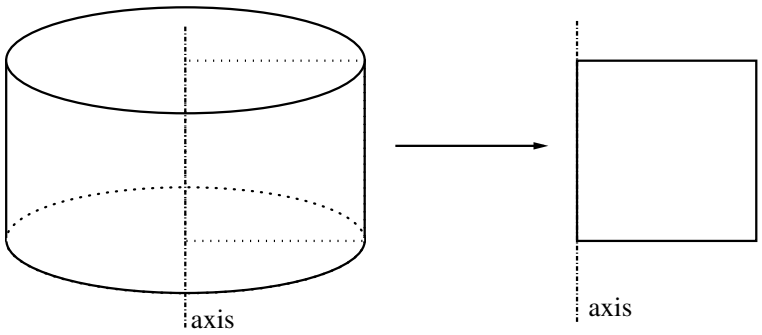

Fig. 3: Transformation of the 3D cylindrical domain to the 2D rectangular domain

Theorem 4.4 (Existence and uniqueness for the viscoelastic problem) *Assume that the same conditions as in the case of the elastic problem hold. In addition, let*

- $f \in L^2\left(0,T;L^2(\Gamma_2)\right)$
- $\boldsymbol{u}_0 \in V, \quad \boldsymbol{\tau}_0 \in P$
- $\exists \eta_0 : \quad 0 < \eta_0 \leq \eta(\boldsymbol{x}) \quad$ *a.e. in* Ω.

Then Problem (4.59) admits unique solutions $\boldsymbol{u}$, φ_1, $\boldsymbol{\tau}$, $\boldsymbol{\sigma}$ *lying in the spaces*

$$\boldsymbol{\sigma} \in \mathcal{C}([0,T];P),\ \boldsymbol{u} \in \mathcal{C}([0,T];V),\ \varphi_1 \in \mathcal{C}([0,T];F),\ \boldsymbol{\tau} \in \mathcal{C}([0,T];P). \qquad (4.105)$$

Furthermore, these solutions are continuously dependent on the initial conditions $\boldsymbol{u}_0$, $\boldsymbol{\tau}_0$ *and the boundary condition* f.

5 Formulation in Cylindrical Coordinates

So far, we have made very few assumptions concerning the studied domain and the imposed boundary condition f. From this section on, however, we put the general 3D problem aside and concentrate on the special case of a cylindrical domain with a cylindrically symmetric vertical load. A schematical drawing of such a domain was shown on Figure 2. Since the problem possesses cylindrical symmetry, it can be reduced to a pseudo-twodimensional problem. As a result, it suffices to solve the given problem on a 2D domain, a rectangle, which produces the cylinder when it is revolved around one of its sides. This side represents the axis of the symmetry. The situation is depicted on Figure 3.

Solving the 2D problem rather than the full 3D problem greatly reduces the complexity of the problem and hence also the computational time necessary for a simulation. However, the equations must first be rewritten into cylindrical coordinates. Owing to the cylindrical symmetry of the problem, many of the terms will fortunately drop out.

5.1 Displacement, Stress and Strain Components

We consider the cylindrical coordinate system with the radial coordinate r, the azimuthal coordinate φ and the vertical coordinate z, with $\boldsymbol{e}_r$, $\boldsymbol{e}_\varphi$, $\boldsymbol{e}_z$ denoting the corresponding unit vectors.

In such a coordinate system, the divergence of a vector field $\boldsymbol{w}$ can be written as

$$\nabla \cdot \boldsymbol{w} = \frac{\partial w_r}{\partial r} + \frac{w_r}{r} + \frac{1}{r}\frac{\partial w_\varphi}{\partial \varphi} + \frac{\partial w_z}{\partial z} \tag{5.1}$$

and the gradient of a scalar field V is given by the formula

$$\nabla V = \frac{\partial V}{\partial r}\ \boldsymbol{e}_r + \frac{1}{r}\frac{\partial V}{\partial \varphi}\ \boldsymbol{e}_\varphi + \frac{\partial V}{\partial z}\ \boldsymbol{e}_z. \tag{5.2}$$

In the case of cylindrical symmetry, these formulae become:

$$\nabla \cdot \boldsymbol{w} = \frac{\partial w_r}{\partial r} + \frac{w_r}{r} + \frac{\partial w_z}{\partial z} \tag{5.3}$$

$$\nabla V = \frac{\partial V}{\partial r}\ \boldsymbol{e}_r + \frac{\partial V}{\partial z}\ \boldsymbol{e}_z. \tag{5.4}$$

The physical components of the small strain tensor are in the cylindrical coordinates given by the relations

$$\begin{aligned} \varepsilon_{rr} &= \frac{\partial u_r}{\partial r}, & \varepsilon_{rz} &= \frac{1}{2}\left(\frac{\partial u_z}{\partial r} + \frac{\partial u_r}{\partial z}\right), \\ \varepsilon_{\varphi\varphi} &= \frac{1}{r}\frac{\partial u_\varphi}{\partial \varphi} + \frac{u_r}{r}, & \varepsilon_{r\varphi} &= \frac{1}{2}\left(\frac{\partial u_\varphi}{\partial r} + \frac{1}{r}\frac{\partial u_r}{\partial \varphi} - \frac{u_\varphi}{r}\right), \\ \varepsilon_{zz} &= \frac{\partial u_z}{\partial z}, & \varepsilon_{\varphi z} &= \frac{1}{2}\left(\frac{\partial u_\varphi}{\partial z} + \frac{1}{r}\frac{\partial u_z}{\partial \varphi}\right). \end{aligned} \tag{5.5}$$

Considering the cylindrical symmetry of the given problem, we have

$$u_\varphi = 0, \quad \frac{\partial u_r}{\partial \varphi} = \frac{\partial u_z}{\partial \varphi} = 0 \tag{5.6}$$

and the small strain tensor components are simplified to

$$\begin{aligned} \varepsilon_{rr} &= \frac{\partial u_r}{\partial r}, & \varepsilon_{rz} &= \frac{1}{2}\left(\frac{\partial u_z}{\partial r} + \frac{\partial u_r}{\partial z}\right), \\ \varepsilon_{\varphi\varphi} &= \frac{u_r}{r}, & \varepsilon_{r\varphi} &= \varepsilon_{\varphi z} = 0, \\ \varepsilon_{zz} &= \frac{\partial u_z}{\partial z}. \end{aligned} \tag{5.7}$$

Using Hooke's law or the formula describing the Maxwell rheology, one can deduce that the stress tensor components obey

$$\tau_{r\varphi} = \tau_{\varphi z} = 0. \tag{5.8}$$

The other stress tensor components are generally non-zero. From the definition of $\boldsymbol{\sigma}$ it is clear that similar relations hold for $\boldsymbol{\sigma}$ as well.

Thus, in the case of cylindrical symmetry, the problem is reduced to the scalar incremental gravitational potential, two non-zero components for the displacement field and four non-zero components for both the stress and the $\boldsymbol{\sigma}$ field, giving 11 unknowns altogether.

5.2 Weak Formulation of the Problems

Next, we proceed to the weak formulations of a cylindrically symmetric elastic and viscoelastic problem.

The weak formulations (4.20), (4.59) remain essentialy unchanged, we only need to explicitly write out all the bilinear forms

$$a(\boldsymbol{u}, \boldsymbol{U}) = \int_{Z_1}^{Z_2}\int_{0}^{R} \lambda \left(\frac{\partial u_r}{\partial r} + \frac{u_r}{r} + \frac{\partial u_z}{\partial z}\right)\left(\frac{\partial U_r}{\partial r} + \frac{U_r}{r} + \frac{\partial U_z}{\partial z}\right) r \,\mathrm{d}r \,\mathrm{d}z \tag{5.9}$$

$$+ \int_{Z_1}^{Z_2}\int_{0}^{R} 2\mu \left[\frac{\partial u_r}{\partial r}\frac{\partial U_r}{\partial r} + \frac{u_r U_r}{r^2} + \frac{\partial u_z}{\partial z}\frac{\partial U_z}{\partial z} + \frac{1}{2}\left(\frac{\partial u_z}{\partial r} + \frac{\partial u_r}{\partial z}\right)\left(\frac{\partial U_z}{\partial r} + \frac{\partial U_r}{\partial z}\right)\right] r \,\mathrm{d}r \,\mathrm{d}z$$

$$b(\boldsymbol{u}, \boldsymbol{U}) = \int_{Z_1}^{Z_2}\int_{0}^{R} \left[\rho_0 g_0 \left(\frac{\partial u_z}{\partial r}U_r - \frac{\partial u_r}{\partial r}U_z - \frac{u_r}{r}U_z\right) + \rho_0 u_z U_z \frac{\mathrm{d}g_0}{\mathrm{d}z}\right] r \,\mathrm{d}r \,\mathrm{d}z \tag{5.10}$$

$$c(\boldsymbol{u}, \Phi) = \int_{Z_1}^{Z_2}\int_{0}^{R} \rho_0 \left(\frac{\partial \Phi}{\partial r}u_r + \frac{\partial \Phi}{\partial z}u_z\right) r \,\mathrm{d}r \,\mathrm{d}z \tag{5.11}$$

$$d(\boldsymbol{u}, \boldsymbol{\mathcal{T}}) = \int_{Z_1}^{Z_2}\int_{0}^{R} 2\mu \left[\frac{\partial u_r}{\partial r}T_{rr} + \frac{u_r}{r}T_{\varphi\varphi} + \frac{\partial u_z}{\partial z}T_{zz} + \left(\frac{\partial u_r}{\partial z} + \frac{\partial u_z}{\partial r}\right)T_{rz}\right] r \,\mathrm{d}r \,\mathrm{d}z \tag{5.12}$$

$$+ \int_{Z_1}^{Z_2}\int_{0}^{R} \lambda \left(\frac{\partial u_r}{\partial r} + \frac{u_r}{r} + \frac{\partial u_z}{\partial z}\right)(T_{rr} + T_{\varphi\varphi} + T_{zz})\, r \,\mathrm{d}r \,\mathrm{d}z$$

$$e\,(\boldsymbol{u},\boldsymbol{\mathcal{S}}) \equiv \int_{Z_1}^{Z_2}\int_{0}^{R} 2\frac{\mu^2}{\eta}\left[\frac{\partial u_r}{\partial r}S_{rr} + \frac{u_r}{r}S_{\varphi\varphi} + \frac{\partial u_z}{\partial z}S_{zz} + \left(\frac{\partial u_r}{\partial z} + \frac{\partial u_z}{\partial r}\right)S_{rz}\right] r\ \mathrm{d}r\ \mathrm{d}z \tag{5.13}$$

$$-\int_{Z_1}^{Z_2}\int_{0}^{R} \frac{2}{3}\ \frac{\mu^2}{\eta}\left(\frac{\partial u_r}{\partial r} + \frac{u_r}{r} + \frac{\partial u_z}{\partial z}\right)(S_{rr} + S_{\varphi\varphi} + S_{zz})\, r\ \mathrm{d}r\ \mathrm{d}z,$$

scalar products

$$(\boldsymbol{\tau},\boldsymbol{\mathcal{T}})_P = \int_{Z_1}^{Z_2}\int_{0}^{R} (\tau_{rr}T_{rr} + \tau_{\varphi\varphi}T_{\varphi\varphi} + \tau_{zz}T_{zz} + 2\ \tau_{rz}T_{rz})\, r\ \mathrm{d}r\ \mathrm{d}z \tag{5.14}$$

$$(\varphi_1,\Phi)_F = \int_{-\infty}^{+\infty}\int_{0}^{+\infty}\left(\frac{\partial\varphi_1}{\partial r}\,\frac{\partial\Phi}{\partial r} + \frac{\partial\varphi_1}{\partial z}\,\frac{\partial\Phi}{\partial z}\right) r\ \mathrm{d}r\ \mathrm{d}z \tag{5.15}$$

and linear forms

$$F_1(\boldsymbol{U}) \equiv \int_{0}^{R} f(r)\, U_z\, r\ \mathrm{d}r \tag{5.16}$$

$$F_2(\Phi) \equiv \int_{0}^{R} \frac{f(r)}{g_R}\,\Phi\, r\ \mathrm{d}r \tag{5.17}$$

in cylindrical coordinates.

The 2D domain corresponding to Ω as well as the boundary parts corresponding to Γ_1 and Γ_2 will still be denoted by the same symbols. By performing the transformation to the 2D rectangular domain, we have obtained a fictitious boundary at $r = 0$, which will be denoted Γ_3. The displacement field is physically acceptable only if the condition

$$u_r = 0 \qquad \text{at} \quad r = 0 \tag{5.18}$$

is met. In the weak formulation, it is satisfied by choosing an appropriate solution space for the displacement. The forces due to the stress acting at the axis $r = 0$ are cynlindrically symmetric only if

$$\tau_{rz} = 0 \qquad \text{at} \quad r = 0. \tag{5.19}$$

However, this stress condition applies only in the classical formulation.

It is evident, that the previously derived existence and uniqueness results hold in the case of cylindrical symmetry as well, since it is only a special case of the general problem. Nevertheless, it would require a more precise notion of the solution spaces in such case and we do not intend to go into details here.

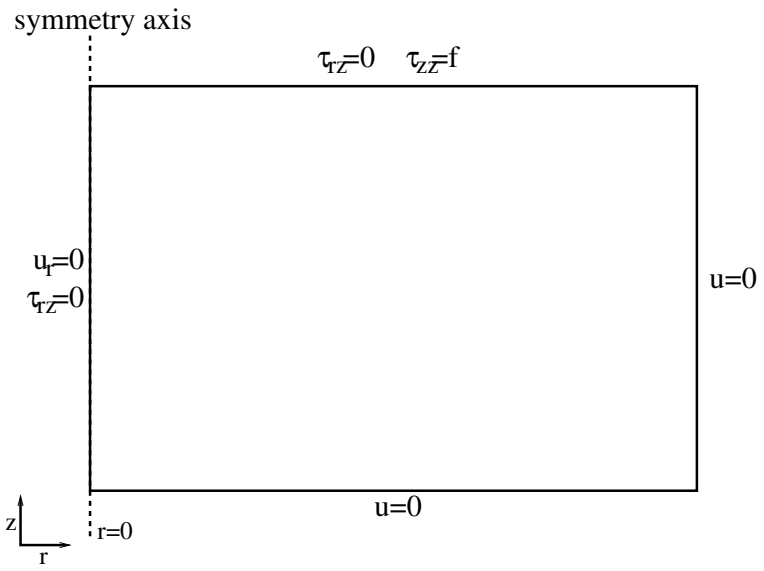

Fig. 4: Boundary conditions imposed in the 2D problem (classical formulation)

6 Numerical Approach

For the numerical calculations, we adopted the so-called Cowling approximation, which means that the effect of the incremental gravitational potential is completely neglected. There are several reasons for doing this. First of all, the complexity of the associated problem is much higher than for the remaining unknowns. Methods for solving such problems on unbounded domains are known, e.g. the infinite element method [23] or the better-known boundary element method (BEM). The weak formulation of Poisson's equation derived in the present work is readily usable for the infinite element method, whereas for BEM it has to be done using a different approach. However, practical implementation of these methods in the adopted FEM code would be very difficult and time-consuming. Furthermore, the values of the incremental gravitational potential itself are of very little interest in the postglacial rebound studies. The effect of the Cowling approximation has been studied e.g. in [19]. For local problems it is reasonable to leave the incremental gravitational potential out.

It might seem that the stress tensor components could be calculated a posteriori, because it is given explicitly and doesn't appear in the other equations. However, the results obtained using such an approach were deteriorated, most likely due to the discontinuities in the Lamé coefficients. This retrospectively confirms the necessity to include the stress in the weak formulation.

6.1 Time Discretization

The standard θ-scheme with an automatic time step control was used for the time discretization. For $\theta = 0$, the scheme corresponds to the forward Euler scheme, for $\theta = 1$ to the backward Euler scheme and for $\theta = 0.5$ to the Crank-Nicolson scheme.

The considered time interval $(0, T)$ will be divided into time steps $0 = t^0 < t^1 < ... < t^n = T$. We will denote the time-step size $\Delta t^i = t^{i+1} - t^i$. Equation (4.59d) describing the Maxwell rheology is the only equation involving a time derivative. Using the θ-scheme, we can proceed from the time layer t^i to the next time layer t^{i+1} by

$$\left(\frac{\boldsymbol{\sigma}^{i+1} - \boldsymbol{\sigma}^i}{\Delta t^i}, \boldsymbol{\mathcal{S}}\right)_P + \left(\frac{\mu}{\eta}[\theta\boldsymbol{\sigma}^{i+1} + (1-\theta)\boldsymbol{\sigma}^i], \boldsymbol{\mathcal{S}}\right)_P + e\left(\theta\boldsymbol{u}^{i+1} + (1-\theta)\boldsymbol{u}^i, \boldsymbol{\mathcal{S}}\right) = 0, \tag{6.1}$$

which can be rewritten in the form

$$\begin{aligned}\left(\boldsymbol{\sigma}^{i+1}, \boldsymbol{\mathcal{S}}\right)_P + A\ \left(\frac{\mu}{\eta}\boldsymbol{\sigma}^{i+1}, \boldsymbol{\mathcal{S}}\right)_P + A\ e\left(\boldsymbol{u}^{i+1}, \boldsymbol{\mathcal{S}}\right) = \\ = \left(\boldsymbol{\sigma}^i, \boldsymbol{\mathcal{S}}\right)_P - B\ \left(\frac{\mu}{\eta}\boldsymbol{\sigma}^i, \boldsymbol{\mathcal{S}}\right)_P - B\ e\left(\boldsymbol{u}^i, \boldsymbol{\mathcal{S}}\right),\end{aligned} \tag{6.2}$$

where we have defined $A = \theta.\Delta t^i$, $B = (1-\theta).\Delta t^i$.

The time step error control is accomplished in the following way [20]. Let us suppose that the solution vector x^i at time t^i is known. First, the solution at time t^{i+1} is calculated in a single time step. We denote this solution $\tilde{x}^{i+1}$. Next, a time step of size $\Delta t^i/2$ starting at t^i is performed and the solution is denoted $x^{i+\frac{1}{2}}$. Then we perform another time step of size $\Delta t^i/2$ starting at $t^{i+\frac{1}{2}}$ and denote the solution x^{i+1}. One such time step is depicted on Figure 5. By taking a suitable norm of the difference of solutions x^{i+1} and $\tilde{x}^{i+1}$, we obtain an error indicator, which we want to be roughly equal to the prescribed tolerance,

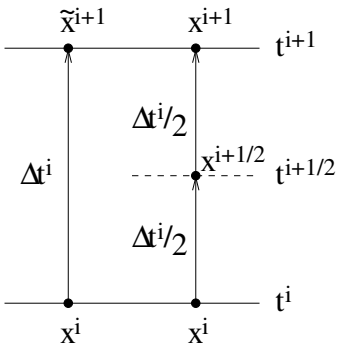

Fig. 5: Time-step for error control

$$\left\|x^{i+1} - \tilde{x}^{i+1}\right\| \approx \mathrm{TOL}. \tag{6.3}$$

If the error is too large, we redo the last time step with a smaller step size, otherwise we consider x^{i+1} to be the correct solution.

To estimate the optimal size for the following time step, we adopt a well-known formula from the numerical methods for ODR:

$$\Delta t^{i+1} = \Delta t^i.\left(\frac{TOL}{\left\|x^{i+1} - \tilde{x}^{i+1}\right\|}\right)^{p+1}, \tag{6.4}$$

Fig. 6: The elements used and their degrees of freedom

where p is the order of the used time stepping scheme (for the Euler schemes $p = 1$, for the Crank-Nicolson scheme $p = 2$).

It remains to discuss, which of the presented schemes is the best for the problem at hand. The forward Euler has the advantage of being explicit, so the time needed to calculate one time-step is smaller. However, explicit schemes are known to have only conditional stability. Furthermore, both Euler schemes have the disadvantage of being only first order methods. The backward Euler scheme is known to perform very well for stiff problems and the problem at hand was expected to exhibit a certain degree of stiffness. None the less, all three methods were tried and it was found out that the Crank-Nicolson scheme performs most efficiently, while the forward Euler scheme proved to be practically unusable, because the stability domain is not known. The backward Euler scheme gave similar results as the Crank-Nicolson scheme. However, significantly smaller time-steps were necessary in the case of the backward Euler scheme.

6.2 Space Discretization

The space discretization is performed using the finite element method. The shape of the used elements is quadrilateral. The domain Ω is covered by a set of elements $\mathcal{T}_h$. The set of the nodes lying on the boundary part Γ_1, Γ_2, Γ_3 will be denoted G_1, G_2, G_3, respectively.

Let us introduce the following finite element spaces:

$$V_h \equiv \Big\{ \boldsymbol{v} \in [\mathcal{C}(\Omega)]^2 ; v_i\big|_T \in Q_2(T)\ \forall T \in \mathcal{T}_h, i = r, z; \quad (6.5)$$
$$\boldsymbol{v}(N) = 0\ \forall N \in G_1; v_r(N) = 0\ \forall N \in G_3 \Big\}$$
$$P_h \equiv \Big\{ \boldsymbol{p} \in \left[L^2(\Omega)\right]^4 ; p_i\big|_T \in P_1(T)\ \forall T \in \mathcal{T}_h, i = rr, \varphi\varphi, zz, rz \Big\}, \quad (6.6)$$

i.e. continuous biquadratic elements are used for the displacement field and discontinuous linear elements for the stress and $\boldsymbol{\sigma}$ fields. Figure 6 schematically shows the degrees of freedom of the used elements. The presented choice of the finite element spaces results in 42 degrees of freedom on one element. Considering the adjacency of the elements, it averages to 32 degrees of freedom per element.

In theory, approximation using bilinear elements for the space V and piecewise constant elements for the space P should be sufficient. However, this choice lead to

a problem with the upper-most node at the axis of symmetry. This node exhibited zero displacement in both directions, although the vertical displacement should be non-zero, since there is some force applied to the node. A possible explanation of this phenomenon is that in the weak formulation, the acting force is multiplied by the radius r. At the axis of symmetry $r = 0$, so the node reacts as if no forces were acting on it. This problem does not appear with biquadratic elements.

6.3 Practical Implementation

The numerical calculations were performed using an adaptation of a Navier–Stokes code programmed by Dr. Jaroslav Hron. The capabilities of this code were the main reason for several aspects of the numerical methods used, e.g. the choice of the time-stepping technique, the shape of the elements and so on.

Primarily, it was necessary to replace the Navier–Stokes equations with our system of equations, choose the element spaces and input the boundary condition. Since the Navier–Stokes equations are essentially non-linear, whereas our equation system is linear, certain changes were made to improve the efficiency for the linear case. The adaptive time-stepping algorithm was already included in the code, slight modifications were necessary, however. The GMRES method with ILU preconditioning included in the *splib* solver package was used as the linear solver.

The output of the simulations are data files including the values of the unknowns and other predefined quantities at all the time levels. These files can be visualized using the freely available *GMV* software [6]. It is also possible to generate movies of the time evolution using the *gmvmpeg* tool [7] developed for the *Featflow* software. Although the use of these readily available post-processing tools saved an immense amount of time, it lead to certain drawbacks. For example, it was impossible to include the glacier shape as well as the time dependence of the boundary condition in the movies. Also the boundaries between the domains with different viscosity could not be visualized in the graphs. Especially the latter fact made the analysis of the results significantly more difficult.

It was necessary to program some additional pre- and post-processing tools, e.g. a simple mesh generator, a program for calculating the dissipation rate over the whole domain, etc.

7 Geophysical Models

In this section, the various geophysical components of the simulations will be presented, namely all the geophysical quantities appearing as coefficients in the equations and the surface load. While the values of the initial density, the initial gravitational acceleration and the Lamé coefficients are generally assumed to be well-

determined and only vertically-dependent, the viscosity distributions widely vary from area to area and depend on the horizontal direction as well. Thus, several viscosity distributions will be considered. The surface load is given by the shape and size of the glacier present on the Earth's surface. The load may be time-dependent.

7.1 PREM

The Preliminary Reference Earth Model (PREM), presented in [3], is used as a widely-accepted standard for the description of the depth variation of seismic velocities (shear and compressional) and the density, based on seismological data. The Earth is separated into 13 spherical layers and the above mentioned physical quantities are approximated by polynomials of at most 3rd degree in each of the layers. The table in Appendix B gives the polynomials as functions of the normalized radius $\alpha = z/R_E$, where R_E is the Earth's radius. The resulting density is in g/cm^3 and the velocities in km/s. In our case we left the upper-most (ocean) layer out and expanded the upper crust layer all the way up to 6371 km.

Once knowing the seismic velocities and the density, values of other quantities can be derived. The values of the Lamé coefficients are obtained from

$$v_S^2 = \frac{\mu}{\rho}, \qquad v_P^2 = \frac{\lambda + 2\mu}{\rho}. \tag{7.1}$$

The depth variation of the gravitational acceleration can be calculated as

$$g(z) = \frac{4\pi G}{z^2} \int_0^z \rho(\xi)\xi^2 \, \mathrm{d}\xi, \tag{7.2}$$

from which it easily follows that the gradient of the gravitational potential obeys

$$\nabla g(z) = \left(4\pi G\rho(z) - \frac{2}{z} g(z) \right) \boldsymbol{e}_z. \tag{7.3}$$

The graphs of the depth-variations of these quantities can be found in Appendix B.

7.2 Glacier Models

In all the simulations performed, we assumed a glacier of constant radius, only the thickness (height) was allowed to vary in time. Two different shapes of glacier were used in the calculations—the rectangular and the parabolic profile depicted on Figure 7. The dependence of the glacier's thickness on the distance from the axis of symmetry r is in the case of the parabolic profile given by the formula

$$h(r) = h_{max} \cdot \sqrt{1 - r/r_{max}}, \tag{7.4}$$

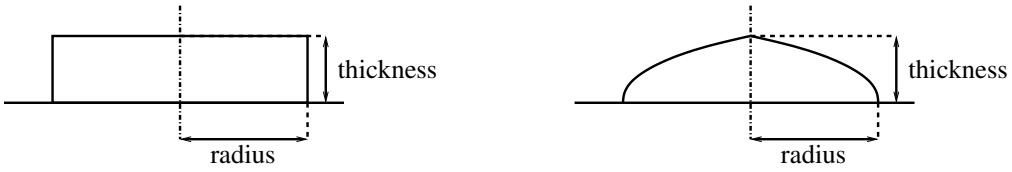

(a) Rectangular (b) Parabolic

Fig. 7: The considered glacier profiles

where r_{max} is the glacier's radius and h_{max} is the thickness in the glacier's center at the time of the glacial maximum. It is interesting to observe, that the parabolic glacier meets the Earth's surface at right angle and has a sharp peak.

The surface load due to the glacier's presence can be calculated as

$$f(r,t) = \rho_g \,.\, g_R \,.\, h(r) \,.\, l(t), \tag{7.5}$$

where the glacier's density was taken to be $\rho_g = 1000$ kg/m^3 and the gravitational acceleration at the Earth's surface g_R was computed from PREM. The loading history function $l(t)$ will be discussed separately.

Apart from the Benchmark model, we always took the parameters of the Scandinavian glacier, $h_{max} = 2.5$ km, $r_{max} = 890$ km.

7.3 Loading History

Three different models for the loading history were considered. Heaviside loading, a simple saw-tooth glaciation cycle and a realistic glaciation cycle. The two latter loading histories are graphed on Figure 8.

The Heaviside loading corresponds to the situation, where there is initially no surface load present and the glacier appears instantaneously with the maximum thickness. This is modeled by calculating the elastic response to the glacier's presence and then taking the result as the initial condition for a viscoelastic simulation.

Evidence shows that in the past million years there were glaciation cycles, each of duration approximately 100 kyrs (kyrs = 1000 years). A simple saw-tooth model for a glaciation cycle was proposed in [21]. The glacier's thickness starts from zero and linearly grows to the maximum, which is achieved at 90 kyrs. In the next 10 kyrs it drops linearly back to zero. We also studied the periodic case with the saw-tooth cycle repeated several times.

For the realistic glaciation cycle, the data from [17] were adopted. Siddall et al. analysed oxygen isotope records from Red Sea sediment cores to reconstruct the history of water residence times in Red Sea. Then a hydraulic model of the water

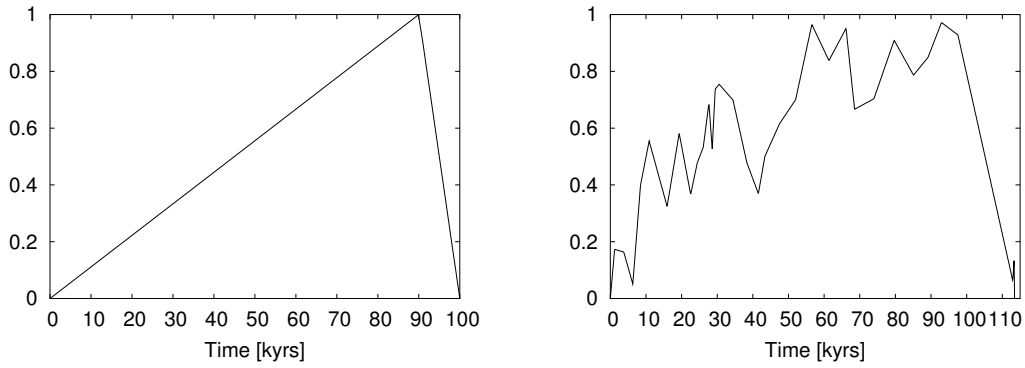

(a) Saw-tooth (b) Realistic

Fig. 8: The various loading histories

exchange between Red Sea and the world ocean was used to derive the global sea-level over the past 470 kyrs. A decrease of sea-level corresponds to a proportional increase of glacier volume and vice-versa. We will restrict our model to the last glaciation cycle, which started approximately 110 kyrs ago.

7.4 Viscosity profiles

For the benchmark model discussed below, the viscosity was assumed only vertically dependent. For the other models the viscosity varies laterally as well. The uppermost layer (the crust) has a thickness of approximately 100 km and is always assumed to be elastic. Under the crust is the upper mantle—a layer of low viscosity ($\sim 10^{21}$ Pa.s), extending down to the distance of 5701 km from the Earth's center. Below is the lower mantle, which has a higher viscosity ($\sim 10^{22}$–10^{23} Pa.s) and extends to 3480 km. In our models, the lateral variations in viscosity appear only in the upper mantle and result from the presence of the asthenosphere—a region of very low viscosity ($\sim 10^{19}$ Pa.s). The assumed viscosity distributions are shown on Figure 9. The asthenosphere was taken to extend outwards from different radii A, namely $A = 550$ km, $A = 890$ km and $A = 1200$ km.

8 Discussion of Results

Numerous calculations were performed, but due to the limitations of the written form, we will present and discuss only the most interesting results. Movies showing the time evolution of some physical quantities for several of the models can be found on the enclosed CD. For some cases we present graphs in Appendix C. The quantities

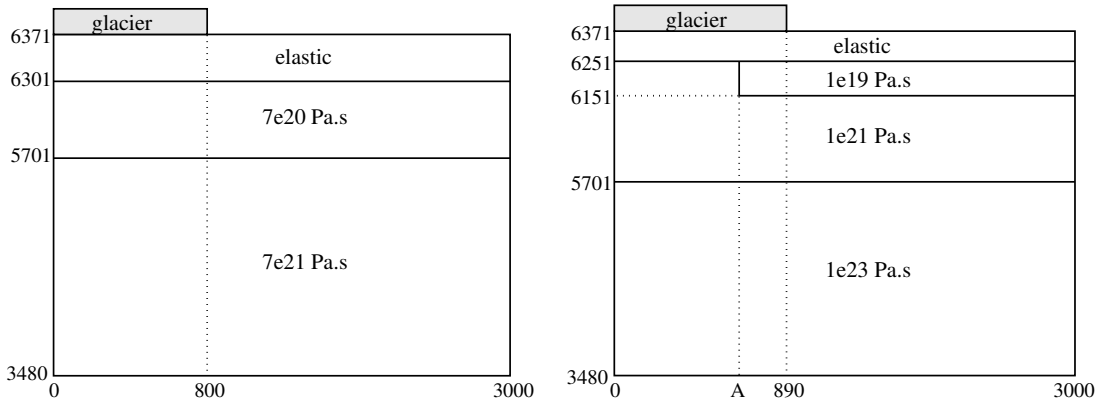

(a) Benchmark (b) Model with the asthenosphere

Fig. 9: The viscosity distributions (distances in km)

shown are: both components of the displacement (in meters), all four components of the stress (in GPa), the Euclidean norm of the $\boldsymbol{\sigma}$ tensor (in GPa) and the local dissipation density (in 3×10^{-9} W.m^{-3}). For many cases, we present graphs of the vertical and horizontal surface displacement (in meters), the maximum local dissipation density (in 3×10^{-9} W.m^{-3}) vs. time and dissipation integrated over the whole cylindrical domain (in 10^6 W) vs. time.

8.1 Benchmark Comparison

To have at least the basic idea that our computer program gives reliable results, we performed a benchmark simulation proposed by [11]. The loading history is Heaviside, the glacier has 800 km radius and 1 km thickness. The output of the model should be the vertical and the horizontal displacement at the Earth's surface in times 0, 1, 2, 5, 10 kyrs after loading. The problem was to be calculated using Legendre polynomials and for a spherical Earth.

Figure 12 shows the results presented at [11] as well as our own results. The vertical displacements are in very good quantitative agreement, our horizontal displacements seem to evolve faster in time, e.g. our result for 5 kyrs corresponds quite well to the benchmark result for 10 kyrs. However, in both cases the lines have the same characteristic shape with the minima at the edge of the glacier. The slight discrepancies in the horizontal displacement could have resulted from the flat-earth approximation.

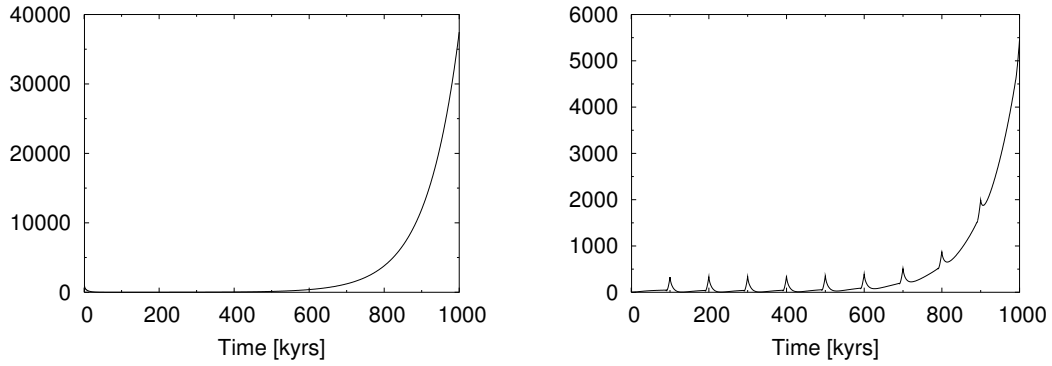

(a) Heaviside load (char. time 115 kyrs) (b) Saw-tooth load (char. time 113 kyrs)

Fig. 10: The Rayleigh–Taylor instability

8.2 Instability of PREM

The viscoelastic Earth model with the density distribution given by PREM is known to be unstable. This so-called Rayleigh–Taylor instability has been studied e.g. in [16] for PREM and in [10] for simpler models, but also analytically. In the case of PREM, it was found that this instability may typically have a characteristic time of the order of 10^7 years, but for very low viscosities in the asthenosphere it may be as low as 6×10^3 years. We were interested in finding out when such an instability would become apparent in our models.

Two simulations ranging over the time interval of one million years were perfomed. One with the Heaviside loading history for model 1 viscosity with $A = 890$ km, the other one with the saw-tooth cycle repeated 10 times for model 1 viscosity with $A = 1200$ km. For the Heaviside loading a ten times smaller time-stepping tolerance was used to make sure that the observed phenomenon is not caused by accumulation of numerical error. The appearance of the instability can be well visualized by plotting the total dissipation over the whole cylindrical domain vs. time (Figure 10). The exponential growth of the dissipation is evident and its characteristic times were found to be approximately 10^5 years in both cases.

8.3 Other interesting results

One model with load periodic in time was tried in order to see in how many cycles the solution would become periodic. The loading history was taken to be several saw-tooth cycles, each following right after the previous came to zero. Because of the Rayleigh–Taylor instability, only the first four or five cycles can be considered as reliable. The surface displacement at times 50, 100, 150, 200, 250, 300, 350 and

400 kyrs for such a case is visualized on Figures 14 and 15. From these graphs, it is apparent that only the first cycle substantially differs, otherwise the solution is already periodic. We can arrive at the same conclusion by looking at the graph of the total dissipation on Figure 13.

The most interesting results seem to be the graphs of the dissipation variation over time. The dissipation itself has deserved very little attention in the literature so far. We expected that the total dissipation would reflect the rate of change of the surface load. This appeared to be true to a certain extent. However, for the saw-tooth cycle, it was found that right after the switch from glaciation to deglaciation, there was a moment during which the total dissipation slightly decreased. The maximum dissipation density exhibited even more complicated behaviour. At some times, the graphs manifested jumps in the derivative, although the surface load was smooth. This is most likely due to the significant stress redistribution following such a glaciation-deglaciation switch, which results in a change of the position of the maximum. These positions can be well observed on the graphs showing the dissipation density in the whole domain (Figure 25. To our great astonishment, when the radial position of the boundary between the asthenosphere and the crust coincided with the position of the edge of the rectangular glacier ($A = 890$ km), the maximum for the dissipation density appeared later than the maximum for the total dissipation. In all other studied saw-tooth simulations, both maxima appeared simultaneously at 100 kyrs. Further calculations are necessary to find out whether the later maximum is caused by the switch to the following glaciation period or not and whether it appears for other values of A near 890 km as well. The realistic time-cycle (again $A = 890$ km) also reveals that a secondary peak usually appears after a sharp decrease of maximum dissipation density. Unfortunately, the realistic loading history was studied only with the parabolic glacier profile.

As to the stresses, an interesting phenomenon to observe is the reaction of the stress fields to the deglaciation. While during the glaciation the stress components are significant only in the upper part of the domain, during the deglaciation they decrease near the top, but become quite significant in the middle or even lower part of the domain. In fact, their values in these parts reach maximum at the time, when zero load is present on the surface. This phenomenon was observed not only in the case of the saw-tooth cycle, but also for the realistic loading history.

9 Conclusions

We succeeded in deriving the weak formulation of both the elastic and the viscoelastic problem. The existence and uniqueness were proved in both cases. A simple numerical approach was developed. The introduction of the auxiliary tensor field $\boldsymbol{\sigma}$, corresponding to the inelastic part of the stress tensor, seems very promising for

development more complicated time-stepping techniques. Using such an approach the evolutionary problem could be decoupled into an evolutionary and a stationary problem, thus enabling use of more efficient time-stepping algorithms.

Using the finite element approach, lateral variations of viscosity may be easily incorporated into the calculations. A program for numerical solution of the elastic and viscoelastic problem was developed and tested on a benchmark problem. Using the program, several simulations were performed for some model glacier profiles and loading histories and one simulation even for a realistic loading history. Furthermore, different positions of the asthenosphere are considered. The graphs of the deformation, stress tensor components and dissipation are shown for some of the problems. All simulations are visualised in the form of movies, which may be found on the enclosed CD. The graphs of the total dissipation as well as those of the maximum local dissipation density exhibit very complicated behaviour. The instability of PREM was studied for two different loading histories and the characteristic times were determined. Some other remarkable results were obtained and discussed. In some cases, further studies are necessary to confirm and explain the phenomena observed.

Bibliography

[1] Biot M.: *Mechanics of Incremental Deformations*, J. Wiley and Sons, New York, 1965.

[2] Dahlen F.A., Tromp J.: *Theoretical Global Seismology*, Princeton Univ. Press, Princeton, 1998.

[3] Dziewonski A.M., Anderson D.L.: Preliminary reference Earth model, *Phys. Earth Planet. Inter.*, 25, pp. 297–356, 1981.

[4] Evans L.C.: *Partial Differential Equations*, Amer. Math. Society, Providence, 1998.

[5] Galdi G.P.: *An Introduction to the Mathematical Theory of the Navier–Stokes Equations*, Springer–Verlag, New York, 1994.

[6] *GMV*, http://www-xdiv.lanl.gov/XCM/gmv/GMVHome.html

[7] *gmvmpeg*, http://www.featflow.de (Software/Download the tools)

[8] Hanyk L.: *Viscoelastic Response of the Earth: Initial-Value Approach*, Ph.D. Thesis, Prague, 1999.

[9] Hanyk L., Matyska C., Yuen D.A.: Energy pumping into the Earth's mantle by glacial forcing, in preparation.

[10] Hanyk L., Matyska C., Yuen D.A.: Secular gravitational instability of a compressible viscoelastic sphere, *Geophys. Res. Letters*, 26, no.5, pp. 557–560, 1999.

[11] Kaufmann G., Johnston P.: *Benchmark Comparisons for Models of Glacial Isostatic Adjustment*, www.rses.anu.edu.au/geodynamics/GIA_benchmark/, 1997.

[12] Kaufmann G., Wu P., Guoying Li: Glacial isostatic adjustment in Fennoscandia for a laterally heterogeneous Earth, *Geophys. J. Int.*, 143, pp. 262–273, 2000.

[13] Martinec Z.: Free oscillations of the Earth, *Travaux Géophysiques*, No. 591, 1984.

[14] Martinec Z.: Spectral–finite element approach to three-dimensional viscoelastic relaxation in a spherical Earth, *Geophys. J. Int.*, 142, pp. 117–141, 2000.

[15] Nečas J., Hlaváček I.: *Mathematical Theory of Elastic and Elastoplastic Bodies: An Introduction*, Elsevier, Amsterdam, 1981.

[16] Plag H.-P., Jüttner H.-U.: Rayleigh–Taylor instabilities of a self-gravitating Earth, *J. Geodynamics*, 20, pp. 267–288, 1995.

[17] Siddall M. et al.: Sea-level fluctuations during the last glacial cycle, *Nature*, 423, pp. 853–858, 2003.

[18] Su W., Dziewonski A.M.: Predominance of long-wavelength heterogeneity in the mantle, *Nature*, 352, pp. 121–126, 1991.

[19] Tamisiea M.E. et al.: Effects of the Cowling approximation on predictions of glacial isostatic adjustment, *Eos. Trans. AGU*, 82(47), Fall Meet. Suppl., 2001.

[20] Turek S.: *Efficient Solvers for Incompressible flow problems*, Springer–Verlag, Heidelberg. 1999.

[21] Wu P., Ni Z., Kaufmann G.: Postglacial rebound with lateral heterogeneities: From 2D to 3D modeling, in *Dynamics of the Ice Age Earth: A Modern Perspective*, pp. 557–582, Wu P. ed., Trans Tech, Switzerland, 1998.

[22] Wu P., Johnston P.: Validity of using flat-earth finite element models in the study of postglacial rebound, in *Dynamics of the Ice Age Earth: A Modern Perspective*, pp. 191–202, Wu P. ed., Trans Tech, Switzerland, 1998.

[23] Ying L.: *Infinite Element Methods*, Peking University press, Peking, 1995.

A Homogeneous Sobolev Spaces

Only those properties of the homogeneous Sobolev spaces that were used throughout the preceding text, are cited below. For further information and proofs, see [5].

The homogeneous Sobolev spaces $D^{m,q}(\Omega),\ \Omega \subseteq \mathcal{R}^n$, are defined as

$$D^{m,q}(\Omega) \equiv \left\{u \in L^1_{loc}(\Omega); D^\alpha u \in L^q(\Omega), \forall\, |\alpha| = m\right\}, \tag{A.1}$$

where $m \in \mathcal{N}, m \geq 0$ and $q \in \mathcal{R}, q \geq 1$.

Let us introduce the seminorm

$$|u|_{m,q} \equiv \left(\sum_{|\alpha|=m} \int_\Omega |D^\alpha u|^q\right)^{1/q}. \tag{A.2}$$

Then the space $\{D^{m,q},\ |\cdot|_{m,q}\}$ is a complete normed space, provided that two functions $u_1, u_2 \in D^{m,q}(\Omega)$ are identified, whenever $|u_1 - u_2|_{m,q} = 0$.

Along with the spaces $D^{m,q}$ we also introduce the spaces $D_0^{m,q}(\Omega)$ defined as the completion of $\mathcal{C}_0^\infty(\Omega)$ in the above-defined seminorm. Evidently, $D_0^{m,q}(\Omega) \subseteq D^{m,q}(\Omega)$.

Lemma A.1 *Let $\Omega \subseteq \mathcal{R}^n,\ n \geq 1$. Then $\{D^{m,q}(\Omega),\ |\cdot|_{m,q}\}$ is a Banach space. In particular, if $q = 2$, it is a Hilbert space with the scalar product*

$$(u, v)_m = \sum_{|\alpha|=m} \int_\Omega D^\alpha u\ D^\alpha v. \tag{A.3}$$

Lemma A.2 *The spaces $D^{m,q}$ and $D_0^{m,q}$ are separable for $1 \leq q < \infty$ and reflexive for $1 < q < \infty$.*

Lemma A.3 *If $u \in D^{m,q}(\Omega)$ then $u \in W^{m,q}_{loc}(\Omega)$.*

Lemma A.4 *Let $u \in D_0^{m,q},\ 1 \leq q < n$. Then $u \in L^s,\ s = nq/(n-q)$ and the Sobolev inequality holds:*

$$\|u\|_s \leq \frac{q(n-1)}{2(n-q)\sqrt{n}}\, |u|_{1,q}. \tag{A.4}$$

Lemma A.5 *Let $u \in D_0^{1,q},\ 1 \leq q < n$. Then*

$$\left\| \frac{u}{|\boldsymbol{x} - \boldsymbol{x}_0|} \right\|_q < \infty, \qquad \forall \boldsymbol{x}_0 \in \mathcal{R}^n \tag{A.5}$$

and, moreover,

$$\left\| \frac{u}{|\boldsymbol{x} - \boldsymbol{x}_0|} \right\|_q \leq \frac{q}{n-q}\, |u|_{1,q}. \tag{A.6}$$

B Definition of PREM

Region	Radius [km]	ρ	v_P	v_S
Inner Core	0–1221.5	13.0885 $-8.8381\alpha^2$	11.2622 $-6.3640\alpha^2$	3.6678 $-4.4475\alpha^2$
Outer Core	1221.5–3480	12.5815 -1.2638α $-3.6426\alpha^2$ $-5.5281\alpha^3$	11.0487 -4.0362α $+4.8023\alpha^2$ $-13.5732\alpha^3$	0
D”	3480–3630	7.9565 -6.4761α $+5.5283\alpha^2$ $-3.0807\alpha^3$	15.3891 -5.3181α $+5.5242\alpha^2$ $-2.5514\alpha^3$	6.9254 $+1.4672\alpha$ $-2.0834\alpha^2$ $+0.9783\alpha^3$
Lower Mantle	3630–5600	7.9565 -6.4761α $+5.5283\alpha^2$ $-3.0807\alpha^3$	24.9520 -40.4673α $+51.4832\alpha^2$ $-26.6419\alpha^3$	11.1671 -13.7818α $+17.4575\alpha^2$ $-9.2777\alpha^3$
	5600–5701	7.9565 -6.4761α $+5.5283\alpha^2$ $-3.0807\alpha^3$	29.2766 -23.6027α $+5.5242\alpha^2$ $-2.5514\alpha^3$	22.3459 -17.2473α $-2.0834\alpha^2$ $+0.9783\alpha^3$
Transition Zone	5701–5771	5.3197 -1.4836α	19.0957 -9.8672α	9.9839 -4.9324α
	5771–5971	11.2494 -8.0298α	39.7027 -32.6166α	22.3512 -18.5856α
	5971–6151	7.1089 -3.8045α	20.3926 -12.2569α	8.9496 -4.4597α
LVZ	6151–6291	2.6910 $+0.6924\alpha$	4.1875 $+3.9382\alpha$	2.1519 $+2.3481\alpha$
LID	6291–6346.6	2.6910 $+0.6924\alpha$	4.1875 $+3.9382\alpha$	2.1519 $+2.3481\alpha$
Crust	6346.6–6356	2.9	6.8	3.9
	6356–6368	2.6	5.8	3.2
Ocean	6368–6371	1.020	1.45	0

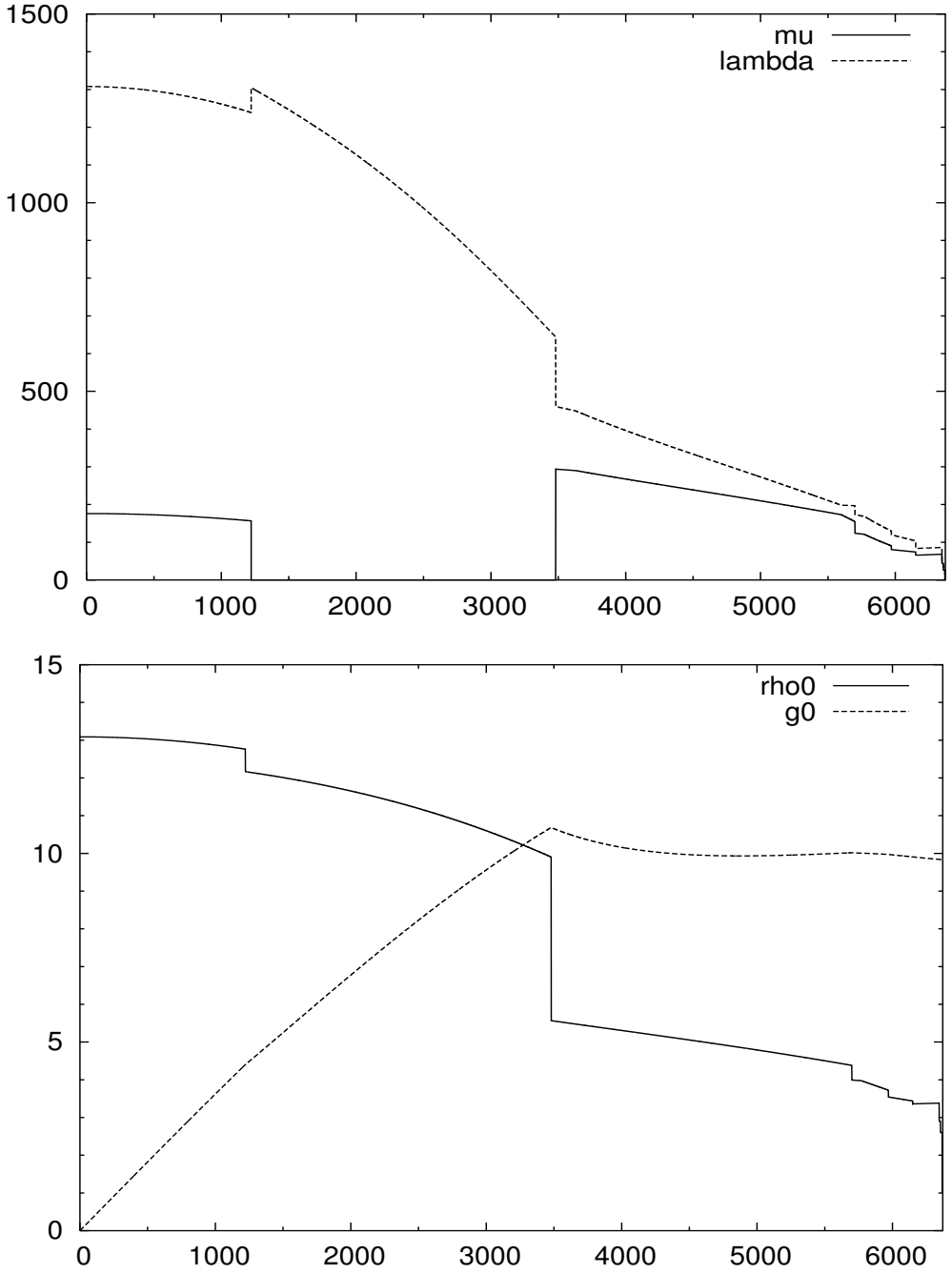

Fig. 11: The variations of the elastic Lamé coefficients (in GPa), the initial density (in g.cm^{-3}) and the initial gravitational acceleration (in m.s^{-2}) according to PREM

C Graphs of Results

Benchmark results

horizontal displacement

vertical displacement

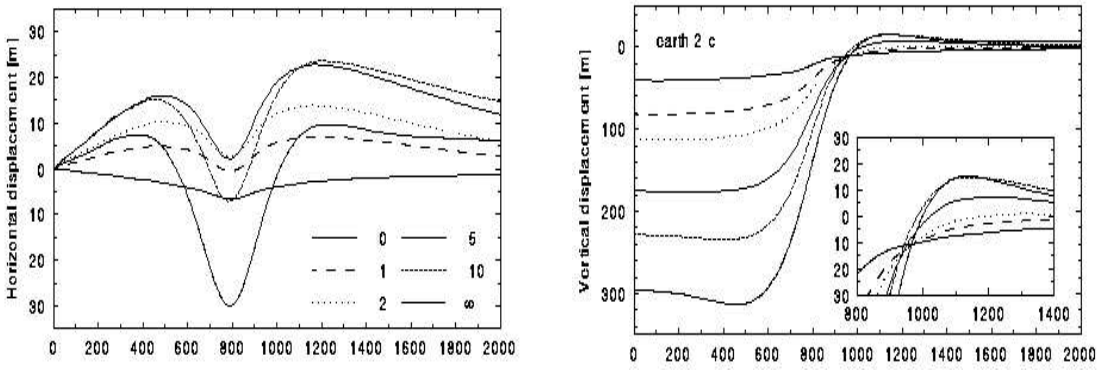

Our results

horizontal displacement

vertical displacement

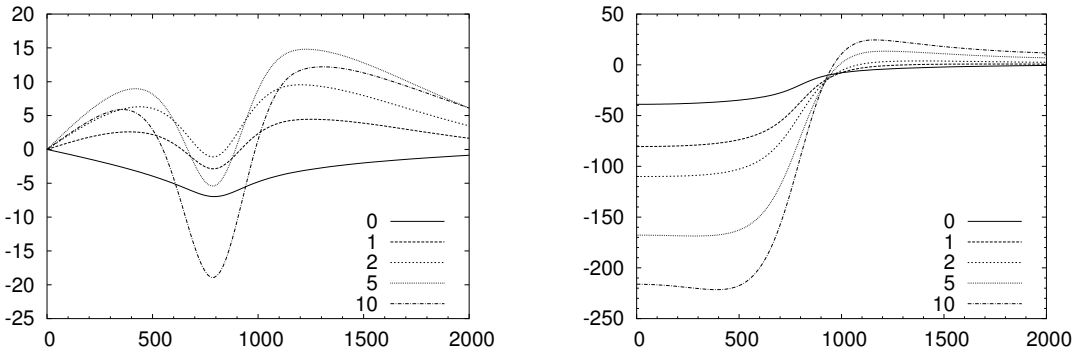

Fig. 12: Benchmark comparison (x-axis—radial distance from cylindrical axis (km), y-axis—surface displacement (m), time in kyrs)

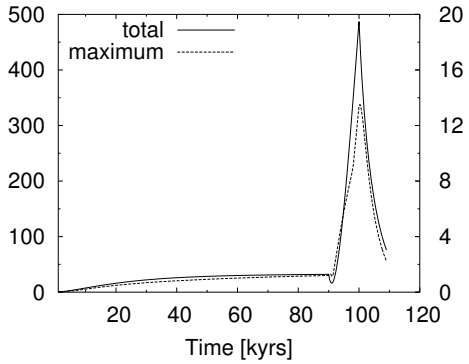

saw-tooth, rect., A=550 km

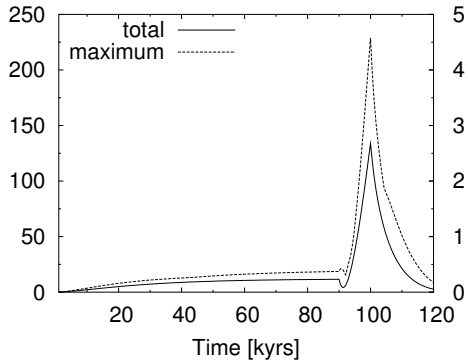

saw-tooth, parab., A=890 km

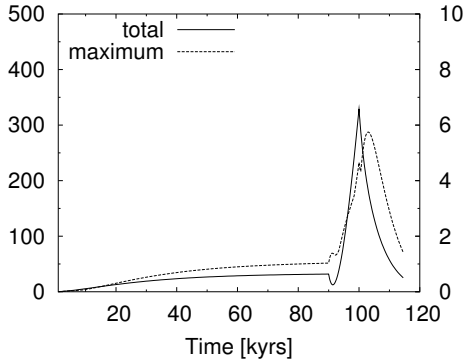

saw-tooth, rect., A=890 km

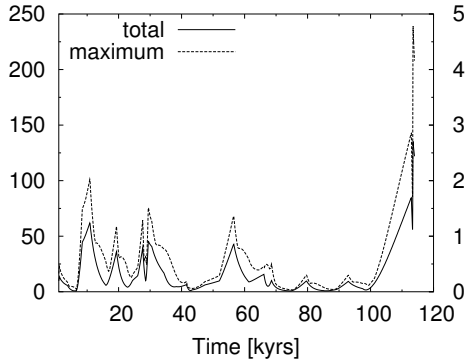

realistic, parab., A=890 km

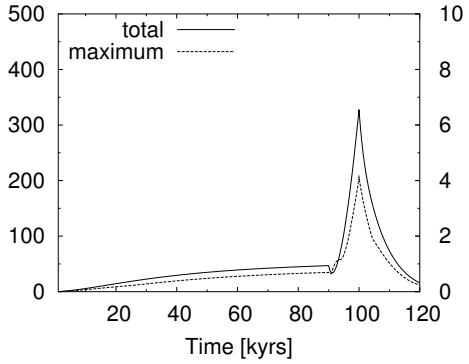

saw-tooth, rect., A=1200 km

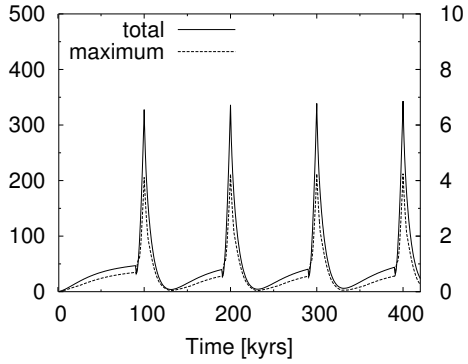

4× saw-tooth, rect., A=1200 km

Fig. 13: Local dissipation densities (right scales, in 3×10^{-9} W/m^3) and total dissipations over the whole cylinder (left scales, in 10^6 W)

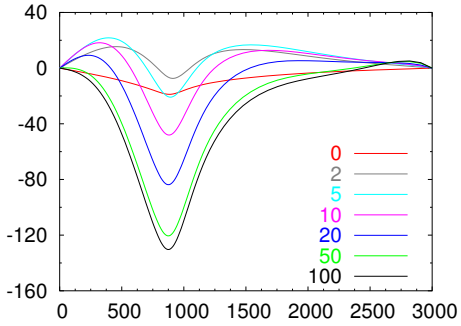

Heaviside, rect., A=890 km

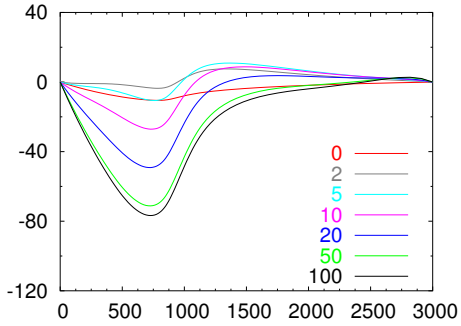

Heaviside, parab., A=890 km

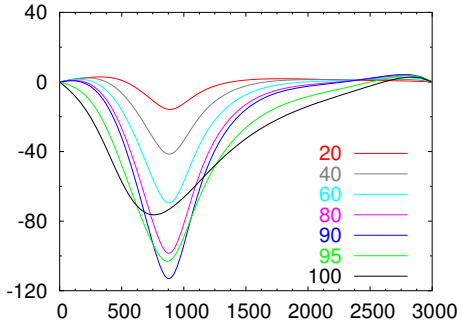

saw-tooth, rect., A=550 km

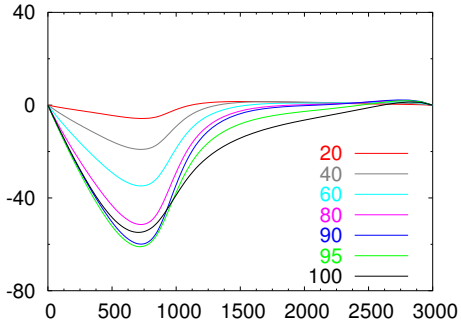

saw-tooth, parab., A=890 km

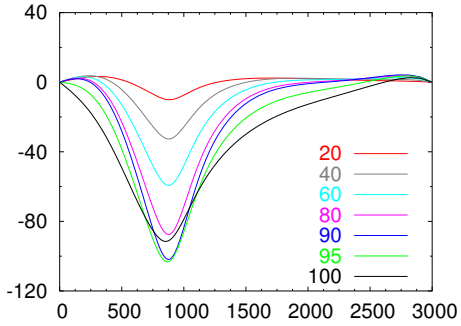

saw-tooth, rect., A=890 km

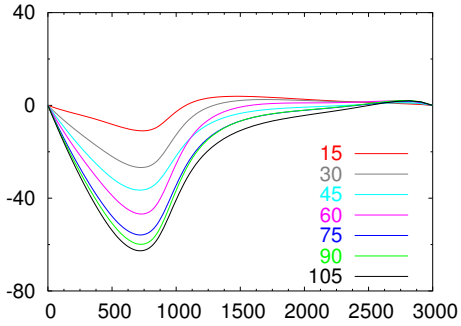

realistic, parab., A=890 km

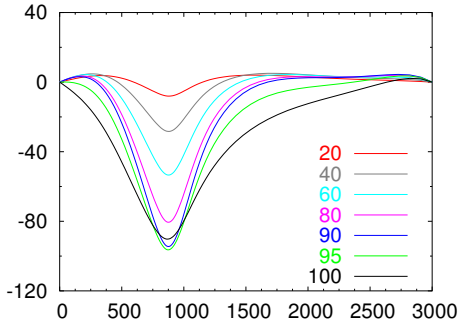

saw-tooth, rect., A=1200 km

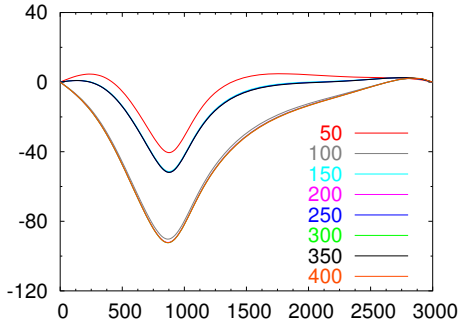

4× saw-tooth, rect., A=1200 km

Fig. 14: The horizontal displacement (in meters) at the surface (time in kyrs)

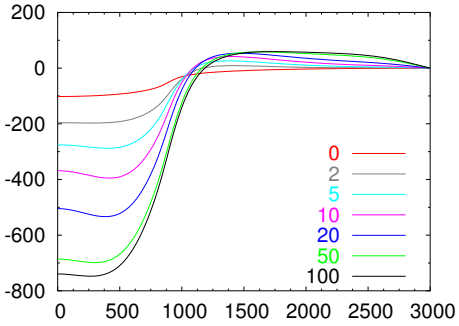

Heaviside, rect., A=890 km

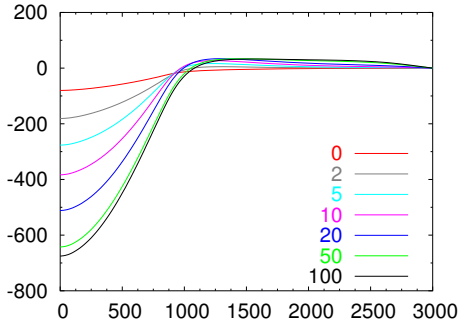

Heaviside, parab., A=890 km

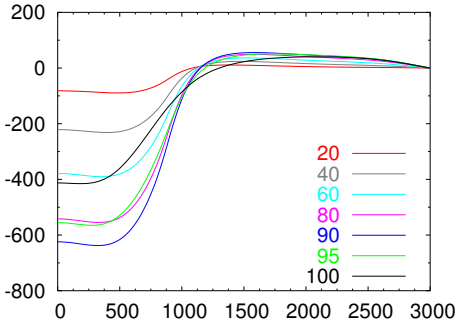

saw-tooth, rect., A=550 km

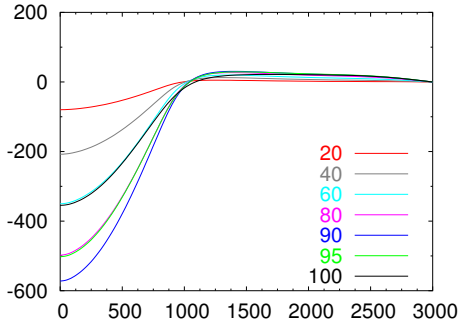

saw-tooth, parab., A=890 km

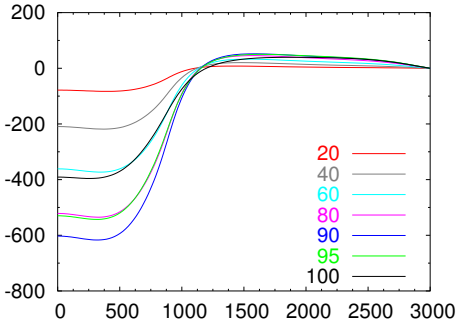

saw-tooth, rect., A=890 km

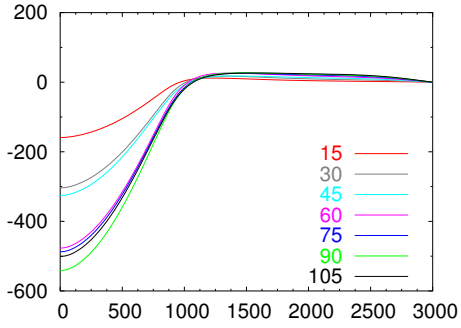

realistic, parab., A=890 km

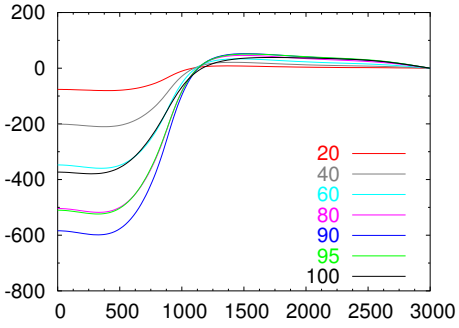

saw-tooth, rect., A=1200 km

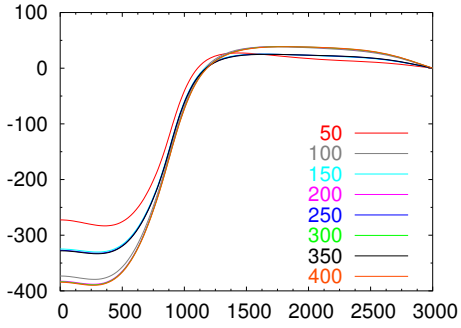

4× saw-tooth, rect., A=1200 km

Fig. 15: The vertical displacement (in meters) at the surface (time in kyrs)

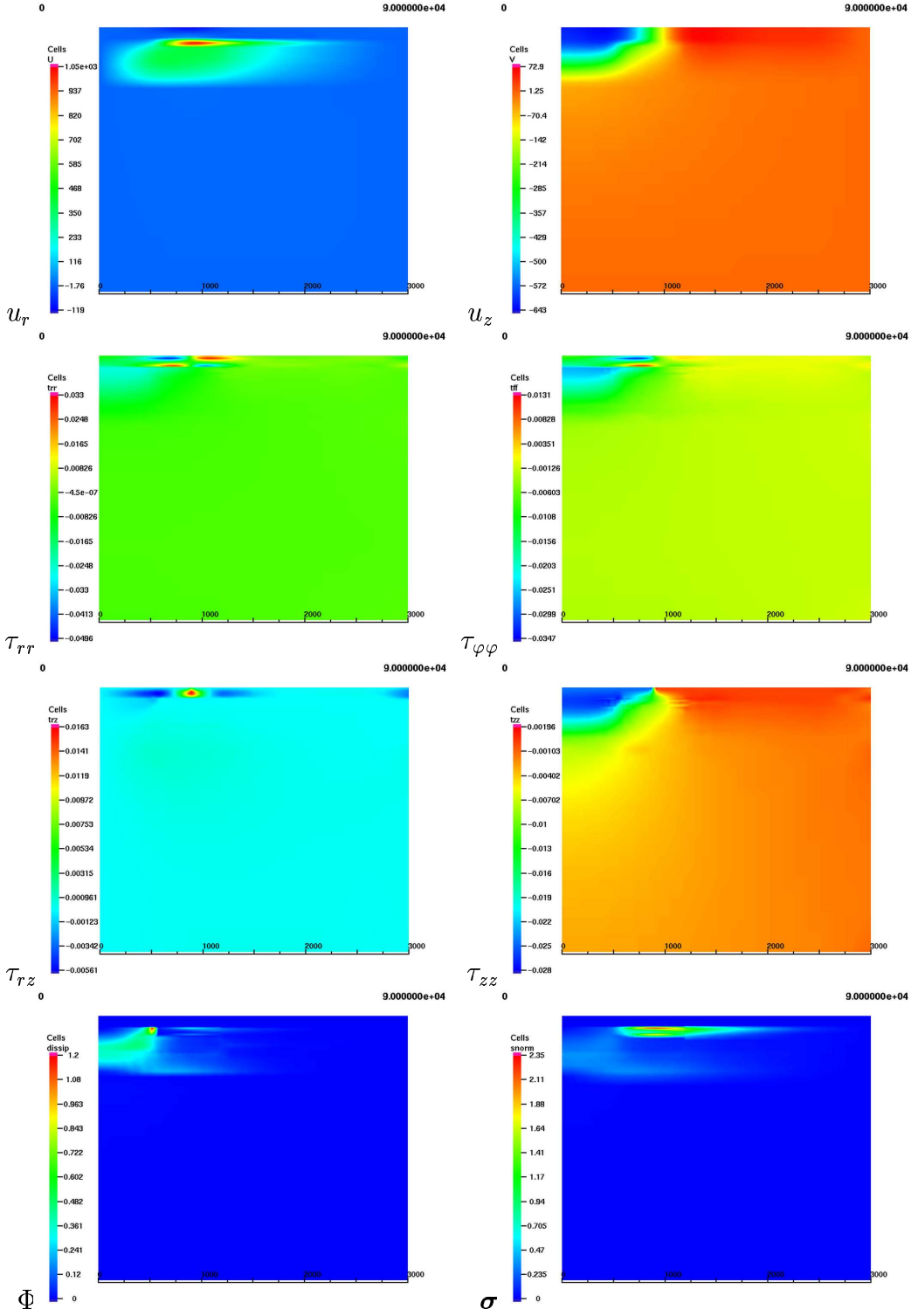

Fig. 16: Results at t=90 kyrs, rectang. glac., saw-tooth load, A=550 km

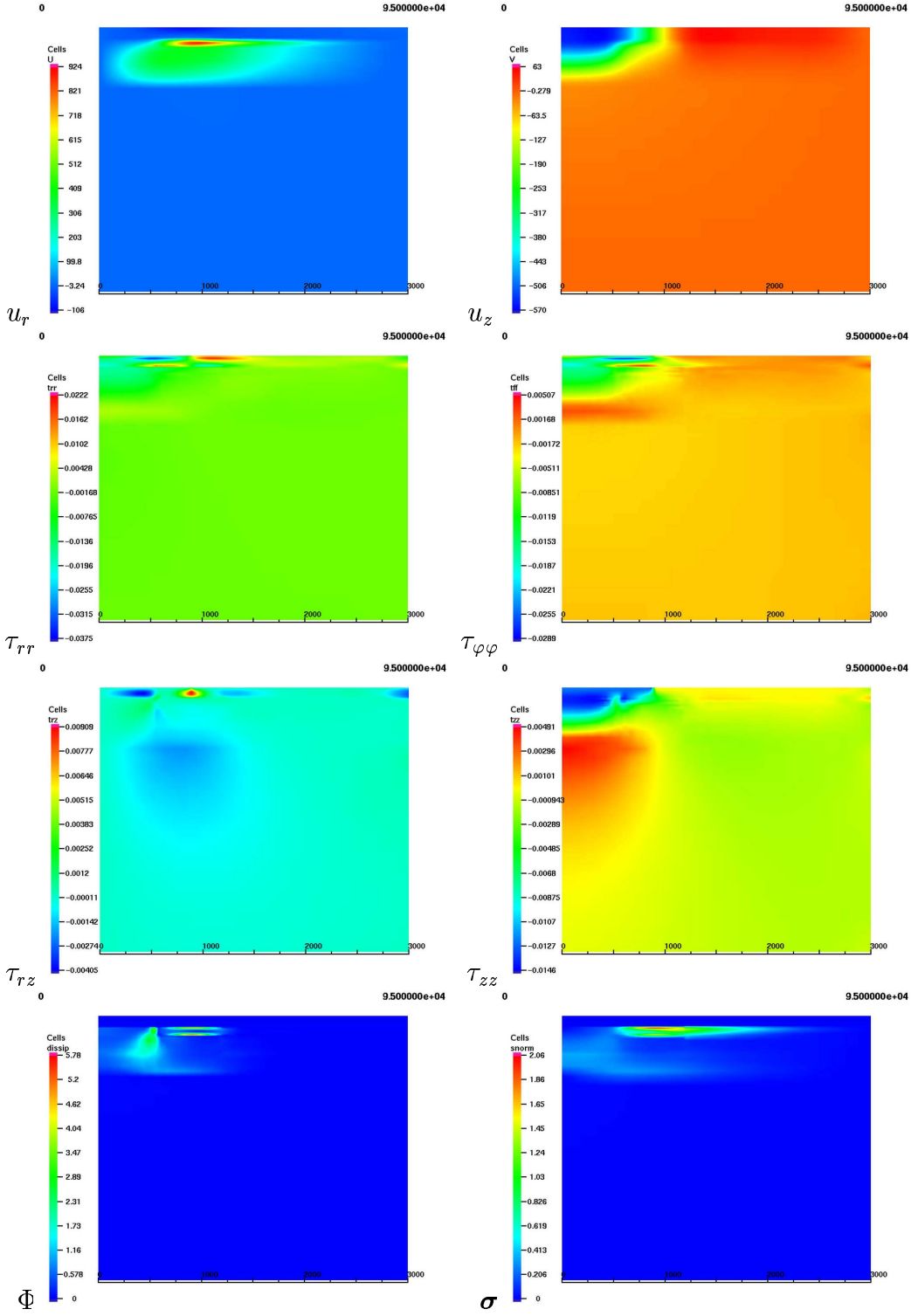

Fig. 17: Results at t=95 kyrs, rectang. glac., saw-tooth load, A=550 km

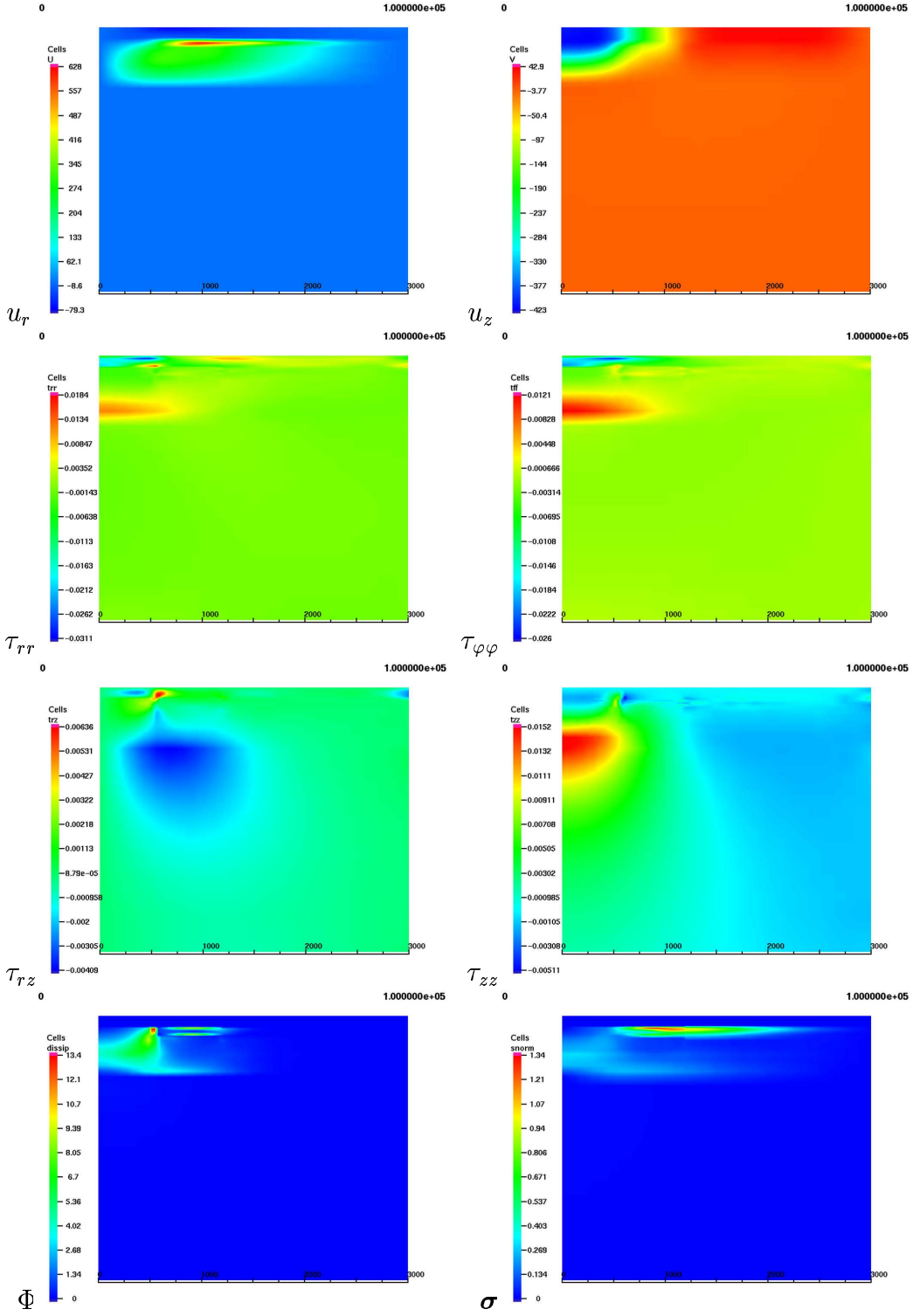

Fig. 18: Results at t=100 kyrs, rectang. glac., saw-tooth load, A=550 km

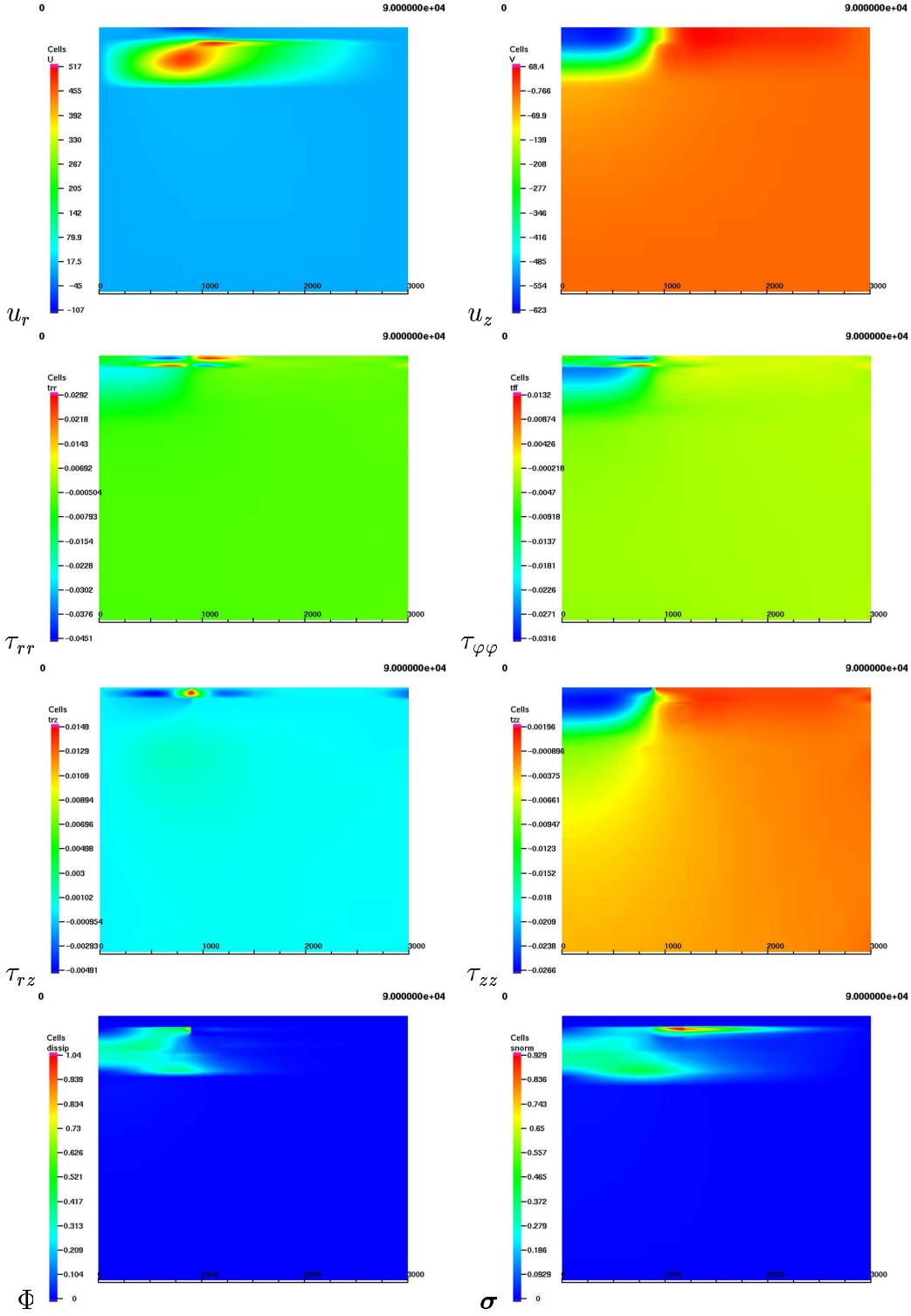

Fig. 19: Results at t=90 kyrs, rectang. glac., saw-tooth load, A=890 km

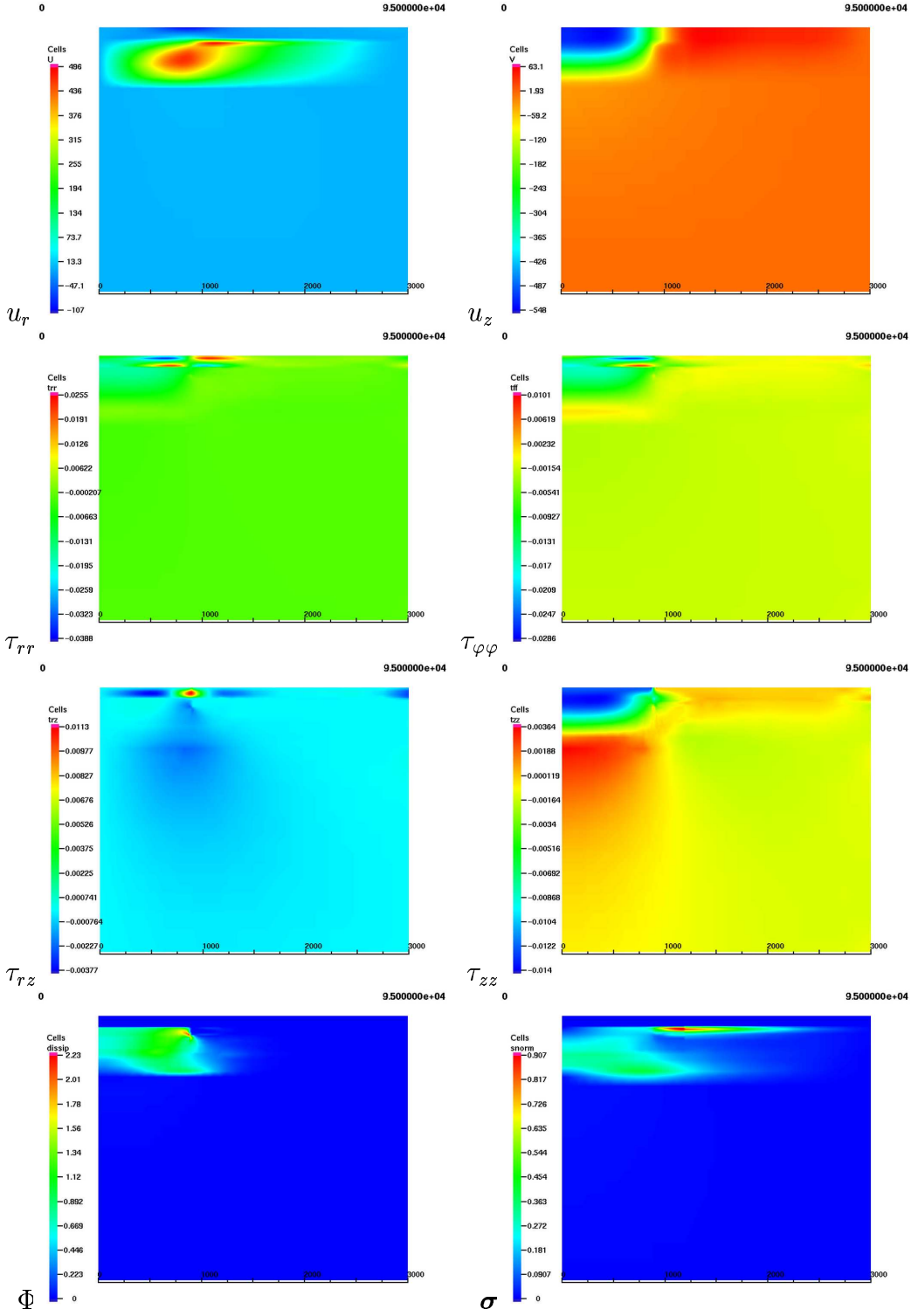

Fig. 20: Results at t=95 kyrs, rectang. glac., saw-tooth load, A=890 km

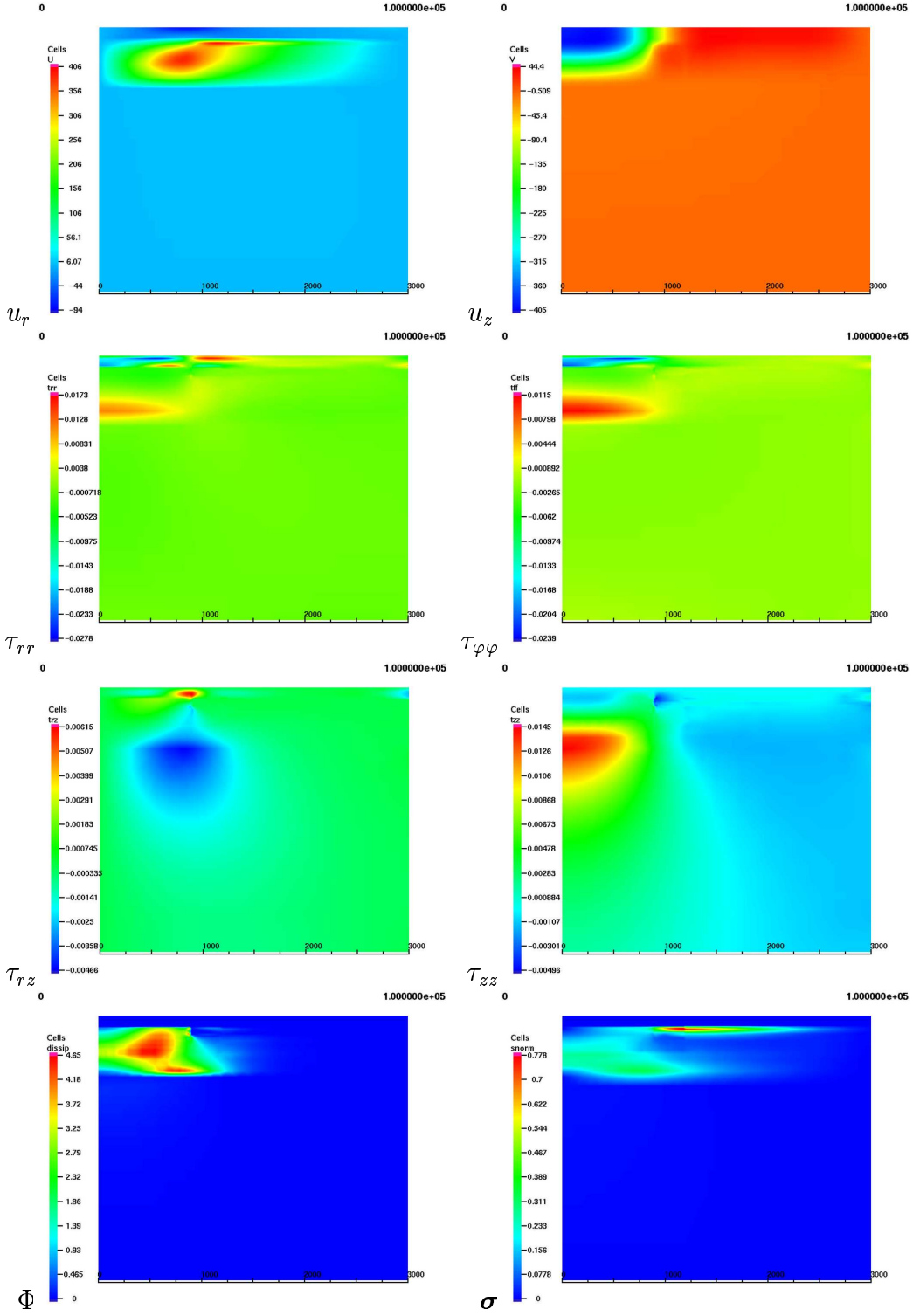

Fig. 21: Results at t=100 kyrs, rectang. glac., saw-tooth load, A=890 km

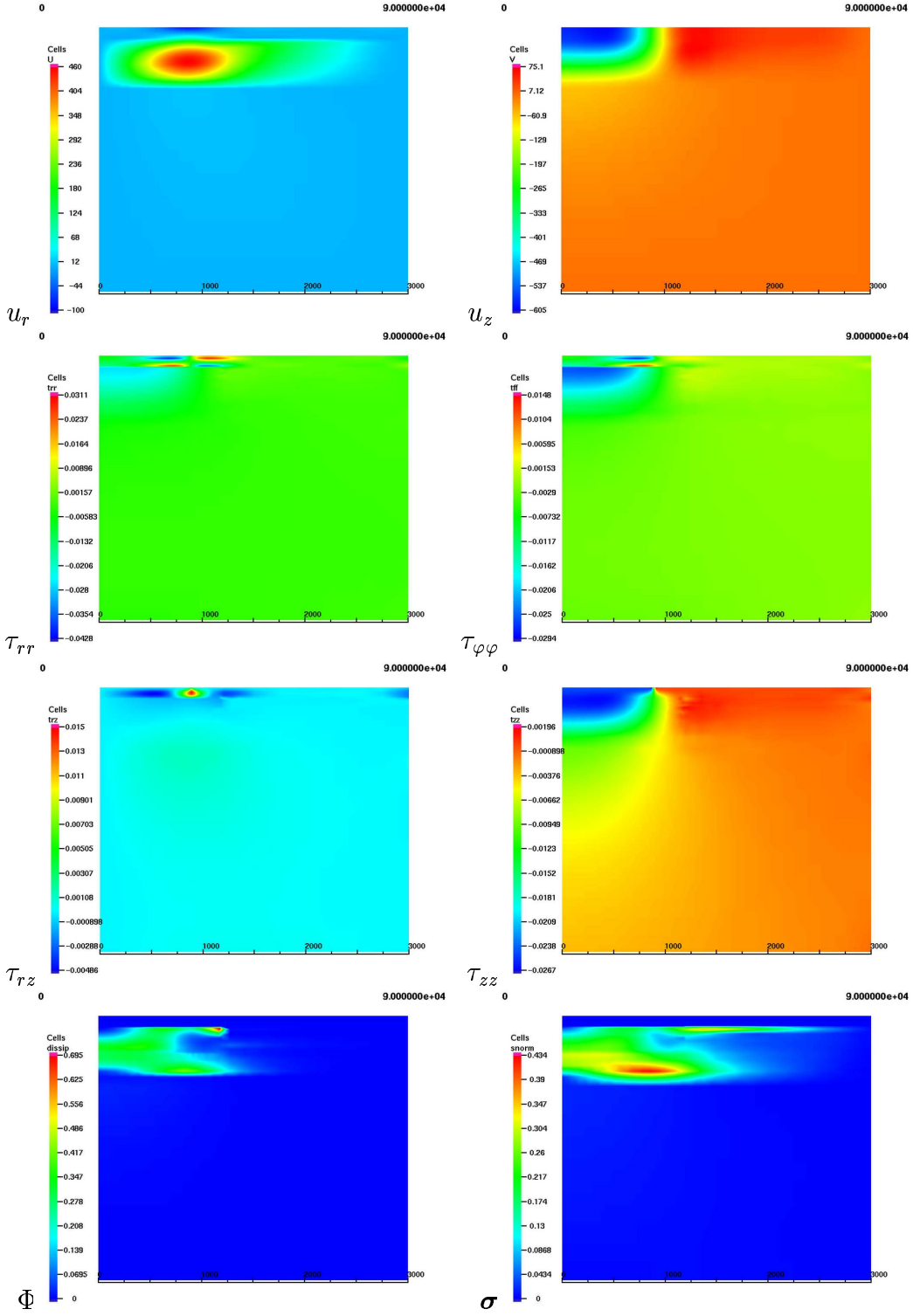

Fig. 22: Results at t=90 kyrs, rectang. glac., saw-tooth load, A=1200 km

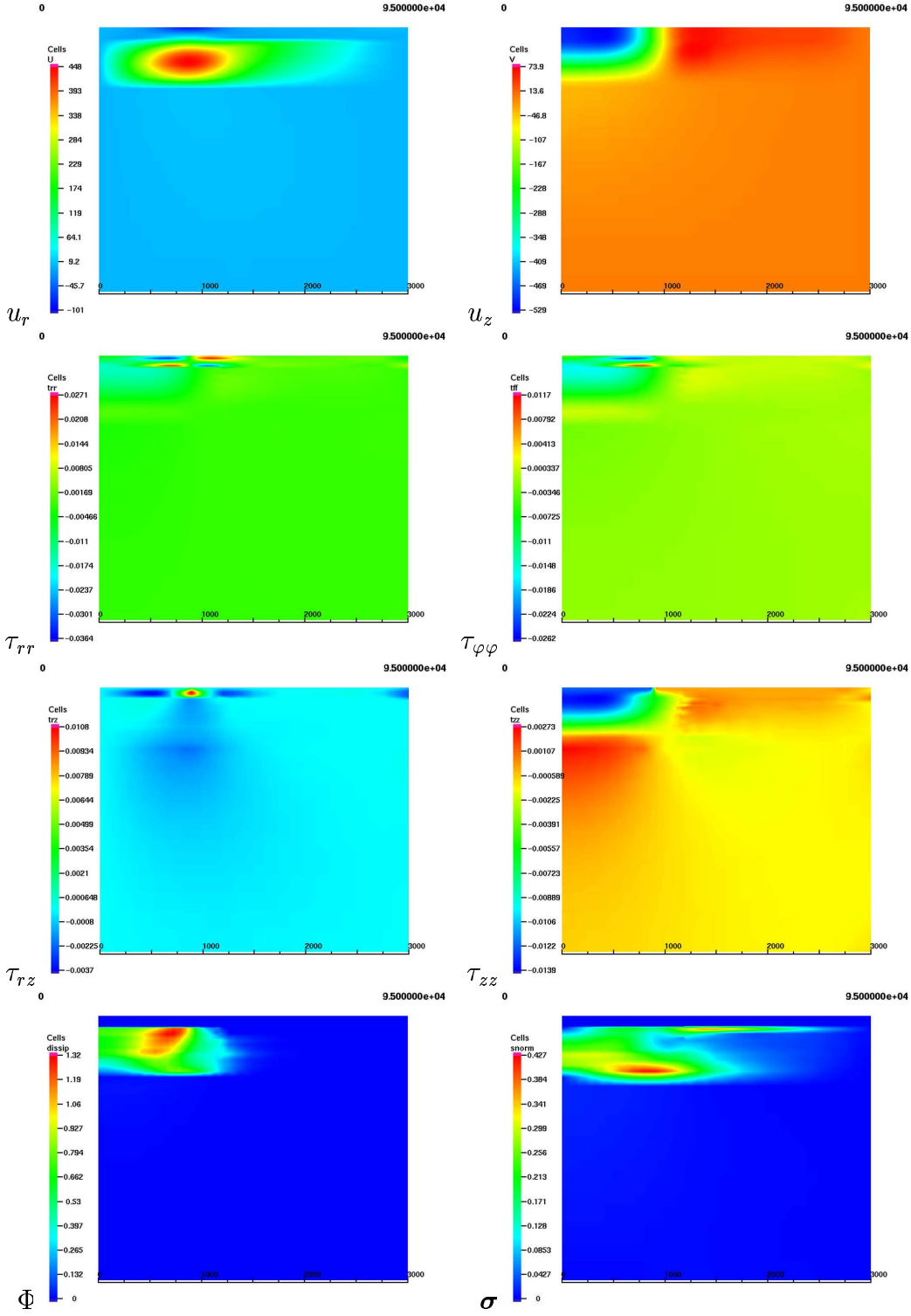

Fig. 23: Results at t=95 kyrs, rectang. glac., saw-tooth load, A=1200 km

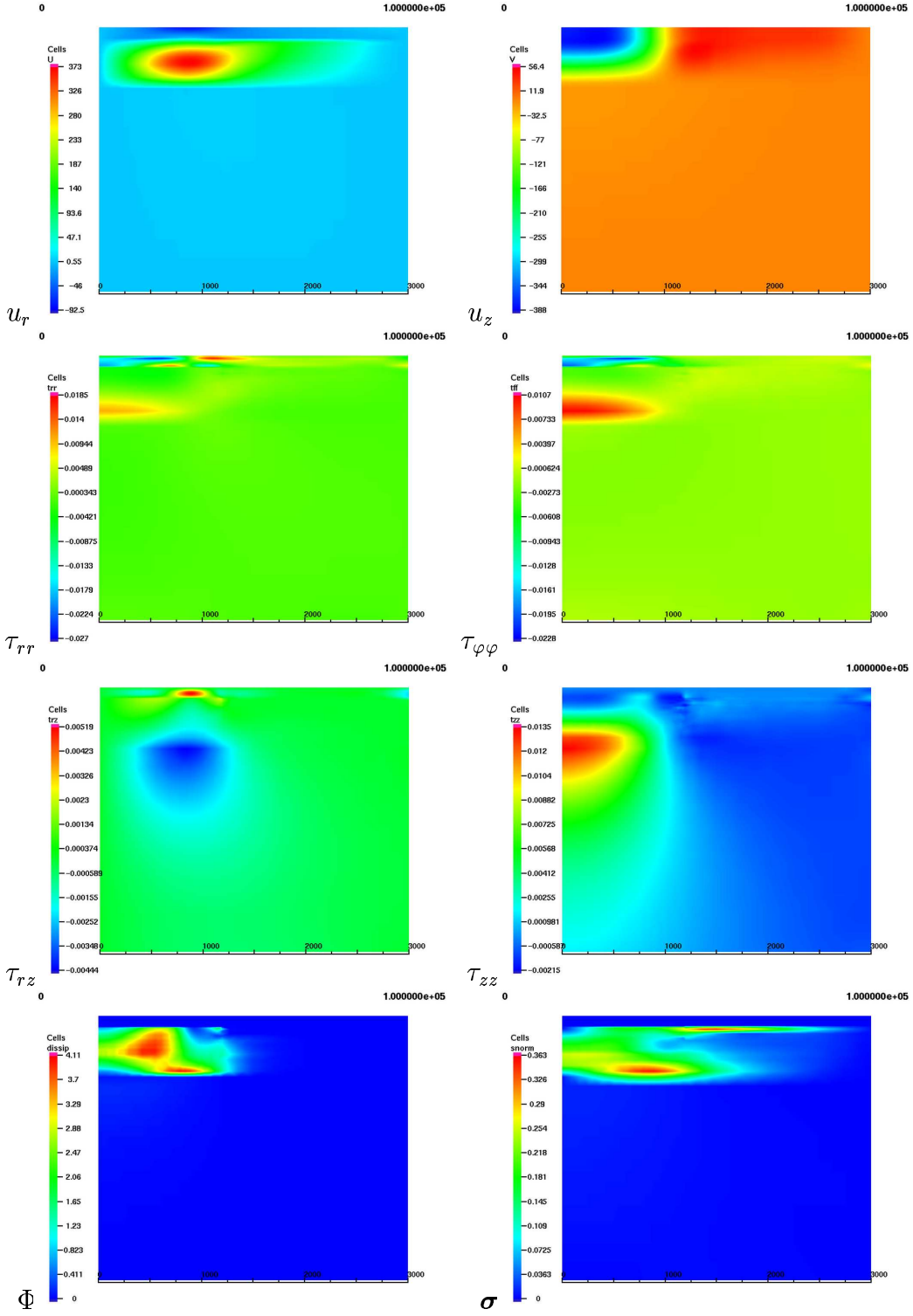

Fig. 24: Results at t=100 kyrs, rectang. glac., saw-tooth load, A=1200 km

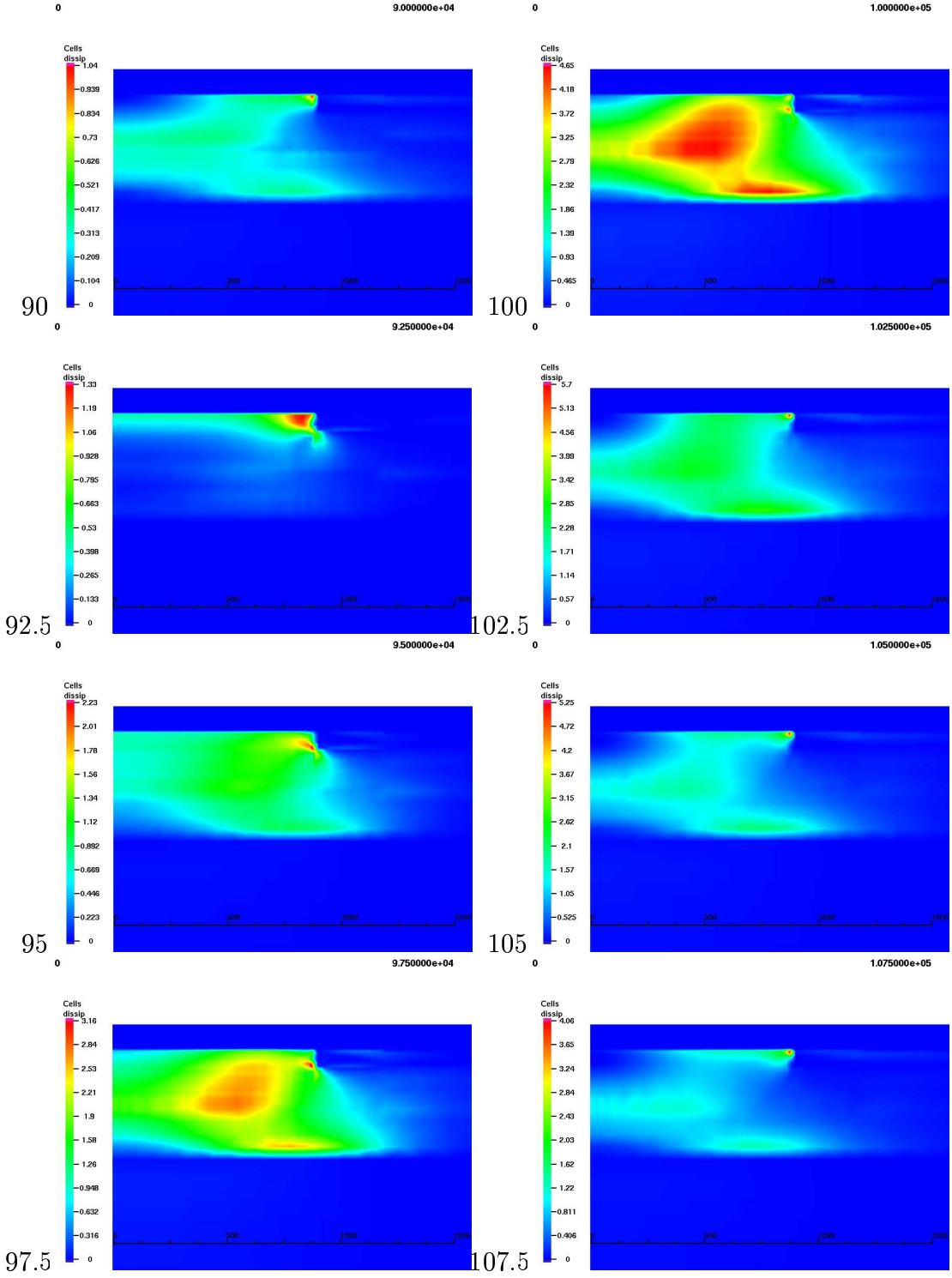

Fig. 25: Dissipation densities at various times (in kyrs) for rectang. glac., saw-tooth load, A=890 km